

Black Marble User Guide (Collection 2.0)

Product's Principal Investigator:
Zhuosen Wang

List of Contributors:
Miguel O. Román, Ranjay Shrestha, Tian Yao, and Virginia Kalb.

October 2024



Contents

1 Introduction.....	1
2 Algorithm.....	2
2.1 Overview of the Algorithm.....	2
2.2 Atmospheric Correction.....	3
2.3 BRDF Correction	4
2.3 Monthly and Yearly Nighttime Light Composite.....	5
3 Data Product Formats	6
3.1 Metadata.....	6
3.2 Filenames	6
3.3 Projection	7
4. Product generation.....	8
5 Scientific Data Sets (SDSs) from Black Marble Product Suite	10
5.1 The VNP46A1/VJ146A1 Daily At-sensor TOA Nighttime Lights Product	10
5.2 The VNP46A2/VJ146A2 Daily Moonlight-adjusted Nighttime Lights (NTL) Product	15
5.3 The VNP46A3/VJ146A3 Monthly and VNP46A4/VJ146A4 Yearly Moonlight-adjusted Nighttime Lights (NTL) Product	17
5.4 Examples of the Black Marble Product Suite.....	23
6 Evaluation and Validation of the Product.....	26
7 Data Archives	29
8 Data Usage and Citation Policies	29
9 Contact Information.....	29
10 Related Publications	29
References.....	31
Appendix A: Metadata (Attributes) in VNP46A1 Product.....	38
Appendix B: Metadata (Attributes) in VNP46A2 Product.....	43
Appendix C: Metadata (Attributes) in VNP46A3 Product.....	45
Appendix D: Metadata (Attributes) in VNP46A4 Product.....	49

List of Figures

Figure 1 Overview of NASA's Black Marble retrieval strategy (<i>cf.</i> , Equation 1). During the ~50% portion of the lunar cycle when moonlight is present at the time of satellite observation, the surface upward radiance from artificial light emissions, L_{NTL} [units of $\text{nWatts}\cdot\text{cm}^{-2}\cdot\text{sr}^{-1}$], can be extracted from at-sensor nighttime radiance at TOA (L_{DNB}). L_{path} is the nighttime path radiance, $a(\theta_m)$ is the VIIRS-derived actual surface albedo. The atmospheric backscatter is given by ρ_a . $T_{\downarrow}(\tau, \theta_v)$ and $T_{\uparrow}(\tau, \theta_v)$ are the total transmittances along the lunar-ground and ground-sensor paths (respectively). $P_{\uparrow}(\theta_v)$ is the probability of the upward transmission of NTL emissions through the urban vegetation canopy.....	4
Figure 2 The Suomi-NPP VIIRS linear latitude/longitude (or geographic) grid consists of 460 non-overlapping Land tiles, which measure approximately $10^{\circ}\times 10^{\circ}$ region.	7
Figure 3 Algorithm processing cycle and ancillary parameters used by NASA's Black Marble product suite.....	9
Figure 4 Black Marble product suite components for a $10^{\circ}\times 10^{\circ}$ Level 3 tile over France and the Balearic Sea region (h18v04; DOY 2015-091). The full-moon-illuminated and 51% cloud-contaminated scene illustrates the challenges of nighttime cloud masking over snow-covered surfaces (e.g., the French Alps and the Pyrenees).....	24
Figure 5 VNP46 product suite components for a $10^{\circ}\times 10^{\circ}$ Level 3 tile over Sweden and Finland (h20v02; DOY 2013-080). The half-moon-illuminated and 30% cloud-contaminated scene is shown to capture extraneous light emissions north of the Gulf of Bothnia caused by the Aurora Borealis.	25
Figure 6 VNP46A3 monthly (upper) and VNP46A4 yearly (bottom) NTL composite (left), the associated number of observations for the composite (middle) and quality (right) for a $10^{\circ}\times 10^{\circ}$ Level 3 tile h06v05 in 2016.	26
Figure 7 The NTL radiance at the Pitahaya farmland site in Cabo Rojo, PR on 1st, 2nd and 3rd March 2017. The top-right image shows the setup of the stable point source. TOA and VNP46A2 values are in $\text{nW}\cdot\text{cm}^{-2}\cdot\text{sr}^{-1}$. VCM = 0 represents cloud free overpasses. LZA is lunar zenith angle, and the values larger than 108° correspond to moonless nights.	28

List of Tables

Table 1 Black Marble VNP46A1 product input files	8
Table 2 Black Marble VNP46A2 product input files	8
Table 3 Black Marble VNP46A3 product input files	8
Table 4 Black Marble VNP46A4 product input files	8
Table 5 Scientific datasets included in the VNP46A1/VJ146A1 daily at-sensor TOA nighttime radiance product.	11
Table 6 Value of QF_Cloud_Mask in the VNP46A1/VJ146A1 product.	13
Table 7 Value of QF_DNB and QF of VIIRS band M10/11/12/13/15/16 in the VNP46A1/VJ146A1 product.	14
Table 8 Scientific datasets included in VNP46A2/VJ146A2 daily moonlight-adjusted NTL product.....	15
Table 9 Values of the Mandatory_Quality_Flag in VNP46A2/VJ146A2 product.....	16
Table 10 Values of the Snow_Flag in VNP46A2/VJ146A2 product.	17
Table 11 Scientific datasets included in VNP46A3/A4 (VJ146A3/A4) NTL composite products.....	15
Table 12 Values of the Quality Flag in VNP46A3/A4 (VJ146A3/A4) product.....	23
Table 13 Values of the DNB_Platform in VNP46A3/A4 (VJ146A3/A4) product.....	23
Table 14 Key performance metrics established for NASA's Black Marble product suite.	26

Acronyms

AERONET	Aerosol Robotic Network
AOD	Aerosol Optical Depth
BRDF	Bidirectional Reflectance Distribution Function
BRF	Bidirectional Reflectance Factor
DMSP	Defense Meteorological Satellite Program
DNB	Day/Night Band
EOS	Earth Observing System
GEO	Group on Earth Observations
GIS	Geographic Information System
HAM	Half-angle Mirror
HDF-EOS	Hierarchical Data Format - Earth Observing System
IR	Infrared
L1B	Level-1 B
L2G	Level-2 Gridded
LAI	Leaf Area Index
LANCE	The Land, Atmosphere Near real-time Capability for EOS
LZA	Lunar Zenith Angle
JPSS	Joint Polar Satellite System
NASA	National Aeronautics and Space Administration
NBAR	Nadir BRDF-Adjusted Reflectance
NCEP	National Centers for Environmental Prediction
NDVI	Normalized Difference Vegetation Index
NDSI	Normalized Difference Snow Index
NIR	Near-infrared
NRT	Near Real-Time
NTL	Nighttime Lights
nW	Nanowatt (One billionth (10^{-9}) of a watt)
Pgap	Gap Fraction Probability
PGE	Product Generation Executable
PRWGLP	Puerto Rico's Working Group on Light Pollution
QA	Quality Assurance
QF	Quality Flag
RTA	Rotating Telescope Assembly
SDS	Scientific Data Set
SIPS	Science Investigator-led Processing System
S-NPP	Suomi National Polar-orbiting Platform
TOA	Top of Atmosphere
UTC	Coordinated Universal Time
VCM	VIIRS Cloud Mask
VCST	VIIRS Calibration Support Team
VIIRS	Visible Infrared Imaging Radiometer Suite
VNP09	VIIRS Surface Reflectance product
VNP46	NASA's Black Marble nighttime lights product suite
VNP46A1	Suomi-NPP Daily at-sensor TOA nighttime lights product
VNP46A2	Suomi-NPP Daily moonlight-adjusted nighttime lights product
VNP46A3	Suomi-NPP Monthly moonlight-adjusted nighttime lights product
VNP46A4	Suomi-NPP Yearly moonlight-adjusted nighttime lights product
VJ146A1	NOAA-20/JPSS-1 Daily at-sensor TOA nighttime lights product

VJ146A2	NOAA-20/JPSS-1 Daily moonlight-adjusted nighttime lights product
VJ146A3	NOAA-20/JPSS-1 Monthly moonlight-adjusted nighttime lights product
VJ146A4	NOAA-20/JPSS-1 Yearly moonlight-adjusted nighttime lights product

1 Introduction

The Day/Night Band (DNB) sensor of the Visible Infrared Imaging Radiometer Suite (VIIRS), on-board the Suomi-National Polar-orbiting Partnership (S-NPP) and Joint Polar Satellite System (JPSS) satellite platforms, provides global daily measurements of nocturnal visible and near-infrared (NIR) light that are suitable for Earth system science and applications studies. The VIIRS DNB's ultra-sensitivity in lowlight conditions allows for the generation of new science-quality nighttime products as a result of significant improvements to sensor resolution and calibration compared to those provided previously by the Defense Meteorological Satellite Program's (DMSP) generation of nighttime lights imagery. These improvements allow us to better monitor both the magnitude and signature of nighttime phenomena and anthropogenic sources of light emissions.

Since the launch of the S-NPP satellite in 2011, multiple studies have used the VIIRS DNB as the primary data source in a wide range of study topics. They include: (1) feature extraction techniques to detect severe weather impacts to urban infrastructure (Cao et al., 2013; Cole et al., 2017; Mann et al., 2016; Molthan and Jedlovec, 2013; Román et al., 2019); (2) detection of sub-pixel scale features, e.g., fires (Polivka et al., 2016), shipping vessels (Asanuma et al., 2016; Elvidge et al., 2015; Straka et al., 2015), lightning flashes (Bankert et al., 2011), surface oil slicks (Hu et al., 2015), and gas flares (Elvidge et al., 2015; Liu et al., 2017; Chakraborty et al., 2023); (3) impacts on vegetation phenology (Meng et al., 2022; Kim et al., 2024); and (4) techniques for monitoring nighttime atmospheric optical properties, including clouds (Minnis et al., 2016; Walther et al., 2013), aerosols (Johnson et al., 2013; McHardy et al., 2015; Zhang et al., 2023), particulate matter (Wang et al., 2016), aurora detection (Kalb et al., 2023) and gravity waves in the upper atmosphere via nightglow (Miller et al., 2015).

As with early research that utilized the DMSP's Operational Line Scanner (OLS) (Huang et al., 2014), recent studies using the VIIRS DNB have employed statistical analyses and correlation discovery methods to confirm established empirical relationships with a wide range of human-linked patterns and processes. They include socioeconomic variables (Chen and Nordhaus, 2015; Chen et al., 2015; Levin and Zhang, 2017; Li et al., 2013; Ma et al., 2014; Shi et al., 2014; Yu et al., 2015), as well as changes driven by urban expansion (Guo et al., 2015; Sharma et al., 2016; Shi et al., 2014), energy use (Coscieme et al., 2014; Román and Stokes, 2015), and carbon emissions (Oda et al., 2017; Ou et al., 2015).

To realize the full potential of the VIIRS DNB time series record, NASA has developed a new suite of standard products that represent the current state-of-the-art in nighttime lights (NTL) applications, NASA's Black Marble product suite (VNP46/VJ146). NASA's Black Marble nighttime lights product, at 15 arc-second spatial resolution, is available from January 2012-present with data from the VIIRS DNB sensor. The VNP46/VJ146 product suite is being processed on a daily basis within 3-5 hours of

acquisition, which enables both near-real-time uses and long-term monitoring applications. The VNP46/VJ146 product suite includes the daily at-sensor top of atmosphere (TOA) nighttime lights (NTL) product (VNP46A1/VJ146A1), daily moonlight-adjusted nighttime lights product (VNP46A2/VJ146A2), monthly moonlight-adjusted nighttime lights product (VNP46A3/VJ146A3), and yearly moonlight-adjusted nighttime lights product (VNP46A4/VJ146A4). The retrieval algorithm, developed and implemented for routine global processing at NASA's Land Science Investigator-led Processing System (SIPS), utilizes all high-quality, cloud-free, atmospheric-, terrain-, snow-, lunar-, and stray light-corrected radiance to estimate daily nighttime lights and other intrinsic surface optical properties. The VIIRS Black Marble product has been used for global mapping of human activity patterns, such as tracking shipping and fishing vessels, gas flares, in addition to their application to humanitarian efforts, such as assessment of conflict-associated demographic changes and mapping impoverishment.

This user guide provides an overview of NASA's Collection 2 VIIRS Level 3 Black Marble nighttime lights product suite (VNP46/VJ146) to users. This document describes the theoretical basis for the algorithms, the operational processing, evaluation and validation of the product, and how to access the product. Additional details are available in related publications in section 10.

2 Algorithm

2.1 Overview of the Algorithm

NASA's operational Black Marble product suite ingests multiple-source input datasets and ancillary data to output the highest quality pixel-based estimates of NTL. These NTL estimates are accompanied by pixel-level quality flags. The principal features of the algorithm are summarized in the following sections. More details of the algorithm are available in related publications in section 10.

NASA's Black Marble algorithm produces cloud-free images that have been corrected for atmospheric, terrain, lunar BRDF, thermal, and straylight effects. The corrected nighttime radiance, resulting in a superior retrieval of nighttime lights at short time scales and a reduction in background noise, enables quantitative detection and analyses of daily, seasonal and annual variations. Key algorithm enhancements include: (1) lunar irradiance modeling to resolve non-linear changes in phase and libration; (2) vector radiative transfer and lunar bidirectional surface anisotropic reflectance modeling to correct for atmospheric and bidirectional reflectance distribution function (BRDF) effects; and (3) temporal gap-filling to reduce persistent data gaps.

2.2 Atmospheric Correction

NASA’s Black Marble retrieval strategy combines daytime VIIRS DNB surface reflectance, BRDF, surface albedo, nadir BRDF-adjusted reflectance (NBAR), and lunar irradiance values to minimize the biases caused by extraneous artifacts in the VIIRS NTL time series record.

Using this novel “turning off the Moon” approach, illustrated in Figure 1, the upward surface radiance from artificial light emissions, L_{NTL} [units of $\text{nWatts}\cdot\text{cm}^{-2}\cdot\text{sr}^{-1}$], can be extracted from at-sensor nighttime radiance at TOA, L_{DNB} , using the following equation:

$$L_{NTL} = \left[\left(\frac{L_{DNB} - L_{path}}{T_{\uparrow}(\tau\theta_v)} \right) (1 - a(\theta_m)\rho_a) - L_m T_{\downarrow}(\tau\theta_v) \right] / P_{\uparrow}(\theta_v) \quad (1)$$

where L_{path} is the nighttime path radiance (*i.e.*, the radiance generated by scattering within the atmosphere), and $a(\theta_m)$ is the VIIRS-derived actual (or blue-sky) surface albedo; incorporating the directional influence of sky radiance and multiple scattering effects between the ground and the atmosphere (Román et al., 2010). For the latter, a snow albedo retrieval scheme is used if the VIIRS current day snow status flag is activated (Klein and Stroeve, 2002; Liu et al., 2017, Liu et al., 2017; Moustafa et al., 2017; Wang et al., 2012). $P_{\uparrow}(\theta_v)$ is the probability of the upward transmission of NTL emissions through the urban vegetation canopy, defined in Equation 4. The atmospheric backscatter is given by ρ_a , and $T_{\downarrow}(\tau\theta_v)$ and $T_{\uparrow}(\tau\theta_v)$ are the total transmittance (including direct and diffuse radiation) along the lunar-ground and ground-sensor paths, respectively. The latter two are a function of view-illumination geometry and the total atmospheric column optical depth (τ) due to mixed gases, water vapor, and aerosol particles. The retrieval uses a modified algorithm based on the VIIRS Surface Reflectance product (VNP09) to estimate the values of L_{path} , ρ_a , $T_{\downarrow}(\tau\theta_v)$, and $T_{\uparrow}(\tau\theta_v)$ for a given set of surface and atmospheric conditions (Roger et al., 2016; Skakun et al., 2018). Additional input datasets include the standard VIIRS Cloud Mask (VCM) (Kopp et al., 2014), atmospheric profiles obtained from the National Centers for Environmental Prediction (NCEP) model (*i.e.*, water vapor, ozone, and surface pressure) (Moorthi et al., 2001), and the VIIRS aerosol model combined with daytime-to-daytime averaged aerosol optical depth (AOD) at $0.550\text{ }\mu\text{m}$ to extrapolate the nighttime AOD.

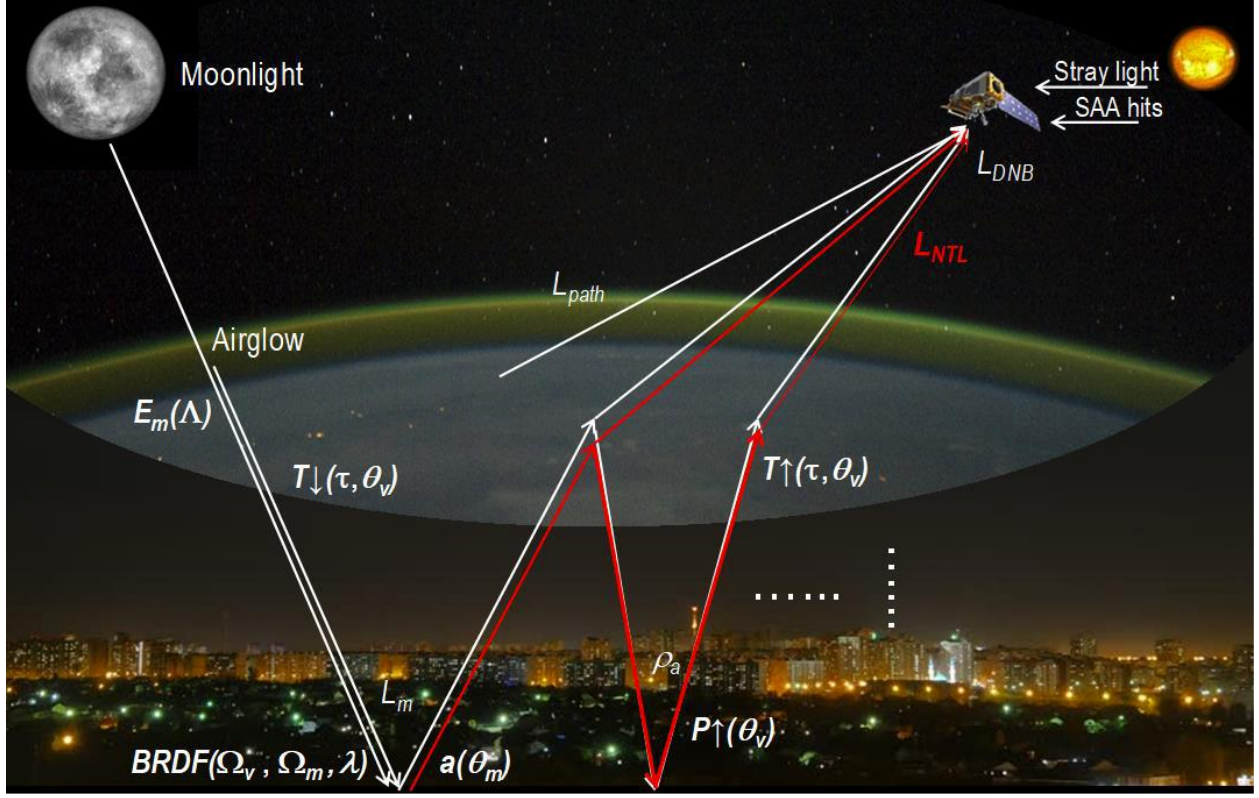


Figure 1 Overview of NASA's Black Marble retrieval strategy (*cf.* Equation 1). During the ~50% portion of the lunar cycle when moonlight is present at the time of satellite observation, the surface upward radiance from artificial light emissions, L_{NTL} [units of $\text{nWatts}\cdot\text{cm}^{-2}\cdot\text{sr}^{-1}$], can be extracted from at-sensor nighttime radiance at TOA (L_{DNB}). L_{path} is the nighttime path radiance, $a(\theta_m)$ is the VIIRS-derived actual surface albedo. The atmospheric backscatter is given by ρ_a . $T_{\downarrow}(\tau, \theta_v)$ and $T_{\uparrow}(\tau, \theta_v)$ are the total transmittances along the lunar-ground and ground-sensor paths (respectively). $P_{\uparrow}(\theta_v)$ is the probability of the upward transmission of NTL emissions through the urban vegetation canopy.

2.3 BRDF Correction

The Black Marble algorithm estimates the actual moonlight, aerosol, and surface albedo contribution through analytical BRDF model inversion. This model has proven effective in removing biases introduced by extraneous sources of nighttime light emissions.

The surface BRDF, or reflectance anisotropy is governed by the angle and intensity of illumination – whether that illumination is solar or lunar or from airglow – and by the structural complexity of the surface, resulting in variations in brightly illuminated regions and highly shadowed areas. The semi-empirical Ross Thick-Li Sparse Reciprocal (RTLSR, or Ross-Li) BRDF model (Román et al., 2010; Roujean et al., 1992; Schaaf et al., 2002, Schaaf et al., 2011; Strahler et al., 1999) is advantageous in this regard since (1) it is the most likely kernel-driven combination to capture the wide range of conditions affecting the VIIRS DNB on a global basis; (2) it allows robust analytical model inversion

with a pixel-specific estimate of the uncertainty in the model parameters and linear combinations thereof (Lucht and Roujean, 2000); and (3) the scheme is flexible enough to allow us to easily adapt other kernels should any become available, and demonstrate its superiority for a particular scenario.

For VIIRS DNB acquisitions over snow-free and snow-covered surfaces, we define the spectral radiance contribution from moonlight, L_m ,

$$L_m(\Omega_v, \Omega_m, \Lambda) = \frac{E_m(\Lambda)}{\pi} BRF(\Omega_v, \Omega_m, \Lambda) \cos(\theta_m) \quad (2)$$

in terms of the Ross-Li model:

$$BRDF(\Omega_v, \Omega_m, \Lambda) \approx \frac{BRF(\Omega_v, \Omega_m, \Lambda)}{\pi} = f_{iso}(\Lambda) + f_{vol}(\Lambda)K_{vol}(\Omega_v, \Omega_m) + f_{geo}(\Lambda)K_{geo}(\Omega_v, \Omega_m) \quad (3)$$

Here, we define the wavelength for the narrowband instrument of interest as the weighted center, Λ , of the VIIRS DNB spectral band [0.5–0.9 μm]. Parameter $f_{iso}(\Lambda)$ is the isotropic scattering component and equal to the bidirectional reflectance for a pixel viewing zenith angle $\theta_v = 0$ and a lunar zenith angle $\theta_m = 0$. Parameter $f_{geo}(\Lambda)$ is the coefficient of the LiSparse-reciprocal geometric scattering kernel K_{geo} , derived for a sparse ensemble of surface casting shadows on a Lambertian background (Li and Strahler, 1992). Parameter $f_{vol}(\Lambda)$ is the coefficient for the RossThick volume scattering kernel K_{vol} , so-called for its assumption of a dense leaf canopy (Ross, 2012).

To achieve a high-quality BRDF retrieval, NASA's Black Marble algorithm collects all available daytime, atmospherically corrected, VIIRS DNB bidirectional reflectance factor (BRF) over a multi-date period (normally 16-days) to establish the analytical solution for the Ross-Li BRDF model parameter values, $f_k(\Lambda)$. Note that during moon-free nights, when atmospheric airglow is the dominant emission source, the VNP46 algorithm sets the illumination geometry to near-nadir ($\theta_m = 10^\circ$) and the lunar irradiance to $E_m(\Lambda) = 0.26 \text{ nW} \cdot \text{m}^{-2}$ (Liao et al., 2013). This enables a BRDF correction even in the absence of moonlight.

2.3 Monthly and Yearly Nighttime Light Composite

Monthly and yearly NTL composites (Wang et al., 2022) are generated from daily atmospherically- and lunar-BRDF-corrected NTL radiance to remove the influence of extraneous artifacts and biases. NTL outliers are excluded according to Boxplot metrics (Tukey 1977). The observations that fall out of the range of $Q1 - 1.5 * IQR$ and $Q3 + 1.5 * IQR$ are identified as outliers and excluded from the NTL composite. Interquartile range (IQR) score is the range between 25th (Q1) and the 75th (Q3) percentile. Unlike Z-score (Kreyszig 1979), the IQR score method does not require normal distribution of the observations. The monthly and yearly NTL composite are then calculated from the mean values of the remaining

observations. To remove any residual background noise, the NTL composite values with radiances less than $0.5 \text{ nW}\cdot\text{cm}^{-2}\cdot\text{sr}^{-1}$ are set to zero. Aurora-contaminated pixels are filled with gap-filled values.

Users should be aware that artificial lights derived from VIIRS DNB data show a strong angular effect (Li et al., 2019; Wang et al., 2021), impacting retrievals, particularly across dense urban centers where NTL radiance at nadir can be significantly higher than off-nadir observations. The presence of nighttime snow also enhances the scattering of reflected NTL due to the increased surface reflectance. Accordingly, NASA's Black Marble monthly and yearly NTL composites are generated for multiple view-angle categories (i.e., near-nadir, off-nadir, and all angles) and snow status (snow-covered and snow-free) along with ancillary metrics of standard deviation, the number of observations, and mandatory QA flags. Users are encouraged to carefully use these NTL composite values (either separately or jointly) to meet their specific science research and application needs.

3 Data Product Formats

NASA's Black Marble product suite includes the daily at-sensor TOA nighttime radiance (VNP46A1/VJ146A1), the daily moonlight and atmosphere-corrected NTL (VNP46A2/VJ146A2), monthly moonlight and atmosphere-corrected NTL (VNP46A3/VJ146A3), and yearly moonlight and atmosphere-corrected NTL (VNP46A4/VJ146A4) products at a 15 arc-second geographic linear latitude/longitude (lat/lon) grid. The data are provided in the standard land Hierarchical Data Format - Earth Observing System (HDF-EOS) format.

3.1 Metadata

Metadata (data attributes) provide information about data acquisition, input products, geographic location, the output of the data product, satellite instrument, processing environment, and other aspects of the retrieval. More details of the VNP46A1/VJ146A1, VNP46A2/VJ146A2, VNP46A3/VJ146A3, and VNP46A4/VJ146A4 product metadata are listed in Appendix A, B, C, and D.

3.2 Filenames

The filenames follow a naming convention, which gives useful information regarding the specific product. For example, the filename VNP46A1.A2018001.h08v05.002.2023184124809.h5 indicates:

- (1) VNP46A1: Product Short Name;
- (2) A2018001: Julian Date of Acquisition (A-YYYYDDD);
- (3) h08v05: Tile Identifier (horizontalXXverticalYY);
- (4) .002: Collection Version;

(5) .2023184124809: Julian Date of Production (YYYYDDDHHMMSS);

(6) .h5: Data Format (HDF5).

3.3 Projection

NASA's Black Marble product suite employs the standard VIIRS science algorithms and software that produce the DNB standard (radiance-based) products, and their corresponding ancillary layers in gridded (Level 2G, Level 3) geographic linear lat/lon format (Figure 2). The gridding algorithms were modified to work with the VIIRS DNB's unique viewing geometry, which, unlike the VIIRS moderate and imagery bands, has a ground pixel footprint at a nearly constant size (742 m). The rationale behind the VIIRS DNB gridding approach is to select the nighttime observations from available 6-min swath granules (2366 km along track, ~3100 km across-track), that are of high quality as indicated by the quality flags and are the least affected by cloud cover and off-nadir viewing observations. The goal is to increase signal-to-noise, while maximizing coverage within a cell of the gridded projection (Tan et al., 2006; Wolfe et al., 2002). By implementing this combined gridding strategy and geographic linear lat/lon projection formats, we seek to improve the efficiency of processing and reprocessing the Black Marble product suite, preserve the satellite location and observation footprints, while also enabling the ingest of the products into accessible software for geographic information system (GIS)-friendly analysis and mapping.

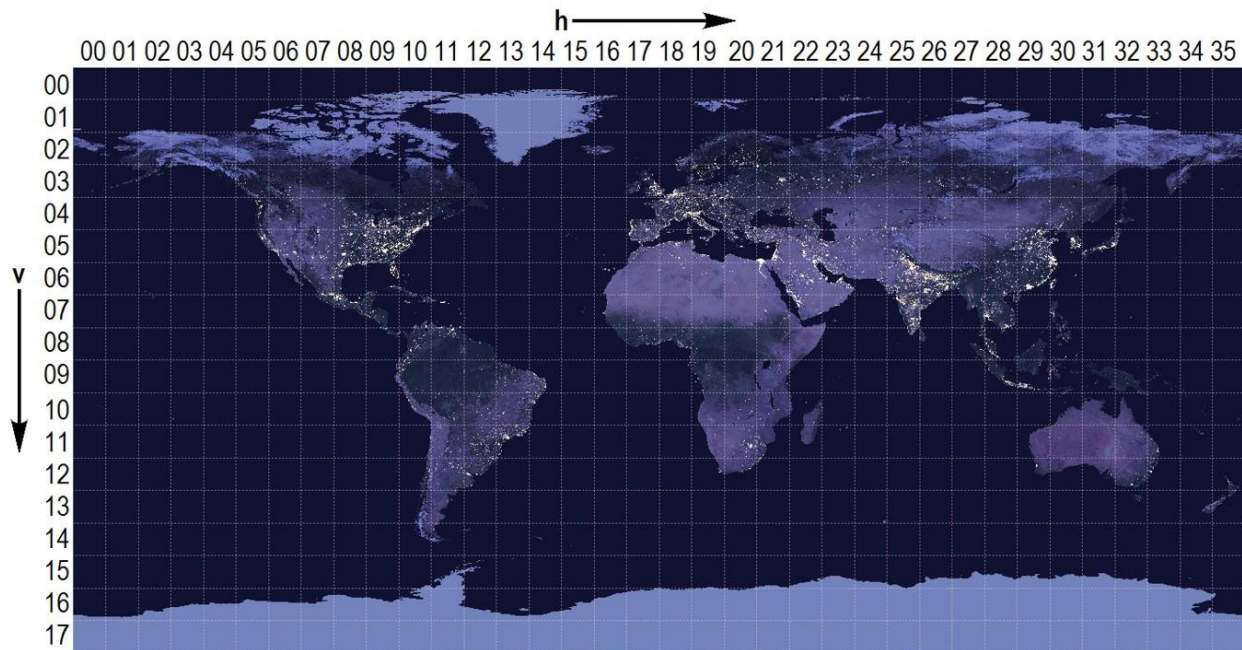


Figure 2 The Suomi-NPP VIIRS linear latitude/longitude (or geographic) grid consists of 460 non-overlapping Land tiles, which measure approximately $10^\circ \times 10^\circ$ region.

4. Product generation

Data product inputs to NASA's Black Marble algorithm are listed in Table 1 and Table 2. The algorithm processing flow is depicted in Figure 3. The algorithm processing cycle is divided into daytime and nighttime branches, and each processing branch produces a unique set of ancillary and quality assurance (QA) flags.

Table 1 Black Marble VNP46A1 product input files

Input File	Description
VNP02DNB	VIIRS/NPP Day/Night Band 6-Min L1B Swath 750m (L1B DNB)
VNP02MOD	VIIRS/NPP Moderate Resolution 6-Min L1B Swath 750m (L1B moderate bands)
NPP_DNBN*	VIIRS L2G DNB radiance
NPP DNBN angles*	VIIRS L2G DNB angles
VNP03MOD	VIIRS moderate bands geolocation
NPP PTDN*	VIIRS DNB pointer files
VNP03DNB	VIIRS DNB geolocation
VNP35	VIIRS cloud mask

* Intermediate Products.

Table 2 Black Marble VNP46A2 product input files

Input file	Description
VNP46A1	VIIRS/NPP TOA Daily Gridded Day Night Band Linear Lat Lon Grid Night
VNP43LGDNBA1	VIIRS/NPP DNB BRDF/Albedo Model Parameters Daily L3 Global LLL Grid
VNPLG09GA	VIIRS/NPP Surface Reflectance Daily L2G Global Linear Lat Lon Grid
VNP04LGA	VIIRS/NPP Aerosols Optical Thickness Daily L2G Global Linear Lat Lon Grid

Table 3 Black Marble VNP46A3 product input files

Input file	Description
VNP46A1	VIIRS/NPP TOA Daily Gridded Day Night Band Linear Lat Lon Grid Night
VNP46A2	VIIRS/NPP Moonlight and Atmosphere corrected Daily Gridded Day Night Band Linear Lat Lon Grid Night

Table 4 Black Marble VNP46A4 product input files

Input file	Description
VNP46A1	VIIRS/NPP TOA Daily Gridded Day Night Band Linear Lat Lon Grid Night
VNP46A2	VIIRS/NPP Moonlight and Atmosphere corrected Daily Gridded Day Night Band Linear Lat Lon Grid Night

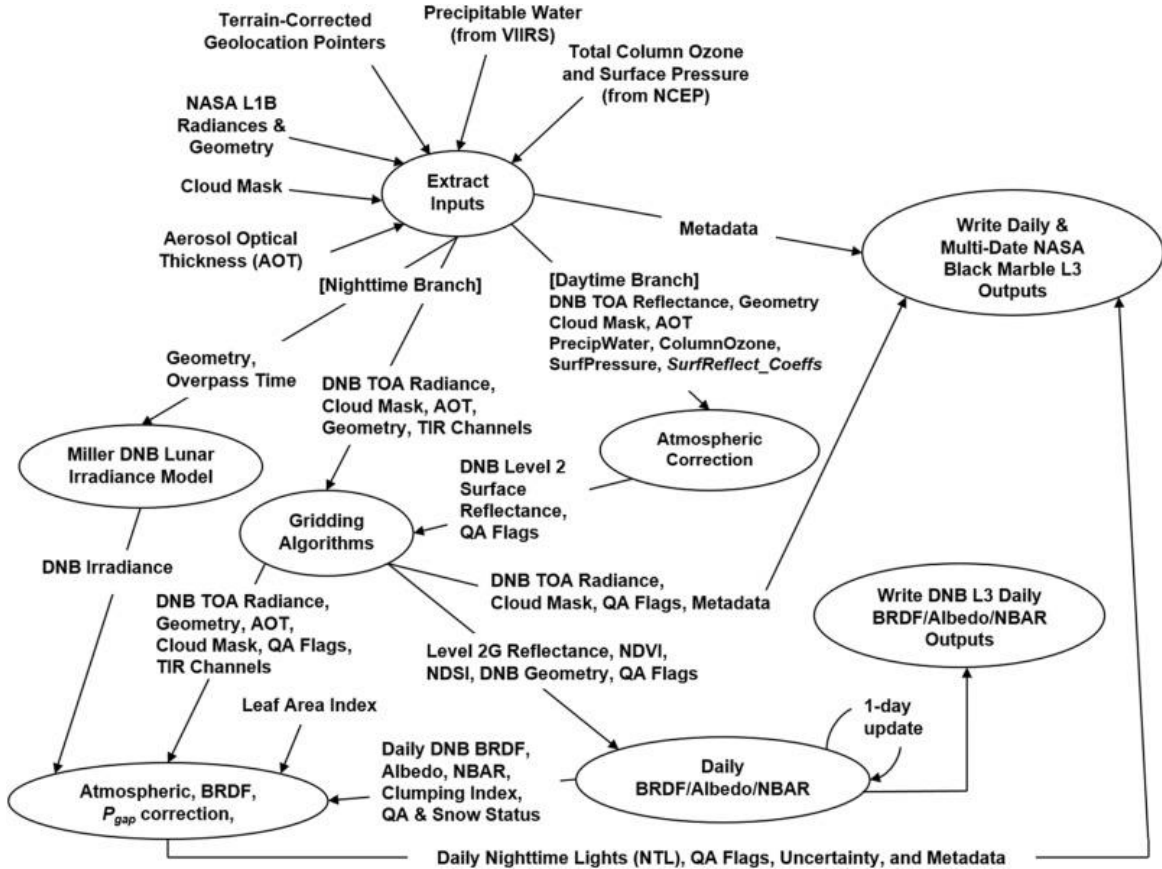


Figure 3 Algorithm processing cycle and ancillary parameters used by NASA's Black Marble product suite.

For the daytime branch, science product generation executables (PGEs) based on the standard suite of VIIRS land products are integrated as part of NASA's Black Marble processing chain. First, a modified version of the operational VIIRS surface reflectance algorithm (Roger et al., 2016; Vermote et al., 2014) is used to generate the DNB surface bidirectional reflectance factor (BRF) using NASA's Level 1B calibrated radiance product as input (i.e., 6-minute granules, or 2366 km along track and ~3100 km across-track). Level 2G DNB surface reflectance is then generated by performing spatial and temporal aggregation to 15 arc-second grid cells over daily time periods (Campagnolo et al., 2016; Pahlevan et al., 2017; Wolfe et al., 1998; Yang and Wolfe, 2001). Daily Level 3 DNB BRDF/Albedo data are then retrieved using the heritage MODIS/VIIRS algorithm (MCD43/VNP43) (Liu et al., 2017, Liu et al., 2017; Wang et al., 2018), and corresponding snow flags are estimated using the VIIRS Normalized Difference Snow Index (NDSI) algorithm (VNP10) (Riggs et al., 2016, Riggs et al., 2017). The NDVI and NDSI values are used to determine the growing, dormant, and snow periods to routinely update the *a priori* global database of the DNB BRDF product (Cescatti et al., 2012; Liu et al., 2017, Liu et al., 2017; Román

et al., 2009). Vegetation correction is not applied in Black Marble Collection 1 and Collection 2 product as requested by the end users.

The nighttime branch describes the path followed to generate the final VNP46/VJ146 products. We begin with the at-sensor TOA nighttime radiance (VNP46A1/VJ146A1), along with the corresponding nighttime cloud mask, multiple solar/viewing/lunar geometry values (including moon-illuminated fraction and phase angles), and the daily snow and aerosol status flags. These science data sets (SDS) enable open access to the primary inputs used to generate NASA's Black Marble NTL time-series record, thus ensuring reproducibility of the final outputs. A series of temporal and spatial gap-filling techniques are also employed to improve the coverage of the VNP46/VJ146 NTL product.

5 Scientific Data Sets (SDSs) from Black Marble Product Suite

5.1 The VNP46A1/VJ146A1 Daily At-sensor TOA Nighttime Lights Product

The daily at-sensor TOA nighttime lights product is available at 15 arc-second spatial resolution from January 2012 onward for SNPP and January 2018 for NOAA-20/JPSS-1. VNP46A1/VJ146A1 product contains 26 SDS layers (Table) including sensor radiance, zenith and azimuth angles at-sensor, solar, and lunar, cloud mask flag, time, shortwave IR radiance, brightness temperatures, VIIRS quality flags, moon phase angle, and moon illumination fraction. Contents of VNP46A1/VJ146A1 product are given in List 1. Table presents detailed information on the layers. Table and Table present the details of the flag description keys and quality flags (QF) of the VNP46A1/VJ146A1 product.

List 1 Datasets in a sample of VNP46A1/VJ146A1 product.



Table 5 Scientific datasets included in the VNP46A1/VJ146A1 daily at-sensor TOA nighttime radiance product.

Scientific Datasets (SDS HDF Layers)	Units	Description	Bit Types	Fill Value	Valid Range	Scale Factor	Offset
DNB_At_Sensor_Radiance ¹	nW·cm ⁻² ·sr ⁻¹	At-sensor DNB radiance	32-bit floating point	-999.9	>=0	1.0	0.0
Sensor_Zenith	Degrees	Sensor zenith angle	16-bit signed integer	-32768	0 - 9000	0.01	0.0

Sensor_Azimuth	Degrees	Sensor azimuth angle	16-bit signed integer	-32768	-18000 – 18000	0.01	0.0
Solar_Zenith	Degrees	Solar zenith angle	16-bit signed integer	-32768	0 – 18000	0.01	0.0
Solar_azimuth	Degrees	Solar azimuth angle	16-bit signed integer	-32768	-18000 – 18000	0.01	0.0
Lunar_Zenith	Degrees	Lunar zenith angle	16-bit signed integer	-32768	0 – 18000	0.01	0.0
Lunar_Azimuth	Degrees	Lunar azimuth angle	16-bit signed integer	-32768	-18000 – 18000	0.01	0.0
Glint_Angle	Degrees	Moon glint angle	16-bit signed integer	-32768	-18000 – 18000	0.01	0.0
UTC_Time	Decimal hours	UTC time	32-bit floating point	-999.9	0 24	1.0	0.0
QF_Cloud_Mask ²	flag, no units	Cloud mask status	16-bit unsigned integer	65535	0 - 65534	N/A	N/A
QF_DNB ³	flag, no units	DNB quality flag	16-bit unsigned integer	65535	0 - 65534	N/A	N/A
Radiance_M10	$\text{W}\cdot\text{m}^{-2}\cdot\mu\text{m}^{-1}\cdot\text{sr}^{-1}$	Radiance in band M10	16-bit unsigned integer	65535	0 - 65534	0.0013	-0.04
Radiance_M11	$\text{W}\cdot\text{m}^{-2}\cdot\mu\text{m}^{-1}\cdot\text{sr}^{-1}$	Radiance in band M11	16-bit unsigned integer	65535	0 - 65534	0.0005	-0.02
BrightnessTemperature_M12	Kelvins	Brightness temperature of band M12	16-bit unsigned integer	65535	0 - 65534	0.0025	203.0
BrightnessTemperature_M13	Kelvins	Brightness temperature of band M13	16-bit unsigned integer	65535	0 - 65534	0.0025	203.0
BrightnessTemperature_M15	Kelvins	Brightness temperature of band M15	16-bit unsigned integer	65535	0 - 65534	0.0041	111.0
BrightnessTemperature_M16	Kelvins	Brightness temperature of band M16	16-bit unsigned integer	65535	0 - 65534	0.0043	103.0
QF_VIIRS_M10 ⁴	flag, no units	Quality flag of band M10	16-bit unsigned integer	65535	0 - 65534	N/A	N/A

QF_VIIRS_M11 ⁴	flag, no units	Quality flag of band M11	16-bit unsigned integer	65535	0 - 65534	N/A	N/A
QF_VIIRS_M12 ⁴	flag, no units	Quality flag of band M12	16-bit unsigned integer	65535	0 - 65534	N/A	N/A
QF_VIIRS_M13 ⁴	flag, no units	Quality flag of band M13	16-bit unsigned integer	65535	0 - 65534	N/A	N/A
QF_VIIRS_M15 ⁴	flag, no units	Quality flag of band M15	16-bit unsigned integer	65535	0 - 65534	N/A	N/A
QF_VIIRS_M16 ⁴	flag, no units	Quality flag of band M16	16-bit unsigned integer	65535	0 - 65534	N/A	N/A
Moon_Phase_Angle	Degrees	Moon phase angle	16-bit signed integer	-32768	0 – 18000	0.01	0.0
Moon_Illumination_Fraction	Percentage	Moon illumination fraction	16-bit signed integer	-32768	0 – 10000	0.01	0.0
Granule	Unitless	Number of selected Granule	8-bit unsigned integer	255	0 - 254	1.0	0.0
lat	Degrees_north	Latitude	64-bit floating point	-999.9	-90 - 90	NA	NA
lon	Degrees_east	Longitude	64-bit floating point	-999.9	-180 - 180	NA	NA

¹ Note that the need to use fill-values can arise from various scenarios such as bad quality data or if the solar zenith angle < 102 degrees since that is the nighttime cut-off used in the code. ² Details of QF_Cloud_Mask are shown in Table 6. ³ The scale and offset are for nighttime. Users should check the quality flags and metadata for specific values. ⁴ Details of QF_DNB and QF for VIIRS band M10/11/12/13/15/16 are shown in Table 7.

Table 6 Value of QF_Cloud_Mask in the VNP46A1/VJ146A1 product.

Bit	Flag description key	Interpretation
0	Day/Night	0 = Night 1 = Day
1-3	Land/Water Background	000 = Land & Desert 001 = Land no Desert

		010 = Inland Water 011 = Sea Water 101 = Coastal
4-5	Cloud Mask Quality	00 = Poor 01 = Low 10 = Medium 11 = High
6-7	Cloud Confidence	00 = Confident Clear 01 = Probably Clear 10 = Probably Cloudy 11 = Confident Cloudy
8	Shadow Detected	1 = Yes 0 = No
9	Cirrus Detection (IR) (BTM15 – BTM16)	1 = Cloud 0 = No Cloud
10	Snow/ Ice Surface	1 = Snow/Ice 0 = No Snow/Ice
11	VI used	1 = Yes 0 = No
12	Aurora Detected	1 = Yes 0 = No
13	Lunar Eclipse Detected	1 = Yes 0 = No

Table 7 Value of QF_DNB and QF of VIIRS band M10/11/12/13/15/16 in the VNP46A1/VJ146A1 product.

SDS Layer	Flag Mask Values and Descriptions
QF_DNB	1 = Substitute_Cal 2 = Out_of_Range 4 = Saturation 8 = Temp_not_Nominal 16 = Stray_light 256 = Bowtie_Deleted/Range_bit 512 = Missing_EV 1024 = Cal_Fail 2048 = Dead_Detector
QF_VIIRS_M10	1 = Substitute_Cal
QF_VIIRS_M11	2 = Out_of_Range
QF_VIIRS_M12	4 = Saturation
QF_VIIRS_M13	8 = Temp_not_Nominal
QF_VIIRS_M15	256 = Bowtie_Deleted

QF_VIIRS_M16	512 = Missing_EV 1024 = Cal_Fail 2048 = Dead_Detector
--------------	---

5.2 The VNP46A2/VJ146A2 Daily Moonlight-adjusted Nighttime Lights (NTL) Product

The daily moonlight and atmosphere-corrected NTL is available at 15 arc-second resolution from January 2012-present. The VNP46A2/VJ146A2 product has 7 layers containing information on BRDF-corrected NTL, Gap-filled BRDF-corrected NTL, lunar irradiance, mandatory quality flag, latest high-quality retrieval (number of days), snow flag, and cloud mask flag. Contents of VNP46A2/VJ146A2 product are given in List 2. The detailed VNP46A2/VJ146A2 layer properties are described in Table . Table and Table present the details of quality flags (QF) for the VNP46A2/VJ146A2 product.

List 2 Datasets in a sample of VNP46A2/VJ146A2 product

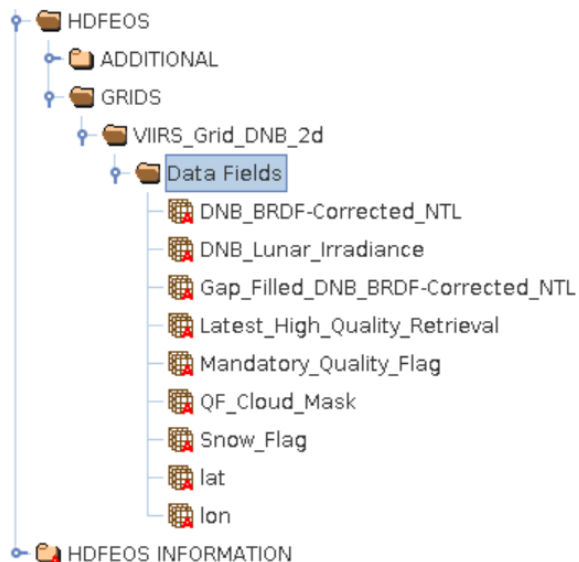


Table 8 Scientific datasets included in VNP46A2/VJ146A2 daily moonlight-adjusted NTL product.

Scientific Data Sets (SDS HDF Layers)	Units	Description	Bit Types	Fill Value	Valid Range	Scale Factor	Offset
DNB_BRDF-Corrected_NTL	nWatts·cm ⁻² ·sr ⁻¹	BRDF corrected DNB Radiance	32-bit floating point	-999.9	>=0	1.0	0.0

Gap_Filled_DNB_BRDF-Corrected_NTL	nWatts·cm ⁻² ·sr ⁻¹	Gap Filled BRDF corrected DNB Radiance	32-bit floating point	-999.9	>=0	1.0	0.0
DNB_Lunar_Irradiance	nWatts·cm ⁻²	DNB Lunar Irradiance	16-bit unsigned integer	65,535	0 – 65,534	0.1	0.0
Mandatory_Quality_Flag ¹	Flag, no units	Mandatory quality flag	8-bit unsigned integer	255	0 – 5	N/A	N/A
Latest_High_Quality_Retrieval	Number of days	Latest high quality BRDF corrected DNB radiance retrieval	8-bit unsigned integer	255	0 – 254	1.0	0.0
Snow_Flag ²	Flag, no units	Flag for snow cover	8-bit unsigned integer	255	0 – 1	N/A	N/A
QF_Cloud_Mask ³	Flag, no units	Quality flag for cloud mask	16-bit unsigned integer	65,535	0 – 65,534	N/A	N/A
lat	Degrees_north	Latitude	64-bit floating point	-999.9	-90 - 90	N/A	N/A
lon	Degrees_east	Longitude	64-bit floating point	-999.9	-180 - 180	N/A	N/A

¹ Details of Mandatory_Quality_Flag are shown in Table 9. ² Details of Snow_Flag are shown in Table 10. ³ Details of QF_Cloud_Mask are shown in Table 6.

Table 9 Values of the Mandatory_Quality_Flag in VNP46A2/VJ146A2 product.

Value	Retrieval quality	Algorithm instance
00	High-quality	Main algorithm
01	Poor-quality	Main Algorithm (Outlier, Potential cloud contamination or other issues)
02	Poor-quality	Main Algorithm (high solar zenith angle 102-108 degrees)
03	Poor-quality	Main Algorithm (Lunar eclipse)
04	Poor-quality	Main Algorithm (Aurora)

05	Poor-quality	Main Algorithm (Glint)
255	No retrieval	Fill value

Table 10 Values of the Snow_Flag in VNP46A2/VJ146A2 product.

Flag description key	Value	Interpretation
Snow/ Ice Surface	00	No Snow/Ice
	01	Snow/Ice
	255	Fill value

5.3 The VNP46A3/VJ146A3 Monthly and VNP46A4/VJ146A4 Yearly Moonlight-adjusted Nighttime Lights (NTL) Product

The monthly and yearly moonlight and atmosphere-corrected NTL composite are available at 15 arc-second resolution from January 2012-present. The composite product has 28 layers containing information on NTL composite, the number of observations, quality, and standard deviation for multi-view zenith angle categories (near-nadir, off-nadir, and all angles) and snow status (snow-covered and snow-free) as well as land water mask, platform, latitude, and longitude. Contents of VNP46A3/A4 (VJ146A3/A4) product are given in List 2. The detailed VNP46A3/A4 (VJ146A3/A4) layer properties are described in Table . Table present the detailed description of quality flags (QF) for the VNP46A3/A4 (VJ146A3/A4) products.

List 3 Datasets in a sample of VNP46A3/A4 (VJ146A3/A4) product



Table 11 Scientific datasets included in VNP46A3/A4 (VJ146A3/A4) NTL composite products.

Scientific Data Sets (SDS HDF Layers)	Units	Description	Bit Types	Fill Value	Valid Range	Scale Factor	Off set
AllAngle_Composite_Snow_Covered	$n\text{Watts}\cdot\text{cm}^{-2}\cdot\text{sr}^{-1}$	Temporal Radiance Composite Using All Observations During Snow-covered Period	32-bit floating point	-999.9	≥ 0	1.0	0.0
AllAngle_Composite_Snow_Covered_Num	Number of observations	Number of Observations of Temporal Radiance Composite Using All Observations During Snow-covered Period	16-bit unsigned integer	65,535	0 – 65,534	1.0	0.0

AllAngle_Composite_Snow_Covered_Quality ¹	flag, no units	Quality Flag of Temporal Radiance Composite Using All Observations During Snow-covered Period	8-bit unsigned integer	255	0 – 254	1.0	0.0
AllAngle_Composite_Snow_Covered_Std	nWatts·cm ⁻² ·sr ⁻¹	Standard Deviation of Temporal Radiance Composite Using All Observations During Snow-covered Period	32-bit floating point	-999.9	>=0	1.0	0.0
AllAngle_Composite_Snow_Free	nWatts·cm ⁻² ·sr ⁻¹	Temporal Radiance Composite Using All Observations During Snow-free Period	32-bit floating point	-999.9	>=0	1.0	0.0
AllAngle_Composite_Snow_Free_Num	Number of observations	Number of Observations of Temporal Radiance Composite Using All Observations During Snow-free Period	16-bit unsigned integer	65,535	0 – 65,534	1.0	0.0
AllAngle_Composite_Snow_Free_Quality ¹	flag, no units	Quality Flag of Temporal Radiance Composite Using All Observations During Snow-free Period	8-bit unsigned integer	255	0 – 254	1.0	0.0
AllAngle_Composite_Snow_Free_Std	nWatts·cm ⁻² ·sr ⁻¹	Standard Deviation of Temporal Radiance Composite Using All Observations During Snow-free Period	32-bit floating point	-999.9	>=0	1.0	0.0
NearNadir_Composite_Snow_Covered	nWatts·cm ⁻² ·sr ⁻¹	Temporal Radiance Composite Using Near Nadir Angle Observations (View Zenith Angle 0-20 degree) During Snow-covered Period	32-bit floating point	-999.9	>=0	1.0	0.0
NearNadir_Composite_Snow_Covered_Num	Number of observations	Number of Observations of Temporal Radiance Composite Using Near Nadir Angle Observations (View	16-bit unsigned integer	65,535	0 – 65,534	1.0	0.0

		Zenith Angle 0-20 degree) During Snow- covered Period					
NearNadir _Composite_Snow_Covered _Quality ¹	flag, no units	Quality Flag of Temporal Radiance Composite Using Near Nadir Angle Observations (View Zenith Angle 0-20 degree) During Snow- covered Period	8-bit unsigned integer	255	0 – 254	1.0	0.0
NearNadir _Composite_Snow_Covered _Std	$n\text{Watts}\cdot\text{cm}^{-2}\cdot\text{sr}^{-1}$	Standard Deviation of Temporal Radiance Composite Using Near Nadir Angle Observations (View Zenith Angle 0-20 degree) During Snow- covered Period	32-bit floating point	-999.9	≥ 0	1.0	0.0
NearNadir _Composite_Snow_Free	$n\text{Watts}\cdot\text{cm}^{-2}\cdot\text{sr}^{-1}$	Temporal Radiance Composite Using Near Nadir Angle Observations (View Zenith Angle 0-20 degree) During Snow- free Period	32-bit floating point	-999.9	≥ 0	1.0	0.0
NearNadir _Composite_Snow_Free_Nu m	Number of observations	Number of Observations of Temporal Radiance Composite Using Near Nadir Angle Observations (View Zenith Angle 0-20 degree) During Snow- free Period	16-bit unsigned integer	65,535	0 – 65,534	1.0	0.0
NearNadir _Composite_Snow_Free_Qu ality ¹	flag, no units	Quality Flag of Temporal Radiance Composite Using Near Nadir Angle Observations (View Zenith Angle 0-20 degree) During Snow- free Period	8-bit unsigned integer	255	0 – 254	1.0	0.0

NearNadir _Composite_Snow_Free_Std	$\text{nWatts}\cdot\text{cm}^{-2}\cdot\text{sr}^{-1}$	Standard Deviation of Temporal Radiance Composite Using Near Nadir Angle Observations (View Zenith Angle 0-20 degree) During Snow-free Period	32-bit floating point	-999.9	≥ 0	1.0	0.0
OffNadir_Composite_Snow_Covered	$\text{nWatts}\cdot\text{cm}^{-2}\cdot\text{sr}^{-1}$	Temporal Radiance Composite Using Off Nadir Angle Observations (View Zenith Angle 40-60 degree) During Snow-covered Period	32-bit floating point	-999.9	≥ 0	1.0	0.0
OffNadir _Composite_Snow_Covered _Num	Number of observations	Number of Observations of Temporal Radiance Composite Using Off Nadir Angle Observations (View Zenith Angle 40-60 degree) During Snow-covered Period	16-bit unsigned integer	65,535 0 – 65,534	1.0	0.0	
OffNadir _Composite_Snow_Covered _Quality ¹	flag, no units	Quality Flag of Temporal Radiance Composite Using Off Nadir Angle Observations (View Zenith Angle 40-60 degree) During Snow-covered Period	8-bit unsigned integer	255 0 – 254	1.0	0.0	
OffNadir _Composite_Snow_Covered _Std	$\text{nWatts}\cdot\text{cm}^{-2}\cdot\text{sr}^{-1}$	Standard Deviation of Temporal Radiance Composite Using Off Nadir Angle Observations (View Zenith Angle 40-60 degree) During Snow-covered Period	32-bit floating point	-999.9	≥ 0	1.0	0.0

OffNadir _Composite_Snow_Free	$\text{nWatts} \cdot \text{cm}^{-2} \cdot \text{sr}^{-1}$	Temporal Radiance Composite Using Off Nadir Angle Observations (View Zenith Angle 40-60 degree) During Snow-free Period	32-bit floating point	-999.9	≥ 0	1.0	0.0
OffNadir _Composite_Snow_Free_Nu m	Number of observations	Number of Observations of Temporal Radiance Composite Using Off Nadir Angle Observations (View Zenith Angle 40-60 degree) During Snow-free Period	16-bit unsigned integer	65,535	0 – 65,534	1.0	0.0
OffNadir _Composite_Snow_Free_Qu ality ¹	flag, no units	Quality Flag of Temporal Radiance Composite Using Off Nadir Angle Observations (View Zenith Angle 40-60 degree) During Snow-free Period	8-bit unsigned integer	255	0 – 254	1.0	0.0
OffNadir _Composite_Snow_Free_Std	$\text{nWatts} \cdot \text{cm}^{-2} \cdot \text{sr}^{-1}$	Standard Deviation of Temporal Radiance Composite Using Off Nadir Angle Observations (View Zenith Angle 40-60 degree) During Snow-free Period	32-bit floating point	-999.9	≥ 0	1.0	0.0
DNB_Platform ²	platform, no units	Platform	8-bit unsigned integer	255	0 – 254	1.0	0.0
Land_Water_Mask ³	land water mask, no units	Land Water Mask	8-bit unsigned integer	255	0 – 254	1.0	0.0
Lat	Degrees_north	Latitude	64-bit floating-point	-999.9	-90 - 90	N/A	N/A

Lon	Degree_east	Longitude	64-bit floating-point	-999.9	-180 - 180	N/A	N/A
-----	-------------	-----------	-----------------------	--------	------------	-----	-----

¹ Details of Quality_Flag are shown in Table 12. ² Details of DNB_Platform are shown in Table 13. ³ Details of Land_Water_Mask are shown in Table 6 bit 1-3 Land/Water Background.

Table 12 Values of the Quality Flag in VNP46A3/A4 (VJ146A3/A4) product.

Value	Retrieval quality	Algorithm instance
00	Good-quality	The number of observations used for the composite is larger than 3
01	Poor-quality	The number of observations used for the composite is less than or equal to 3
02	Gap filled	Gap filled NTL based on historical data
255	Fill value	Fill value

Table 13 Values of the DNB_Platform in VNP46A3/A4 (VJ146A3/A4) product.

Value	Sensors
00	Suomi-NPP
01	NOAA-20
02	NOAA-21
03	NOAA-20 and NOAA-21 combined
255	Fill value

5.4 Examples of the Black Marble Product Suite

The Black Marble product suite is available both retrospectively, via NASA’s Level 1 and Atmosphere Archive and Distribution System Distributed Active Archive Center (LAADS-DAAC), and in forward near-real-time (NRT) data streams, via NASA’s Land, Atmosphere Near-Real-time Capability for EOS (LANCE) with a latency of about three hours. The NRT data are mainly used in response to disasters and other management applications, which require low latency data access.

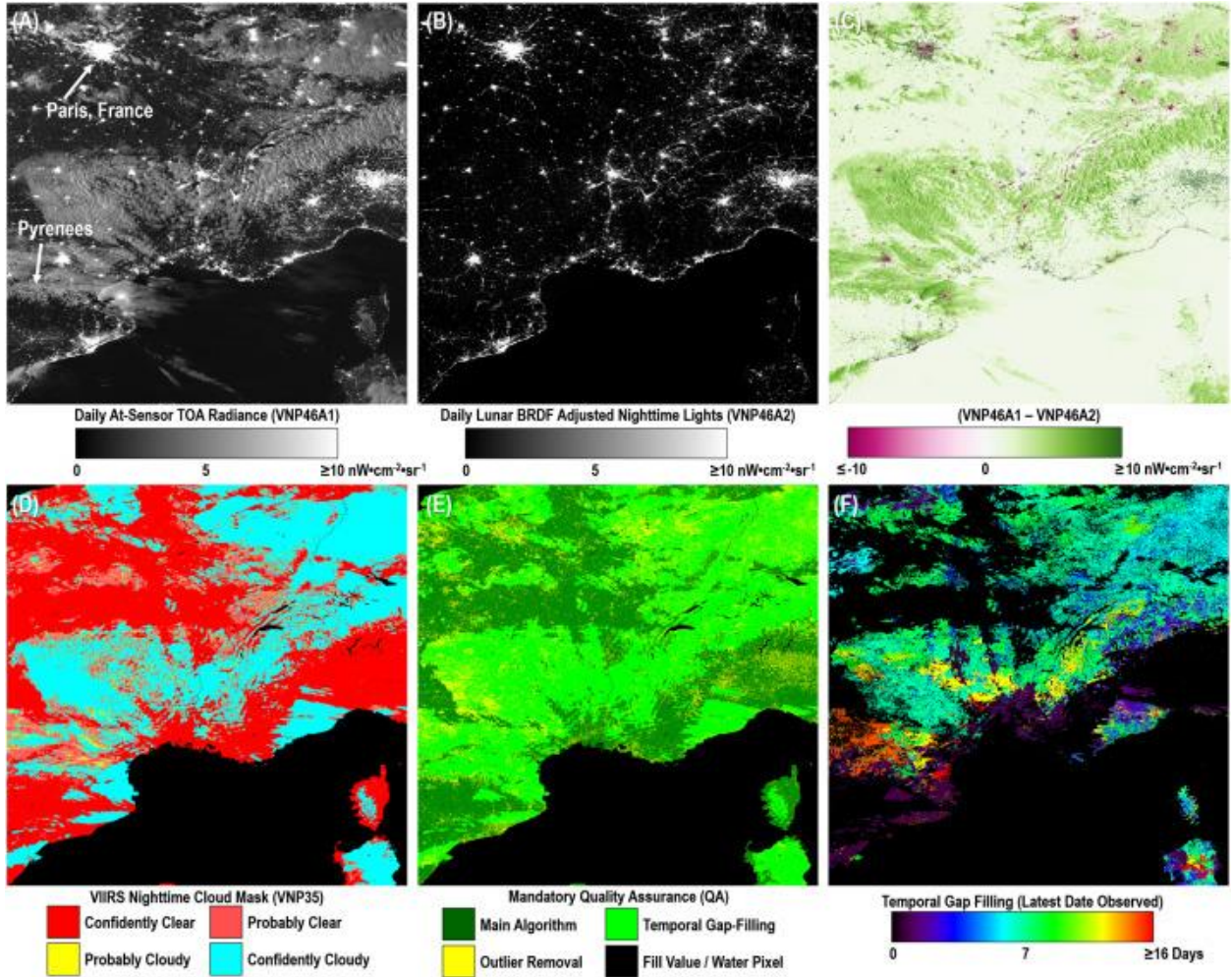


Figure 4 Black Marble product suite components for a $10^\circ \times 10^\circ$ Level 3 tile over France and the Balearic Sea region (h18v04; DOY 2015-091). The full-moon-illuminated and 51% cloud-contaminated scene illustrates the challenges of nighttime cloud masking over snow-covered surfaces (e.g., the French Alps and the Pyrenees).

Figure 4 and Figure 5 illustrate the key processing steps used to retrieve high-quality NTL as part of NASA's Black Marble product suite. Cloud-free, atmospheric-, and moonlight BRDF-corrected DNB nighttime radiance is produced using the nighttime DNB-at-sensor radiance (VNP46A1), nighttime cloud mask, aerosol optical depth values, snow status flag, Ross-Li DNB BRDF model parameters and albedo values, and per-pixel estimates of DNB lunar irradiance and corresponding geometries. A mandatory quality assurance (QA) flag is then provided to establish the pixel-specific estimates of retrieval performance. Note that when the temporal gap-filling routine is called upon, as reported in the mandatory quality assurance (QA) Flags (Table), the latest high-quality date observed (based on retrievals using the main algorithm) is reported as a separate SDS layer. If an outlier is still detected after temporal gap-filling, then the VNP46 algorithm defaults to a monthly climatology, based on the most recently available moonless high QA values. Thus, through judicious use of the VNP46 product quality flag, the end-user can establish whether a particular temporally gap-filled NTL value is based on a recent date or not. This results in a traceable, moonlight-adjusted, NTL product to assess current versus recent NTL conditions, while reducing persistent data gaps caused by nighttime clouds, snow, and other ephemeral artifacts (e.g., the Aurora Borealis - cf., Figure 5). Figure 6 illustrates the monthly (VNP46A3) and yearly (VNP46A4)

NTL composite, the associated the number of valid observations used for the composite, and quality flags generated from daily lunar-BRDF-corrected NTL product (VNP46A2) for tile h06v05 in 2016.

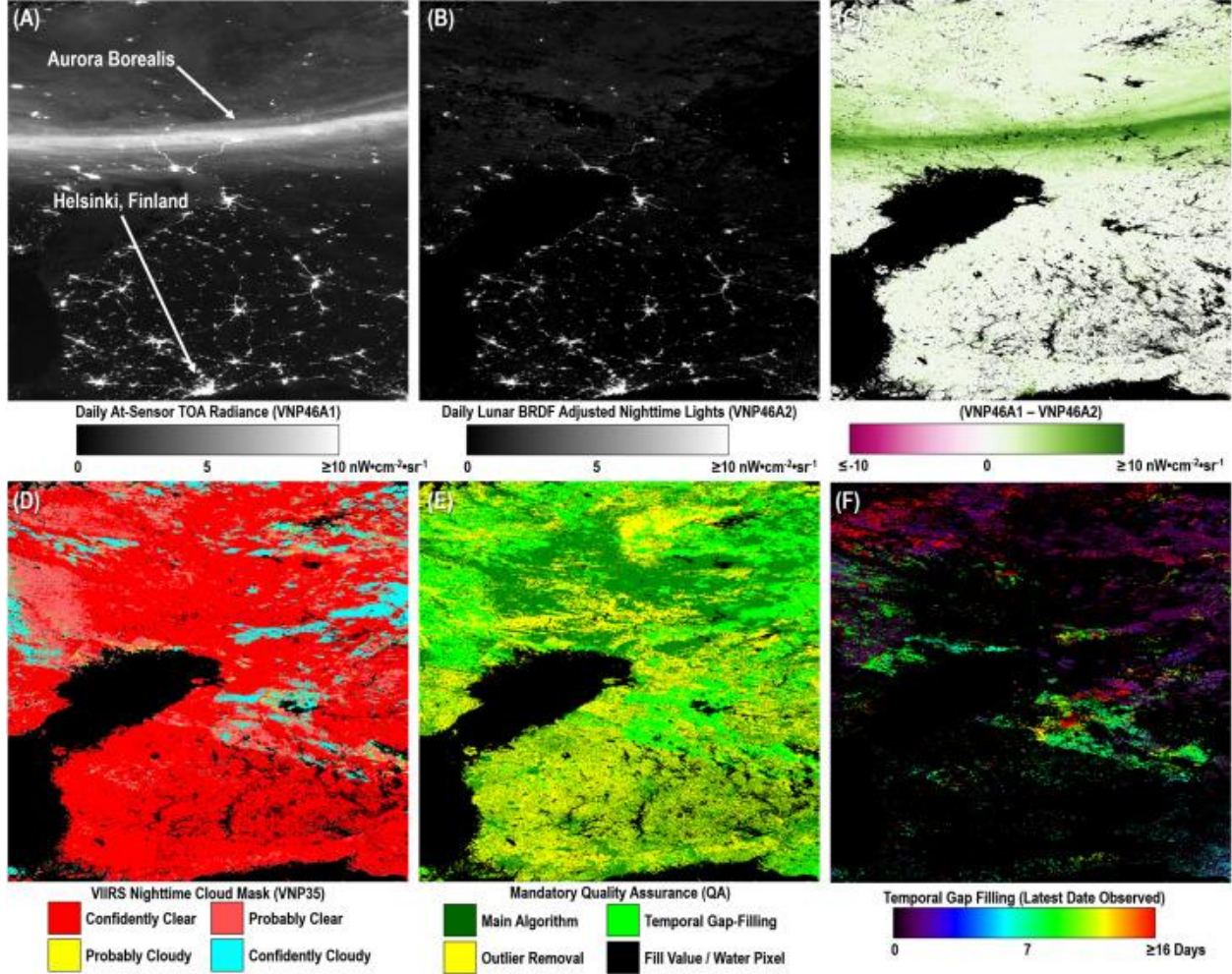
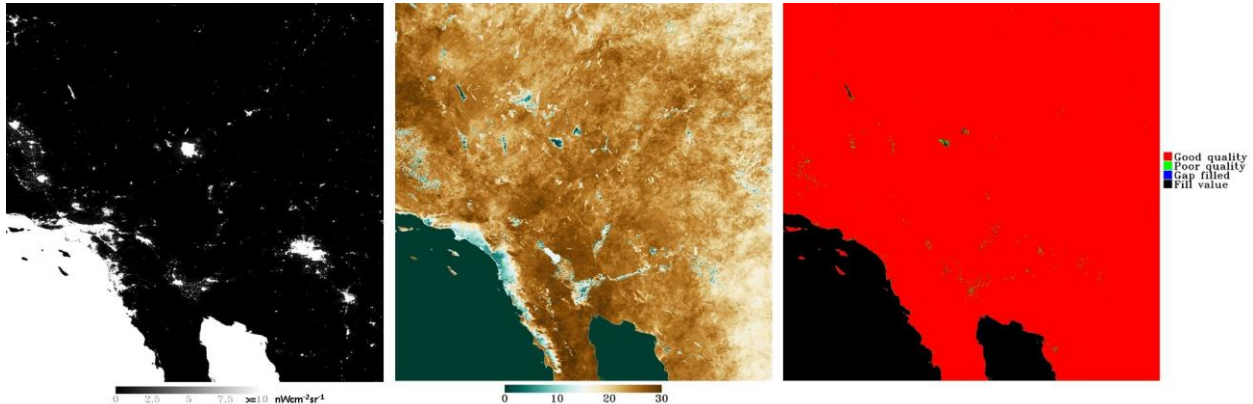


Figure 5 VNP46 product suite components for a $10^\circ \times 10^\circ$ Level 3 tile over Sweden and Finland (h20v02; DOY 2013-080). The half-moon-illuminated and 30% cloud-contaminated scene is shown to capture extraneous light emissions north of the Gulf of Bothnia caused by the Aurora Borealis.



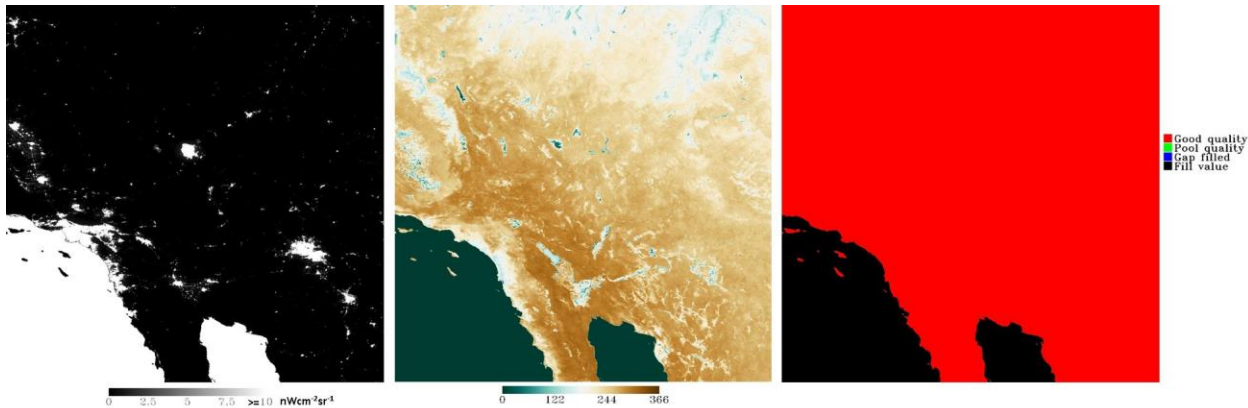


Figure 6 VNP46A3 monthly (upper) and VNP46A4 yearly (bottom) NTL composite (left), the associated number of observations for the composite (middle) and quality (right) for a $10^\circ \times 10^\circ$ Level 3 tile h06v05 in 2016.

6 Evaluation and Validation of the Product

The overarching goal of NASA's Black Marble science product development effort is to achieve a "breakthrough" performance specification (cf., Table) by conducting the following: (1) long-term stability monitoring of the entire VNP46 algorithm processing chain, including the fundamental (Level 1B) VIIRS DNB time series record, terrain-corrected geolocation, stray light correction, and calibration LUTs; and (2) global quality assessment, uncertainty quantification, and product validation. To assess progress, we have developed a series of benchmark tests to quantify product performance at representative spatial and temporal scales. This comprehensive suite of benchmark tests and assessment metrics are meant to ensure that variations in VNP46 product performance can be identified quickly so that improvements can be implemented in a timely fashion. It also enables the end-user to consider the products in their appropriate context, e.g., by anticipating appropriate noise reduction levels under specific retrieval conditions.

Table 14 Key performance metrics established for NASA's Black Marble product suite.

Key performance metrics Goal	Threshold	Breakthrough	Goal
NTL detection limit (Lmin)	$3.0 \text{ nW} \cdot \text{cm}^{-2} \cdot \text{sr}^{-1}$	$0.5 \text{ nW} \cdot \text{cm}^{-2} \cdot \text{sr}^{-1}$	$0.25 \text{ nW} \cdot \text{cm}^{-2} \cdot \text{sr}^{-1}$
NTL robustness (L0)	$\pm 3.0 \text{ nW} \cdot \text{cm}^{-2} \cdot \text{sr}^{-1}$	$\pm 0.10 \text{ nW} \cdot \text{cm}^{-2} \cdot \text{sr}^{-1}$	$\pm 0.05 \text{ nW} \cdot \text{cm}^{-2} \cdot \text{sr}^{-1}$
Stray light error	$0.45 \text{ nW} \cdot \text{cm}^{-2} \cdot \text{sr}^{-1}$	$0.25 \text{ nW} \cdot \text{cm}^{-2} \cdot \text{sr}^{-1}$	$< 0.1 \text{ nW} \cdot \text{cm}^{-2} \cdot \text{sr}^{-1}$
Spatial resolution	$742\text{m } (\pm 5\%)$	$500\text{m } (\pm 5\%)$	$\leq 200\text{m } (\pm 5\%)$
Temporal resolution	Monthly	Daily	Hourly

Geolocation uncertainty	133m	50m	20m
-------------------------	------	-----	-----

A series of benchmark tests were designed to quantify errors inherited from the upstream products (i.e., VIIRS calibrated radiance, cloud mask, aerosol retrieval, etc.), provided a relative assessment of NTL product performance. The initial validation results are presented together with example case studies that are available in related publications in section 10. To establish the absolute accuracy of the final NTL retrievals, one must also assess the NTL products against an independent source of reference data. Unfortunately, quality-assessed *in situ* NTL measurements are not widely available; let alone, at the spatial and temporal densities necessary to capture the full range of retrieval conditions. Recent NASA Black Marble product validation efforts have therefore focused on developing guidelines for accuracy assessment of NTL products through a number of international initiatives.

Figure 7 shows an example of the accuracy assessment of NTL products through a field experiment at the Pitahaya farmland site in Cabo Rojo, PR. During the night of 2 March 2017, at 02:00 local time, the Puerto Rico's Working Group on Light Pollution (PRWGLP) team conducted a validation experiment at the Pitahaya site. A stable point source was reflected by a 30 m^2 Lambertian target to generate an in-band DNB radiance at sensor of $\sim 0.45\text{nW}\cdot\text{cm}^{-2}\cdot\text{sr}^{-1}$. Additional Sky-Quality Meter instrument data recordings (Falchi et al., 2016; Kyba et al., 2011, Kyba et al., 2013; Schnitt et al., 2013) with specialized filters matching the VIIRS relative spectral response, as well as atmospheric measurements from nearby Aerosol Robotic Network (AERONET) sun photometers (Holben et al., 1998) were used to characterize atmospheric conditions.

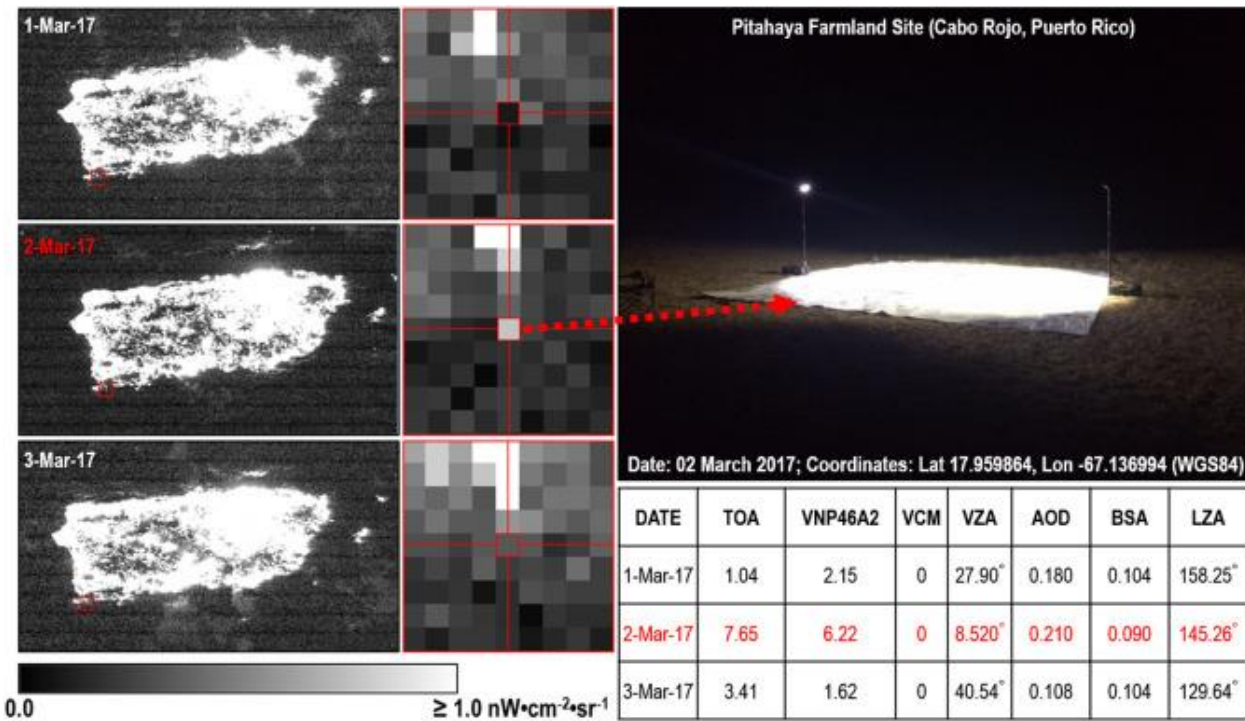


Figure 7 The NTL radiance at the Pitahaya farmland site in Cabo Rojo, PR on 1st, 2nd and 3rd March 2017. The top-right image shows the setup of the stable point source. TOA and VNP46A2 values are in $\text{nW} \cdot \text{cm}^{-2} \cdot \text{sr}^{-1}$. VCM = 0 represents cloud free overpasses. LZA is lunar zenith angle, and the values larger than 108° correspond to moonless nights.

The validation approach follows the assessment method first described in *Cao and Bai (2014)*, which relies on quantitative analysis and stability monitoring of stable light point sources. We used the following parameters to generate our radiative transfer calculations: (1) atmospheric transmittance = 0.8 (based on 6S radiative transfer code and AERONET calculations), a target reflectance = 0.8, and 16 W of total effective irradiance incident on the reflective surface. Results in Figure 7 also illustrate how the detected VIIRS at-sensor cloud-corrected radiance (or TOA) and VNP46A2 estimates over the pixel centered on the reflective point source were within the VNP46A2 product's "breakthrough" requirement specifications for the NTL detection limit, L_{\min} ($0.43 \text{ nW} \cdot \text{cm}^{-2} \cdot \text{sr}^{-1}$) after removing background noise measured the days prior and after activation of the stable light point sources. We found that the final VNP46A2 product resulted in a 16.95% sensitivity enhancement (due to reduced background noise), as confirmed in previous benchmark tests, compared to the at-sensor cloud-corrected radiance product (TOA) under observed moon-free conditions.

7 Data Archives

The VNP46 suite of operational products are archived and supported by NASA's LAADS DAAC data center <https://ladsweb.modaps.eosdis.nasa.gov/>.

The VNP46 suite of near-real-time products with a latency of about three hours are available at the NASA LANCE: NASA Near-Real-time Data and Imagery <https://earthdata.nasa.gov/earth-observation-data/near-real-time>.

8 Data Usage and Citation Policies

Please find detailed information about how to use and how to cite the data on the webpage https://modaps.modaps.eosdis.nasa.gov/services/faq/LAADS_Data-Use_Citation_Policies.pdf.

9 Contact Information

Principal Investigator: Dr. Zhuosen Wang (zhuosen.wang@nasa.gov)

NASA Official: Dr. Virginia L. Kalb (virginia.l.kalb@nasa.gov)

10 Related Publications

Román, M.O., Wang, Z., Sun, Q., Kalb, V., Miller, S.D., Molthan, A., Schultz, L., Bell, J., Stokes, E.C., Pandey, B. and Seto, K.C., et al. (2018). NASA's Black Marble nighttime lights product suite. *Remote Sens. Environ.* 210, 113-143. doi:10.1016/j.rse.2018.03.017.

Román, M.O. and Stokes, E.C. (2015). Holidays in lights: Tracking cultural patterns in demand for energy services. *Earth's Future*, 3, 182–205.

Román, M.O., Stokes, E.C., Shrestha, R., Wang, Z., Schultz, L., Sepúlveda Carlo, E.A., Sun, Q., Bell, J., Molthan, A., Kalb, V., Ji, C., Seto, K.C., McClain, S.N., Enenkel, M., 2019. Satellite-based assessment of electricity restoration efforts in Puerto Rico after Hurricane Maria. *PLoS One*. doi:10.1371/journal.pone.0218883

Wang, Z., Román, M.O., Kalb, V.L., Miller, S.D., Zhang, J., Shrestha, R.M., 2021. Quantifying uncertainties in nighttime light retrievals from Suomi-NPP and NOAA-20 VIIRS Day/Night Band data. *Remote Sensing of Environment* 263, 112557. <https://doi.org/10.1016/J.RSE.2021.112557>

Wang, Z., Shrestha, R.M., Roman, M.O., Kalb, V.L., 2022. NASA's Black Marble Multiangle Nighttime Lights Temporal Composites. *IEEE Geoscience and Remote Sensing Letters* 19. <https://doi.org/10.1109/LGRS.2022.3176616>

Wang, Z., Román, M. O., Sun, Q., Molthan, A. L., Schultz, L. A., and Kalb, V. L. (2018). Monitoring Disaster-related Power Outages Using NASA Black Marble Nighttime Light Product. Int. Arch. Photogramm. Remote Sens. Spatial Inf. Sci., XLII-3, 1853-1856, <https://doi.org/10.5194/isprs-archives-XLII-3-1853-2018>, 2018.

Wang, Z., Shrestha, R. and Román, M. O., (2020). NASA's Black Marble Nighttime Lights Product Suite Algorithm Theoretical Basis Document (ATBD), Version 1.1, July 2020. Available in
https://viirsland.gsfc.nasa.gov/PDF/VIIRS_BlackMarble_ATBD_V1.1.pdf

Cole, T.A., Wanik, D.W., Molthan, A.L., Román, M.O. and Griffin, R.E. (2017). Synergistic use of nighttime satellite data, electric utility infrastructure, and ambient population to improve power outage detections in urban areas. *Remote Sensing*, 9(3), 286. doi:10.3390/rs9030286.

Kalb, V., Kosar, B., Collado-Vega, Y., Davidson, C., 2023. Aurora Detection From Nighttime Lights for Earth and Space Science Applications. *Earth and Space Science* 10,1. doi:10.1029/2022EA002513

References

- Andersson, E., Barthel, S., Borgström, S., Colding, J., Elmquist, T., Folke, C., Gren, Å., 2014. Reconnecting cities to the biosphere: stewardship of green infrastructure and urban ecosystem services. *Ambio* 43, 445–453.
- Asanuma, I., Yamaguchi, T., Park, J., Mackin, K.J., Mittleman, J., 2016. Detection limit of fishing boats by the day night band (DNB) on VIIRS, in: SPIE Optical Engineering+ Applications. International Society for Optics and Photonics, p. 99760P–99760P–8.
- Bankert, R.L., Solbrig, J.E., Lee, T.F., Miller, S.D., 2011. Automated lightning flash detection in nighttime visible satellite data. *Weather Forecast*. 26, 399–408.
- Baret, F., Nightingale, J., Garrigues, S., Justice, C., Nickeson, J.E., 2009. Report on the CEOS Land Product Validation Sub-group Meeting. *Earth Obs.* 21, 26–30.
- Bennett, M.M., Smith, L.C., 2017. Advances in using multitemporal night-time lights satellite imagery to detect, estimate, and monitor socioeconomic dynamics. *Remote Sens. Environ.* 192, 176–197. doi:10.1016/j.rse.2017.01.005
- Bennie, J., Davies, T.W., Inger, R., Gaston, K.J., 2014. Mapping artificial lightscapes for ecological studies. *Methods Ecol. Evol.* 5, 534–540. doi:10.1111/2041-210X.12182
- Bickenbach, F., Bode, E., Nunnerkamp, P., Söder, M., 2016. Night lights and regional GDP. *Rev. World Econ.* 152, 425–447. doi:10.1007/s10290-016-0246-0
- Campagnolo, M.L., Sun, Q., Liu, Y., Schaaf, C., Wang, Z., Román, M.O., 2016. Estimating the effective spatial resolution of the operational BRDF, albedo, and nadir reflectance products from MODIS and VIIRS. *Remote Sens. Environ.* 175, 52–64.
- Cao, C., Bai, Y., 2014. Quantitative Analysis of VIIRS DNB Nightlight Point Source for Light Power Estimation and Stability Monitoring. *Remote Sens.* 6, 11915–11935. doi:10.3390/rs61211915
- Cao, C., Shao, X., Upadhyay, S., 2013. Detecting light outages after severe storms using the Suomi-NPP/VIIRS day/night band radiances. *IEEE Geosci. Remote Sens. Lett.* 10, 1582–1586. doi:10.1109/LGRS.2013.2262258
- Cescatti, A., Marcolla, B., Vannan, S.K.S., Pan, J.Y., Román, M.O., Yang, X., Ciais, P., Cook, R.B., Law, B.E., Matteucci, G., Migliavacca, M., Moors, E., Richardson, A.D., Seufert, G.G., Schaaf, C.B., 2012. Intercomparison of MODIS albedo retrievals and in situ measurements across the global FLUXNET network. *Remote Sens. Environ.* 121, 323–334. doi:10.1016/j.rse.2012.02.019
- Chakraborty, S., Oda, T., Kalb, V.L., Wang, Z., and Román, M.O. 2023. Potentially underestimated gas flaring activities—a new approach to detect combustion using machine learning and NASA's Black Marble product suite. *Environ. Res. Lett.* 18 035001, doi 10.1088/1748-9326/acb6a7
- Chen, H., Xiong, X., Sun, C., Chen, X., Chiang, K., 2017. Suomi-NPP VIIRS day–night band on-orbit calibration and performance. *J. Appl. Remote Sens.* 11, 36019.
- Chen, J.M., Black, T.A., 1991. Measuring leaf area index of plant canopies with branch architecture. *Agric. For. Meteorol.* 57, 1–12.
- Chen, J.M., Menges, C.H., Leblanc, S.G., 2005. Global mapping of foliage clumping index using multi-angular satellite data. *Remote Sens. Environ.* 97, 447–457.
- Chen, X., Nordhaus, W., 2015. A test of the new VIIRS lights data set: Population and economic output in Africa. *Remote Sens.* 7, 4937–4947. doi:10.3390/rs70404937
- Chen, Z., Yu, B., Hu, Y., Huang, C., Shi, K., Wu, J., 2015. Estimating house vacancy rate in metropolitan areas using NPP-VIIRS nighttime light composite data. *IEEE J. Sel. Top. Appl. Earth Obs. Remote Sens.* 8, 2188–2197. doi:10.1109/JSTARS.2015.2418201
- Chopping, M.J., 2006. Progress in retrieving canopy structure parameters from NASA multi-angle remote sensing, in: International, I. (Ed.), Proceedings of the IEEE International Geoscience & Remote Sensing Symposium, IGARSS '06 and the 27th Canadian Remote Sensing Symposium. Denver, CO, pp. 256–259.
- Cinzano, P., Falchi, F., Elvidge, C.D., Baugh, K.E., 2000. The artificial night sky brightness mapped from DMSP satellite Operational Linescan System measurements. *Mon. Not. R. Astron. Soc.* 318, 641–657.
- Cole, T.A., Wanik, D.W., Molthan, A.L., Román, M.O., Griffin, R.E., 2017. Synergistic Use of Nighttime Satellite Data, Electric Utility Infrastructure, and Ambient Population to Improve Power Outage Detections in Urban Areas. *Remote Sens.* 9, 286. doi:10.3390/rs9030286

- Cook, B.D., Corp, L.A., Nelson, R.F., Middleton, E.M., Morton, D.C., McCorkel, J.T., Masek, J.G., Ranson, K.J., Ly, V., Montesano, P.M., 2013. NASA goddard's LiDAR, hyperspectral and thermal (G-LiHT) airborne imager. *Remote Sens.* 5, 4045–4066. doi:10.3390/rs5084045
- Coscieme, L., Pulselli, F.M., Bastianoni, S., Elvidge, C.D., Anderson, S., Sutton, P.C., 2014. A thermodynamic geography: Night-time satellite imagery as a proxy measure of energy. *Ambio* 43, 969–979. doi:10.1007/s13280-013-0468-5
- Elvidge, C.D., Keith, D.M., Tuttle, B.T., Baugh, K.E., 2010. Spectral identification of lighting type and character. *Sensors* 10, 3961–3988.
- Elvidge, C.D., Zhizhin, M., Baugh, K., Hsu, F.-C., 2015a. Automatic boat identification system for VIIRS low light imaging data. *Remote Sens.* 7, 3020–3036.
- Elvidge, C.D., Zhizhin, M., Baugh, K., Hsu, F.-C., Ghosh, T., 2015b. Methods for global survey of natural gas flaring from visible infrared imaging radiometer suite data. *Energies* 9, 14.
- Esch, T., Heldens, W., Hirne, A., Keil, M., Marconcini, M., Roth, A., Zeidler, J., Dech, S., Strano, E., 2017. Breaking new ground in mapping human settlements from space-The Global Urban Footprint. *arXiv Prepr.* arXiv1706.04862.
- Esch, T., Marconcini, M., Felbier, A., Roth, A., Heldens, W., Huber, M., Schwinger, M., Taubenbock, H., Muller, A., Dech, S., 2013. Urban footprint processor-Fully automated processing chain generating settlement masks from global data of the TanDEM-X mission. *IEEE Geosci. Remote Sens. Lett.* 10, 1617–1621. doi:10.1109/LGRS.2013.2272953
- Falchi, F., Cinzano, P., Duriscoe, D., Kyba, C.C.M., Elvidge, C.D., Baugh, K., Portnov, B.A., Rybnikova, N.A., Furgoni, R., 2016. The new world atlas of artificial night sky brightness. *Sci. Adv.* 2, e1600377.
- Griggs, D., Stafford-smith, M., Gaffney, O., Rockström, J., Öhman, M.C., Steffen, W., Glaser, G., Kanie, N., Noble, I., 2015. Policy : Sustainable development goals for people and planet. *Nature* 495, 5–9. doi:10.1038/495305a
- Guo, W., Lu, D., Wu, Y., Zhang, J., 2015. Mapping impervious surface distribution with integration of SNNP VIIRS-DNB and MODIS NDVI data. *Remote Sens.* 7, 12459–12477.
- He, L., Chen, J.M., Pisek, J., Schaaf, C.B., Strahler, A.H., 2012. Global clumping index map derived from the MODIS BRDF product. *Remote Sens. Environ.* 119, 118–130.
- Helios Global, 2017. Helios Global World Trends [WWW Document]. URL <http://www.heliosglobalinc.com/world-trends-watch/> (accessed 10.24.17).
- Heynen, N., Perkins, H.A., Roy, P., 2006. The political ecology of uneven urban green space: the impact of political economy on race and ethnicity in producing environmental inequality in Milwaukee. *Urban Aff. Rev.* 42, 3–25.
- Hill, M.J., Román, M.O., Schaaf, C.B., 2011. Dynamics of vegetation indices in tropical and subtropical savannas defined by ecoregions and Moderate Resolution Imaging Spectroradiometer (MODIS) land cover. *Geocarto Int.* 1–39. doi:doi:10.1080/10106049.2011.626529
- Hillger, D., Kopp, T., Lee, T., Lindsey, D., Seaman, C., Miller, S., Solbrig, J., Kidder, S., Bachmeier, S., Jasmin, T., 2013. First-light imagery from Suomi NPP VIIRS. *Bull. Am. Meteorol. Soc.* 94, 1019–1029.
- Holben, B.N., Eck, T.F., Slutsker, I., Tanré, D., Buis, J.P., Setzer, A., Vermote, E., Reagan, J.A., Kaufman, Y.J., Nakajima, T., Lavenu, F., Jankowiak, I., Smirnov, A., 1998. AERONET—A federated instrument network and data archive for aerosol characterization. *Remote Sens. Environ.* 66, 1–16. doi:doi:10.1016/S0034-4257(98)00031-5
- Hu, C., Chen, S., Wang, M., Murch, B., Taylor, J., 2015. Detecting surface oil slicks using VIIRS nighttime imagery under moon glint: a case study in the Gulf of Mexico. *Remote Sens. Lett.* 6, 295–301.
- Huang, Q., Yang, X., Gao, B., Yang, Y., Zhao, Y., 2014. Application of DMSP/OLS nighttime light images: A meta-analysis and a systematic literature review. *Remote Sens.* 6, 6844–6866. doi:10.3390/rs6086844
- Jim, C.Y., 2004. Green-space preservation and allocation for sustainable greening of compact cities. *Cities* 21, 311–320.
- Johnson, R.S., Zhang, J., Hyer, E.J., Miller, S.D., Reid, J.S., 2013. Preliminary investigations toward nighttime aerosol optical depth retrievals from the VIIRS day/night band. *Atmos. Meas. Tech.* 6, 587–612.
- Kabisch, N., Haase, D., 2014. Green justice or just green? Provision of urban green spaces in Berlin, Germany. *Landsc. Urban Plan.* 122, 129–139.

- Kalb, V., Kosar, B., Collado-Vega, Y., Davidson, C., 2023. Aurora Detection From Nighttime Lights for Earth and Space Science Applications. *Earth and Space Science* 10,1. doi:10.1029/2022EA002513
- Katz, Y., Levin, N., 2016. Quantifying urban light pollution - A comparison between field measurements and EROS-B imagery. *Remote Sens. Environ.* 177, 65–77. doi:10.1016/j.rse.2016.02.017
- Klein, A.G., Stroeve, J., 2002. Development and validation of a snow albedo algorithm for the MODIS instrument. *Ann. Glaciol.* 34, 45–52.
- Knyazikhin, Y., Glassy, J., Privette, J.L., Tian, Y., Lotsch, A., Zhang, Y., Wang, Y., Morisette, J.T., P.Votava, Myneni, R.B., Nemani, R.R., Running, S.W., 1999. MODIS Leaf Area Index (LAI) and Fraction of Photosynthetically Active Radiation Absorbed by Vegetation (FPAR) Product (MOD15) Algorithm Theoretical Basis Document, <http://eospso.gsfc.nasa.gov/atbd/modistables.html>.
- Kopp, T.J., Thomas, W., Heidinger, A.K., Botambekov, D., Frey, R.A., Hutchison, K.D., Iisager, B.D., Brueske, K., Reed, B., 2014. The VIIRS Cloud Mask: Progress in the first year of S - NPP toward a common cloud detection scheme. *J. Geophys. Res. Atmos.* 119, 2441–2456.
- Kreyszig, E. (1979). Advanced Engineering Mathematics (Fourth ed.). Wiley. p. 880, eq. 5. ISBN 0-471-02140-7.
- Kyba, C.C.M., Ruhtz, T., Fischer, J., Höller, F., 2011. Cloud coverage acts as an amplifier for ecological light pollution in urban ecosystems. *PLoS One* 6, e17307.
- Kyba, C.C.M., Wagner, J.M., Kuechly, H.U., Walker, C.E., Elvidge, C.D., Falchi, F., Ruhtz, T., Fischer, J., Höller, F., 2013. Citizen Science Provides Valuable Data for Monitoring Global Night Sky Luminance. *Sci. Rep.* 3, 1835. doi:10.1038/srep01835
- Lacaze, R., Chen, J.M., Roujean, J.-L., Leblanc, S.G., 2002. Retrieval of vegetation clumping index using hot spot signatures measured by POLDER instrument. *Remote Sens. Environ.* 79, 84–95. doi:doi:10.1016/S0034-4257(01)00241-3
- Leblanc, S.G., Chen, J.M., White, H.P., Latifovic, R., Lacaze, R., Roujean, J.-L., 2005. Canada-wide foliage clumping index mapping from multiangular POLDER measurements. *Can. J. Remote Sens.* 31, 364–376.
- Lee, S., Chiang, K., Xiong, X., Sun, C., Anderson, S., 2014. The S-NPP VIIRS Day-Night Band on-orbit calibration/characterization and current state of SDR products. *Remote Sens.* 6, 12427–12446.
- Lee, S., McIntire, J., Oudrari, H., Schwarting, T., Xiong, X., 2015. A New Method for Suomi-NPP VIIRS Day–Night Band On-Orbit Radiometric Calibration. *IEEE Trans. Geosci. Remote Sens.* 53, 324–334. doi:10.1109/TGRS.2014.2321835
- Levin, N., 2017. The impact of seasonal changes on observed nighttime brightness from 2014 to 2015 monthly VIIRS DNB composites. *Remote Sens. Environ.* 193, 150–164. doi:10.1016/j.rse.2017.03.003
- Levin, N., Zhang, Q., 2017. A global analysis of factors controlling VIIRS nighttime light levels from densely populated areas. *Remote Sens. Environ.* 190, 366–382. doi:10.1016/j.rse.2017.01.006
- Li, X., Xu, H., Chen, X., Li, C., 2013. Potential of NPP-VIIRS nighttime light imagery for modeling the regional economy of China. *Remote Sens.* 5, 3057–3081. doi:10.3390/rs5063057
- Li, X., Ma, R., Zhang, Q., Li, D., Liu, S., He, T., Zhao, L., 2019. Anisotropic characteristic of artificial light at night – Systematic investigation with VIIRS DNB multi-temporal observations. *Remote Sens. Environ.* doi:10.1016/j.rse.2019.111357
- Liao, L.B., Weiss, S., Mills, S., Hauss, B., 2013. Suomi NPP VIIRS day-night band on-orbit performance. *J. Geophys. Res. Atmos.* 118, 12705–12718. doi:10.1002/2013JD020475
- Liu, Y., Wang, Z., Sun, Q., Erb, A.M., Li, Z., Schaaf, C.B., Zhang, X., Román, M.O., Scott, R.L., Zhang, Q., 2017. Evaluation of the VIIRS BRDF, Albedo and NBAR products suite and an assessment of continuity with the long term MODIS record. *Remote Sens. Environ.* 201, 256–274.
- Liu, Hu, C., Zhan, W., Sun, C., Murch, B., Ma., L., 2017. Identifying industrial heat sources using time-series of the VIIRS Nightfire product with an object-oriented approach. *Remote Sens. Environ.* doi:10.1016/J.RSE.2017.10.019
- Lucht, W., Roujean, J., 2000. Considerations in the parametric modeling of BRDF and albedo from multiangular satellite sensor observations. *Remote Sens. Rev.* 18, 343–379.
- Ma, T., Zhou, C.H., Pei, T., Haynie, S., Fan, J.F., 2014. Responses of Suomi- NPP VIIRS- derived nighttime lights to socioeconomic activity in China's cities. *Remote Sens. Lett.* 5, 165–174. doi:10.1080/2150704x.2014.890758

- Mann, M.L., Melaas, E.K., Malik, A., 2016. Using VIIRS Day/Night Band to Measure Electricity Supply Reliability: Preliminary Results from Maharashtra, India. *Remote Sens.* 8, 711.
- McHardy, T.M., Zhang, J., Reid, J.S., Miller, S.D., Hyer, E.J., Kuehn, R.E., 2015. An improved method for retrieving nighttime aerosol optical thickness from the VIIRS Day/Night Band. *Atmos. Meas. Tech.* 8, 4773–4783.
- Meng, L., Zhou, Y., Román, M.O., Stokes, E.C., Wang, Z., Asrar, G.R., Mao, J., Richardson, A.D., Gu, L., Wang, Y., 2022. Artificial light at night: an underappreciated effect on phenology of deciduous woody plants, PNAS Nexus, Volume 1, Issue 2, pgac046, <https://doi.org/10.1093/pnasnexus/pgac046>
- Miller, S.D., Combs, C.L., Kidder, S.Q., Lee, T.F., 2012. Assessing Moonlight Availability for Nighttime Environmental Applications by Low-Light Visible Polar-Orbiting Satellite Sensors. *J. Atmos. Ocean. Technol.* 29, 538–557. doi:10.1175/JTECH-D-11-00192.1
- Miller, S.D., Haddock, S.H.D., Elvidge, C.D., Lee, T.F., 2006. Twenty thousand leagues over the seas: the first satellite perspective on bioluminescent “milky seas.” *Int. J. Remote Sens.* 27, 5131–5143. doi:10.1080/01431160600554298
- Miller, S.D., Haddock, S.H.D., Elvidge, C.D., Lee, T.F., 2005. Detection of a bioluminescent milky sea from space. *PNAS* 102, 14181–14184. doi:doi:10.1073/pnas.0507253102
- Miller, S.D., Straka, W., Mills, S.P., Elvidge, C.D., Lee, T.F., Solbrig, J., Walther, A., Heidinger, A.K., Weiss, S.C., 2013. Illuminating the capabilities of the suomi national polar-orbiting partnership (NPP) visible infrared imaging radiometer suite (VIIRS) day/night band. *Remote Sens.* 5, 6717–6766.
- Miller, S.D., Straka, W.C., Yue, J., Smith, S.M., Alexander, M.J., Hoffmann, L., Setvák, M., Partain, P.T., 2015. Upper atmospheric gravity wave details revealed in nightglow satellite imagery. *Proc. Natl. Acad. Sci.* 112, E6728–E6735.
- Miller, S.D., Turner, R.E., 2009. A Dynamic Lunar Spectral Irradiance Data Set for NPOESS/VIIRS Day/Night Band Nighttime Environmental Applications. *IEEE Trans. Geosci. Remote Sens.* 47, 2316–2329. doi:10.1109/TGRS.2009.2012696
- Miller, S., Mills, S.P., Elvidge, C.D., Lindsey, D.T., Lee, T.F., Hawkins, J.D., 2012. Suomi satellite brings to light a unique frontier of nighttime environmental sensing capabilities. *Proc. Natl. Acad. Sci.* 109, 15706–15711. doi:doi:10.1073/pnas.1207034109
- Mills, S., Miller, S., 2016. VIIRS Day/Night Band—Correcting Striping and Nonuniformity over a Very Large Dynamic Range. *J. Imaging* 2, 9. doi:doi:10.3390/jimaging2010009
- Mills, S., Weiss, S., Liang, C., 2013. VIIRS day/night band (DNB) stray light characterization and correction, in: SPIE Optical Engineering+ Applications. International Society for Optics and Photonics, p. 88661P–88661P.
- Minnis, P., Hong, G., Sun-Mack, S., Smith, W.L., Chen, Y., Miller, S.D., 2016. Estimating nocturnal opaque ice cloud optical depth from MODIS multispectral infrared radiances using a neural network method. *J. Geophys. Res. Atmos.* 121, 4907–4932. doi:10.1002/2015JD024456
- Molthan, A., Jedlovec, G., 2013. Satellite observations monitor outages from Superstorm Sandy. *Eos, Trans. Am. Geophys. Union* 94, 53–54.
- Moody, E.G., King, M.D., Schaaf, C.B., Platnick, S., 2008. MODIS-derived spatially complete surface albedo products: Spatial and temporal pixel distribution and zonal averages. *J. Appl. Meteorol. Climatol.* 47, 2879–2894. doi:doi:10.1175/2008JAMC1795.1
- Moorthi, S., Pan, H.-L., Caplan, P., 2001. Changes to the 2001 NCEP operational MRF/AVN global analysis/forecast system. US Department of Commerce, National Oceanic and Atmospheric Administration, National Weather Service, Office of Meteorology, Program and Plans Division.
- Morisette, J.T., Baret, F., Liang, S., 2006. Special issue on global land product validation. *IEEE Trans. Geosci. Remote Sens.* 44, 1695–1697.
- Moustafa, S.E., Rennermalm, A.K., Román, M.O., Wang, Z., Schaaf, C.B., Smith, L.C., Koenig, L.S., Erb, A., 2017. Evaluation of satellite remote sensing albedo retrievals over the ablation area of the southwestern Greenland ice sheet. *Remote Sens. Environ.* 198, 115–125.
- NASM, 2018. Thriving on Our Changing Planet: A Decadal Strategy for Earth Observation from Space. The National Academies Press, Washington, DC. doi:10.17226/24938
- Nicodemus, F.E., 1977. Geometrical considerations and nomenclature for reflectance, in: National Bureau of Standards Monograph, No. 160. Washington, DC, pp. 1–52.
- Nilson, T., 1971. A theoretical analysis of the frequency of gaps in plant stands. *Agric. Meteorol.* 8, 25–38.

- NRC, 2017. A look into Zaatari camp during winter | NRC [WWW Document]. World Bank. URL <https://www.nrc.no/news/2016/february/a-look-into-zaatari-camp-during-winter/> (accessed 10.24.17).
- O'Sullivan, F., 2017. How Built-Out Barcelona Found Space for an Urban Forest - CityLab [WWW Document]. URL <https://www.citylab.com/solutions/2017/05/barcelona-green-urban-forest-climate-plan/526998/> (accessed 6.28.17).
- Oda, T., Lauvaux, T., Lu, D., Rao, P., Miles, N.L., Richardson, S.J., Gurney, K.R., 2017. On the impact of granularity of space-based urban CO₂ emissions in urban atmospheric inversions: A case study for Indianapolis, IN. *Elem Sci Anth* 5.
- Omar, A.H., Winker, D.M., Tackett, J.L., Giles, D.M., Kar, J., Liu, Z., Vaughan, M.A., Powell, K.A., Trepte, C.R., 2013. CALIOP and AERONET aerosol optical depth comparisons: One size fits none. *J. Geophys. Res. Atmos.* 118, 4748–4766.
- Ou, J., Liu, X., Li, X., Li, M., Li, W., 2015. Evaluation of NPP-VIIRS nighttime light data for mapping global fossil fuel combustion CO₂ emissions: a comparison with DMSP-OLS nighttime light data. *PLoS One* 10, e0138310. doi:10.1371/journal.pone.0138310
- Pahlevan, N., Sarkar, S., Devadiga, S., Wolfe, R.E., Román, M., Vermote, E., Lin, G., Xiong, X., 2017. Impact of Spatial Sampling on Continuity of MODIS–VIIRS Land Surface Reflectance Products: A Simulation Approach. *IEEE Trans. Geosci. Remote Sens.* 55, 183–196.
- Park, T., Yan, K., Chen, C., Xu, B., Knyazikhin, Y., Myneni, R., 2017. VIIRS Leaf Area Index (LAI) and Fraction of Photosynthetically Active Radiation Absorbed by Vegetation (FPAR) Product Algorithm Theoretical Basis Document (ATBD), NASA Technical Report.
- Paynter, I., Saenz, E., Genest, D., Peri, F., Erb, A., Li, Z., Wiggin, K., Muir, J., Raumonen, P., Schaaf, E.S., 2016. Observing ecosystems with lightweight, rapid - scanning terrestrial lidar scanners. *Remote Sens. Ecol. Conserv.* 2, 174–189.
- Polivka, T.N., Wang, J., Ellison, L.T., Hyer, E.J., Ichoku, C.M., 2016. Improving Nocturnal Fire Detection With the VIIRS Day–Night Band. *IEEE Trans. Geosci. Remote Sens.* 54, 5503–5519.
- Riggs, G.A., Hall, D.K., Román, M.O., 2017. Overview of NASA's MODIS and VIIRS Snow-Cover Earth System Data Records. *Earth Syst. Sci. Data* 9, 1–13. doi:10.5194/essd-9-765-2017
- Riggs, G.A., Hall, D.K., Román, M.O., 2016. NASA S-NPP VIIRS Snow Products Collection 1 User Guide 1–26. doi:doi:10.5067/VIIRS/VNP10_L2.v001
- Roger, J.C., Vermote, E.F., Devadiga, S., Ray, J.P., 2016. Suomi-NPP VIIRS Surface Reflectance User's Guide.
- Román, M., Schaaf, C.B., Yang, X., Woodcock, C.E., Strahler, A.H., Braswell, R.H., Curtis, P.S., Davis, K.J., D., D., Gu, L., Goulden, M.L., Hollinger, D.Y., Kolb, T.E., Meyers, T.P., Munger, J.W., Privette, J.L., Richardson, A.D., Wilson, T.B., Wofsy, S.C., 2009. The MODIS (Collection V005) BRDF/albedo product: Assessment of spatial representativeness over forested landscapes. *Remote Sens. Environ.* 113, 2476–2498. doi:doi:10.1016/j.rse.2009.07.009
- Román, M.O., Gatebe, C.K., Poudyal, R., Schaaf, C.B., Wang, Z., King, M.D., 2011. Variability in surface BRDF at different spatial scales (30 m–500 m) over a mixed agricultural landscape as retrieved from airborne and satellite spectral measurements. *Remote Sens. Environ.* 115, 2184–2203. doi:10.1016/j.rse.2011.04.012
- Román, M.O., Gatebe, C.K., Shuai, Y., Wang, Z., Gao, F., Masek, J.G., He, T., Liang, S., Schaaf, C.B., 2013. Use of In Situ and Airborne Multiangle Data to Assess MODIS- and Landsat-Based Estimates of Directional Reflectance and Albedo. *IEEE Trans. Geosci. Remote Sens.* 51, 1393–1404. doi:10.1109/TGRS.2013.2243457
- Román, M.O., Schaaf, C.B., Lewis, P., Gao, F., Anderson, G.P., Privette, J.L., Strahler, A.H., Woodcock, C.E., Barnsley, M., 2010. Assessing the coupling between surface albedo derived from MODIS and the fraction of diffuse skylight over spatially-characterized landscapes. *Remote Sens. Environ.* 114, 738–760. doi:10.1016/j.rse.2009.11.014
- Román, M.O., Stokes, E.C., 2015. Holidays in lights: Tracking cultural patterns in demand for energy services. *Earth's Futur.* 3, 182–205. doi:10.1002/2014EF000285
- Román, M.O., Wang, Z., Sun, Q., Kalb, V., Miller, S.D., Molthan, A., Schultz, L., Bell, J., Stokes, E.C., Pandey, B. and Seto, K.C., et al. (2018). NASA's Black Marble nighttime lights product suite. *Remote Sens. Environ.*, 210, 113-143. doi:10.1016/j.rse.2018.03.017.
- Román, M.O., Stokes, E.C., Shrestha, R., Wang, Z., Schultz, L., Sepúlveda Carlo, E.A., Sun, Q., Bell, J., Molthan, A., Kalb, V., Ji, C., Seto, K.C., McClain, S.N., Enenkel, M., 2019. Satellite-based assessment of electricity

- restoration efforts in Puerto Rico after Hurricane Maria. *PLoS One*. doi:10.1371/journal.pone.0218883
- Roujean, J., Leroy, M., Deschanms, P., 1992. A bidirectional reflectance model of the Earth's surface for the correction of remote sensing data. *J. Geophys. Res.* 97, 20,420-455,468. doi:doi:10.1029/92JD01411
- Schaaf, C.B., Gao, F., Strahler, A.H., Lucht, W., Li, X., Tsang, T., Strugnell, N.C., Zhang, X., Jin, Y., Muller, J.P.J.-P., Lewis, P., Barnsley, M., Hobson, P., Disney, M., Roberts, G., Dunderdale, M., Doll, C., d'Entremont, R.P., Hu, B., Liang, S., Privette, J.L., Roy, D.P., 2002. First operational BRDF, albedo nadir reflectance products from MODIS. *Remote Sens. Environ.* 83, 135–148. doi:10.1016/S0034-4257(02)00091-3
- Schaaf, Liu, J., Gao, F., Strahler, A.H., 2011a. MODIS albedo and reflectance anisotropy products from Aqua and Terra, in: Ramachandran, B., Justice, C., Abrams, M. (Eds.), *Land Remote Sensing and Global Environmental Change: NASA's Earth Observing System and the Science of ASTER and MODIS*. Springer-Verlag. ISBN:1441967486., p. 873.
- Schaaf, Wang, Z., Strahler, A., 2011b. Commentary on Wang and Zender—MODIS snow albedo bias at high solar zenith angles relative to theory and to in situ observations in Greenland. *Remote Sens. Environ.* 115, 1296–1300.
- Schaepman-Strub, G., Schaepman, M.E., Painter, T.H., Dangel, S., Martonchik, J. V, 2006. Reflectance quantities in optical remote sensing—definitions and case studies. *Remote Sens. Environ.* 103, 27–42. doi:doi:10.1016/j.rse.2006.03.002
- Schnitt, S., Ruhtz, T., Fischer, J., Hölker, F., Kyba, C., 2013. Temperature stability of the sky quality meter. *Sensors* 13, 12166–12174.
- Seto, K.C., Dhakal, S., 2014. Chapter 12: Human Settlements, Infrastructure, and Spatial Planning. *Clim. Chang. 2014 Mitig. Clim. Chang. Contrib. Work. Gr. III to Fifth Assess. Rep. Intergov. Panel Clim. Chang.* 67–76.
- Sharma, R.C., Tateishi, R., Hara, K., Gharechelou, S., Iizuka, K., 2016. Global mapping of urban built-up areas of year 2014 by combining MODIS multispectral data with VIIRS nighttime light data. *Int. J. Digit. Earth* 9, 1004–1020. doi:10.1080/17538947.2016.1168879
- Shi, K., Huang, C., Yu, B., Yin, B., Huang, Y., Wu, J., Chang, H., Bailang, Y., Bing, Y., Yixiu, H., Jianping, W., 2014. Evaluation of NPP-VIIRS night-time light composite data for extracting built-up urban areas. *Remote Sens. Lett.* 5, 358–366. doi:10.1080/2150704x.2014.905728
- Shuai, Y., Schaaf, C., Zhang, X., Strahler, A., Roy, D., Morisette, J., Wang, Z., Nightingale, J., Nickeson, J., Richardson, A.D., 2013. Daily MODIS 500 m reflectance anisotropy direct broadcast (DB) products for monitoring vegetation phenology dynamics. *Int. J. Remote Sens.* 34, 5997–6016.
- Skakun, S., Justice, C.O., Vermote, E., Roger, J.-C., 2018. Transitioning from MODIS to VIIRS: an analysis of inter-consistency of NDVI data sets for agricultural monitoring. *Int. J. Remote Sens.* 39, 971–992.
- Strahler, A.H., Lucht, W., Schaaf, C.B., Tsang, T., Gao, F., Li, X., Muller, J.-P., Lewis, P., Barnsley, M., 1999. MODIS BRDF/Albedo Product: Algorithm Theoretical Basis Document Version 5.0. Technical Report. NASA EOS-MODIS.
- Straka, W.C., Seaman, C.J., Baugh, K., Cole, K., Stevens, E., Miller, S.D., 2015. Utilization of the suomi national polar-orbiting partnership (npp) visible infrared imaging radiometer suite (viirs) day/night band for arctic ship tracking and fisheries management. *Remote Sens.* 7, 971–989.
- Strugnell, N., Lucht, W., Schaaf, C.B., 2001. A global albedo data set derived from AVHRR data for use in climate simulations. *Geophys. Res. Lett.* 28, 191–194. doi:doi:10.1029/2000GL011580
- Tan, B., Woodcock, C.E., Hu, J., Zhang, P., Ozdogan, M., Huang, D., Yang, W., Knyazikhin, Y., Myneni, R.B., 2006. The impact of gridding artifacts on the local spatial properties of MODIS data: Implications for validation, compositing, and band-to-band registration across resolutions. *Remote Sens. Environ.* 105, 98–114.
- Thaiutsa, B., Puangchit, L., Kjelgren, R., Arunpraparut, W., 2008. Urban green space, street tree and heritage large tree assessment in Bangkok, Thailand. *Urban For. urban Green.* 7, 219–229.
- Tomasi, C., Fuzzi, S., Kokhanovsky, A., 2017. *Atmospheric Aerosols: Life Cycles and Effects on Air Quality and Climate*. John Wiley & Sons.
- Tukey, J. W. (1977), *Exploratory Data Analysis*, Addison-Wesley.
- UNHCR, 2017. Syria Regional Refugee Response - - - Emirati Jordanian Camp (Mujrib al Fhoud) [WWW Document]. URL <http://data.unhcr.org/syrianrefugees/settlement.php?id=224&country=0®ion=0> (accessed 10.25.17).
- Vermote, E., Justice, C.O., Csizar, I., 2014. Early evaluation of the VIIRS calibration, cloud mask and surface reflectance Earth data records. *Remote Sens. Environ.* 148, 134–145. doi:10.1016/j.rse.2014.03.028

- Vermote, E.F., Kotchenova, S., 2008. Atmospheric correction for the monitoring of land surfaces. *J. Geophys. Res.* 113. doi:doi:10.1029/2007JD009662.
- Walther, A., Heidinger, A.K., Miller, S., 2013. The Expected Performance of Cloud Optical and Microphysical Properties derived from Soumi NPP VIIRS Day/Night Band Lunar Reflectance. *J. Geophys. Res. Atmos.* 2013JD020478. doi:10.1002/2013JD020478
- Wang, J., Aegeerter, C., Xu, X., Szykman, J.J., 2016. Potential application of VIIRS Day/Night Band for monitoring nighttime surface PM 2.5 air quality from space. *Atmos. Environ.* 124, 55–63.
- Wang, Z., Schaaf, C.B., Strahler, A.H., Chopping, M.J., Román, M.O., Shuai, Y., Woodcock, C.E., Hollinger, D.Y., Fitzjarrald, D.R., 2014. Evaluation of MODIS albedo product (MCD43A) over grassland, agriculture and forest surface types during dormant and snow-covered periods. *Remote Sens. Environ.* 140, 60–77. doi:10.1016/j.rse.2013.08.025
- Wang, Z., Schaaf, C.B., Strahler, A.H., Wang, J., Woodcock, C.E., Chopping, M.J., Román, M.O., Rocha, A.V., Shuai, Y., 2012. Evaluation of Moderate-resolution Imaging Spectroradiometer (MODIS) snow albedo product (MCD43A) over tundra. *Remote Sens. Environ.* 117, 264–280. doi:doi:10.1016/j.rse.2011.10.002
- Wang, Z., Román, M. O., Sun, Q., Molthan, A. L., Schultz, L. A., and Kalb, V. L. (2018). Monitoring Disaster-related Power Outages Using NASA Black Marble Nighttime Light Product. *Int. Arch. Photogramm. Remote Sens. Spatial Inf. Sci.*, XLII-3, 1853-1856, <https://doi.org/10.5194/isprs-archives-XLII-3-1853-2018>, 2018.
- Wang, Z., Román, M.O., Kalb, V.L., Miller, S.D., Zhang, J., Shrestha, R.M., 2021. Quantifying uncertainties in nighttime light retrievals from Suomi-NPP and NOAA-20 VIIRS Day/Night Band data. *Remote Sensing of Environment* 263, 112557. <https://doi.org/10.1016/J.RSE.2021.112557>
- Wang, Z., Shrestha, R.M., Roman, M.O., Kalb, V.L., 2022. NASA's Black Marble Multiangle Nighttime Lights Temporal Composites. *IEEE Geoscience and Remote Sensing Letters* 19. <https://doi.org/10.1109/LGRS.2022.3176616>
- Wang, Z., Shrestha, R. and Román, M. O., (2018). NASA's Black Marble Nighttime Lights Product Suite Algorithm Theoretical Basis Document (ATBD), Version 1.0, April 2018. Available in https://viirsland.gsfc.nasa.gov/PDF/VIIRS_BlackMarble_ATBD_V1.0.pdf.
- Wickland, D., Gobron, N., Moore, B., Nakajima, M., Sathyendranath, S., Plummer, S., Schmullius, C., Dubayah, R., 2014. CEOS Strategy for Carbon Observations from Space. 40th COSPAR Sci. Assem. Held 2-10 August 2014, Moscow, Russ. Abstr. A0. 1-2-14. 40, 3626.
- WMO, 2016. Observing Systems Capabilities Analysis and Review tool: Rolling Requirements Review process, <http://www.wmo.int/pages/prog/www/OSY/RRR-DB.html> (accessed 8.25.17).
- Wolch, J.R., Byrne, J., Newell, J.P., 2014. Urban green space, public health, and environmental justice: The challenge of making cities “just green enough.” *Landsc. Urban Plan.* 125, 234–244. Wolfe, R.E., Lin, G., Nishihama, M., Tewari, K.P., Tilton, J.C., Isaacman, A.R., 2013. Suomi NPP VIIRS prelaunch and on - orbit geometric calibration and characterization. *J. Geophys. Res. Atmos.* 118.
- Wolfe, R.E., Nishihama, M., Fleig, A.J., Kuyper, J.A., Roy, D.P., Storey, J.C., Patt, F.S., 2002. Achieving sub-pixel geolocation accuracy in support of MODIS land science. *Remote Sens. Environ.* 83, 31–49.
- Wolfe, R.E., Roy, D.P., Vermote, E., 1998. MODIS land data storage, gridding, and compositing methodology: Level 2 grid. *IEEE Trans. Geosci. Remote Sens.* 36, 1324–1338.
- World Bank, 2017. Rebuilding Infrastructure and Improving Access to Employment in Post Crisis Côte d'Ivoire [WWW Document]. World Bank. URL <http://www.worldbank.org/en/results/2016/06/17/rebuilding-infrastructure-and-improving-access-to-employment-in-post-crisis-cote-divoire> (accessed 10.24.17).
- Xiao, Z., Liang, S., Wang, T., Jiang, B., 2016. Retrieval of Leaf Area Index (LAI) and Fraction of Absorbed Photosynthetically Active Radiation (FAPAR) from VIIRS Time-Series Data. *Remote Sens.* 8, 351.
- Xiong, X., Butler, J., Chiang, K., Efremova, B., Fulbright, J., Lei, N., McIntire, J., Oudrari, H., Sun, J., Wang, Z., 2014. VIIRS on - orbit calibration methodology and performance. *J. Geophys. Res. Atmos.* 119, 5065–5078.
- Yang, K., Wolfe, R.E., 2001. MODIS level 2 grid with the ISIN map projection, in: *Geoscience and Remote Sensing Symposium, 2001. IGARSS'01. IEEE 2001 International*. IEEE, pp. 3291–3293.
- Yorks, J., Palm, S., McGill, M., Hlavka, D., Hart, W., Selmer, P., Nowotnick, E., 2015. CATS Algorithm Theoretical Basis Document Level 1 and Level 2 Data Products Release 1.
- Yorks, J.E., McGill, M.J., Palm, S.P., Hlavka, D.L., Selmer, P.A., Nowotnick, E.P., Vaughan, M.A., Rodier, S.D., Hart, W.D., 2016. An overview of the CATS level 1 processing algorithms and data products. *Geophys. Res. Lett.* 43, 4632–4639. doi:10.1002/2016GL068006

Yu, B., Shi, K., Hu, Y., Huang, C., Chen, Z., Wu, J., 2015. Poverty evaluation using NPP-VIIRS nighttime light composite data at the county level in China. *IEEE J. Sel. Top. Appl. Earth Obs. Remote Sens.* 8, 1217–1229. doi:10.1109/JSTARS.2015.2399416

Zhang, Q., Pandey, B., Seto, K.C., 2016. A Robust Method to Generate a Consistent Time Series From DMSP/OLS Nighttime Light Data. *IEEE Trans. Geosci. Remote Sens.* 54, 5821–5831.

Zhang, J., Reid, J. S., Miller, S. D., Román, M., Wang, Z., Spurr, R. J. D., and Jaker, S.: Sensitivity studies of nighttime top-of-atmosphere radiances from artificial light sources using a 3-D radiative transfer model for nighttime aerosol retrievals, *Atmos. Meas. Tech.*, 16, 2531–2546, <https://doi.org/10.5194/amt-16-2531-2023>, 2023.

Zhao, F., Strahler, A.H., Schaaf, C., Yao, T., Yang, X., Wang, Z., Schull, M.A., Román, M.O., Woodcock, C.E., Olofsson, P., Ni-Meister, W., Jupp, D.L.B., Lovell, J.L., Culvenor, D.S., Newnham, G.J., 2012. Measuring Gap Fraction, Element Clumping Index and LAI in Sierra Forest Stands Using a Full-waveform Ground-Based Lidar. *Remote Sens. Environ.* 125, 73–79. doi:10.1016/j.rse.2012.07.007

Zhao, X., Shi, H., Yu, H., Yang, P., 2016. Inversion of Nighttime PM2.5 Mass Concentration in Beijing Based on the VIIRS Day-Night Band. *Atmosphere*, 7, 136.

Appendix A: Metadata (Attributes) in VNP46A1 Product

```
VNP46A1.A2023100.h10v04.002.2024065214519.h5 {
    // global attributes:
    :identifier_product_doi = "10.5067/VIIRS/VNP46A1.002" ;
    :RangeEndingDate = "2023-04-10" ;
    :VerticalTileNumber = "04" ;
    :ReprocessingPlanned = "metadata field" ;
    :NumberofInputGranules = "5" ;
    :DataResolution = "15 arc-second" ;
    :creator_url = "https://ladsweb.modaps.eosdis.nasa.gov" ;
    :SensorShortname = "VIIRS" ;
    :EndTime = "2023-04-10 23:59:59" ;
    :InputPointer_L2G_PNTR =
        "NPP_PTDN.A2023100.h10v04.0536.C2.hdf:NPP_PTDN.A2023100.h10v04.0542.C2.hdf:NPP_PTDN.A2023100.h10v04.0718.C2.hdf:NPP_PTDN.A2023100.h10v04.0724.C2.hdf:NPP_PTDN.A2023100.h10v04.0900.C2.hdf" ;
        :TileID = "61010004" ;
        :NorthBoundingCoord = 50. ;
        :ScienceQualityFlagExplanation = "unknown" ;
        :SatelliteInstrument = "NPP_OPS" ;
        :useCM = "Yes" ;
        :creator_name = "VIIRS Land SIPS Processing Group" ;
        :ReprocessingActual = "metadata field" ;
        :InputPointer_DNB =
            "/MODAPSops4/archive/f20183/running/VNP_L5dglu/57076768/VNP03DNB.A2023100.0536.002.2023100120446.nc:/MODAPSops4/archive/f20183/running/VNP_L5dglu/57076768/VNP03DNB.A2023100.0542.002.2023100120444.nc:/MODAPSops4/archive/f20183/running/VNP_L5dglu/57076768/VNP03DNB.A2023100.0718.002.2023100135952.nc:/MODAPSops4/archive/f20183/running/VNP_L5dglu/57076768/VNP03DNB.A2023100.0724.002.2023100135955.nc:/MODAPSops4/archive/f20183/running/VNP_L5dglu/57076768/VNP03DNB.A2023100.0900.002.2023100152748.nc" ;
        :publisher_name = "LAADS" ;
```

```

:LongName = "VIIRS/NPP Daily Gridded Day Night Band 15 arc-second Linear Lat Lon Grid Night" ;
:ProcessVersion = "002" ;
:naming_authority = "gov.nasa.gsfc.VIIRSland" ;
:InputPointer =
"VNP03MOD.A2023100.0536.002.2023100120446.nc,VNP03MOD.A2023100.0542.002.2023100120444.nc,VNP03MOD.A2023100.0718.002.2023100135952.nc,VNP03MOD.A2023100.0724.002.2023100135955.nc,VNP03MOD.A2023100.0900.002.2023100152748.nc,VNP35_L2.A2023100.0536.002.2023105170610.hdf,VNP35_L2.A2023100.0542.002.2023105170148.hdf,VNP35_L2.A2023100.0718.002.2023105170229.hdf,VNP35_L2.A2023100.0724.002.2023105170130.hdf,VNP35_L2.A2023100.0900.002.2023105170141.hdf,VNP02MOD.A2023100.0536.002.2023100122239.nc,VNP02MOD.A2023100.0542.002.2023100122206.nc,VNP02MOD.A2023100.0718.002.2023100141726.nc,VNP02MOD.A2023100.0724.002.2023100141810.nc,VNP02M OD.A2023100.0900.002.2023100154601.nc,VNP03DNB.A2023100.0536.002.2023100120446.nc,VNP03DNB.A2023100.0542.002.2023100120444.nc,VNP03DNB.A2023100.0718.002.2023100135952.nc,VNP03DNB.A2023100.0724.002.2023100135955.nc,VNP03DNB.A2023100.0900.002.2023100152748.nc,VNP02DNB.A2023100.0536.002.2023100122239.nc,VNP02DNB.A2023100.0542.002.2023100122206.nc,VNP02DNB.A2023100.0718.002.2023100141726.nc,VNP02DNB.A2023100.0900.002.2023100154601.nc" ;
:CMfill = "No" ;
:PGEVersion = "2.0.7" ;
:creator_email = "modis-ops@lists.nasa.gov" ;
:VersionID = "002" ;
:SouthBoundingCoord = 40. ;
:TileMode = "Night" ;
:RangeEndingTime = "23:59:59" ;
:GRingSequence = 1U, 2U, 3U, 4U ;
:identifier_product_doi_authority = "https://doi.org" ;
:comment = "For additional information regarding traceability for reference-based sensor calibration, VIIRS Level-1B measurement uncertainty, and radiometric accuracy, refer to the following DOI: identifier_product_doi = 10.5067/VIIRS/VNP02DNB.002; For additional information regarding geometric correction methods and reference data sources, and geometric accuracy of the L1 data, refer to the following DOI: identifier_product_doi = 10.5067/VIIRS/VNP03DNB.002" ;
:ProcessingCenter = "LandSIPS" ;
:Conventions = "CF-1.6" ;
:InputPointer_Mod =
"/MODAPSops4/archive/f20183/running/VNP_L5dglu/57076768/VNP02MOD.A2023100.0536.002.2023100122239.nc:/MODAPSops4/archive/f20183/running/VNP_L5dglu/57076768/VNP02MOD.A2023100.0718.002.2023100141726.nc:/MODAPSops4/archive/f20183/running/VNP_L5dglu/57076768/VNP02MOD.A2023100.0724.002.2023100141810.nc:/MODAPSops4/archive/f20183/running/VNP_L5dglu/57076768/VNP02MOD.A2023100.0900.002.2023100154601.nc" ;
:ProcessingEnvironment = "Linux minion20183 5.4.0-1082-fips #91-Ubuntu SMP Wed Jul 19 21:56:44 UTC 2023 x86_64 x86_64 x86_64"
GNU/Linux ;
:HorizontalTileNumber = "10" ;
:PGE_Name = "PGE54" ;
:EastBoundingCoord = -70. ;
:InputPointer_CM =
"NPP_CMN.data.A2023100.h10v04.0536.C2.hdf:NPP_CMN.data.A2023100.h10v04.0542.C2.hdf:NPP_CMN.data.A2023100.h10v04.0718.C2.hdf:NPP_CMN.data.A2023100.h10v04.0724.C2.hdf:NPP_CMN.data.A2023100.h10v04.0900.C2.hdf" ;
:PGE_EndTime = "2023-04-10 23:59:59.000000Z" ;
:InputPointer_L2G_DNB =
"NPP_DNBN.data.A2023100.h10v04.0536.C2.hdf:NPP_DNBN.data.A2023100.h10v04.0542.C2.hdf:NPP_DNBN.data.A2023100.h10v04.0718.C2.hdf:NPP_DNBN.data.A2023100.h10v04.0724.C2.hdf:NPP_DNBN.data.A2023100.h10v04.0900.C2.hdf" ;
:GRingLongitude = -80., -80., -70., -70. ;
:ShortName = "VNP46A1" ;
:StartTime = "2023-04-10 00:00:00" ;
:DayNightFlag = "Night" ;
:RangeBeginningTime = "00:00:00" ;
:publisher_url = "https://ladsweb.modaps.eosdis.nasa.gov" ;
:GRingLatitude = 40., 50., 50., 40. ;
:PGENumber = "554" ;
:RangeBeginningDate = "2023-04-10" ;
:InputPointer_L2G_Ang =
"NPP_DNBN.angles.A2023100.h10v04.0536.C2.hdf:NPP_DNBN.angles.A2023100.h10v04.0542.C2.hdf:NPP_DNBN.angles.A2023100.h10v04.0718.C2.hdf:NPP_DNBN.angles.A2023100.h10v04.0724.C2.hdf:NPP_DNBN.angles.A2023100.h10v04.0900.C2.hdf" ;
:PlatformShortName = "SUOMI-NPP" ;
:PGE_StartTime = "2023-04-10 00:00:00.000" ;
:AlgorithmVersion = "NPP_PRDNBdaily 1.0.2" ;
:publisher_email = "modis-ops@lists.nasa.gov" ;
:LocalGranuleID = "VNP46A1.A2023100.h10v04.002.2024065214519.h5" ;
:AlgorithmType = "SCI" ;
:WestBoundingCoord = -80. ;
:ProductionTime = "2024-03-05 21:45:19.000" ;

```

group: HDFEOS {

group: ADDITIONAL {

```

group: FILE_ATTRIBUTES {
} // group FILE_ATTRIBUTES
} // group ADDITIONAL

```

group: GRIDS {

group: VIIRS_Grid_DNB_2d {

```

group: Data\Fields {
dimensions:
phony_dim_0 = 2400 ;
phony_dim_1 = 2400 ;
variables:
 ushort BrightnessTemperature_M12(phony_dim_0, phony_dim_1) ;
    BrightnessTemperature_M12:valid_min = 0 ;
    BrightnessTemperature_M12:valid_max = 65534 ;
    BrightnessTemperature_M12:_FillValue = 65535US ;
    BrightnessTemperature_M12:long_name = "Brightness Temperature of band M12 " ;
    BrightnessTemperature_M12:units = "Kelvins" ;
    BrightnessTemperature_M12:scale_factor = 0.0025f ;
    BrightnessTemperature_M12:add_offset = 203.f ;
 ushort BrightnessTemperature_M13(phony_dim_0, phony_dim_1) ;
    BrightnessTemperature_M13:valid_min = 0 ;
    BrightnessTemperature_M13:valid_max = 65534 ;
    BrightnessTemperature_M13:_FillValue = 65535US ;
    BrightnessTemperature_M13:long_name = "Brightness Temperature of band M13 " ;
    BrightnessTemperature_M13:units = "Kelvins" ;
    BrightnessTemperature_M13:scale_factor = 0.0025f ;
    BrightnessTemperature_M13:add_offset = 203.f ;
 ushort BrightnessTemperature_M15(phony_dim_0, phony_dim_1) ;
    BrightnessTemperature_M15:valid_min = 0 ;
    BrightnessTemperature_M15:valid_max = 65534 ;
    BrightnessTemperature_M15:_FillValue = 65535US ;
    BrightnessTemperature_M15:long_name = "Brightness Temperature of band M15 " ;
    BrightnessTemperature_M15:units = "Kelvins" ;
    BrightnessTemperature_M15:scale_factor = 0.0041f ;
    BrightnessTemperature_M15:add_offset = 111.f ;
 ushort BrightnessTemperature_M16(phony_dim_0, phony_dim_1) ;
    BrightnessTemperature_M16:valid_min = 0 ;
    BrightnessTemperature_M16:valid_max = 65534 ;
    BrightnessTemperature_M16:_FillValue = 65535US ;
    BrightnessTemperature_M16:long_name = "Brightness Temperature of band M16 " ;
    BrightnessTemperature_M16:units = "Kelvins" ;
    BrightnessTemperature_M16:scale_factor = 0.0043f ;
    BrightnessTemperature_M16:add_offset = 103.f ;
float DNB_At_Sensor_Radiance(phony_dim_0, phony_dim_1) ;
    DNB_At_Sensor_Radiance:valid_min = 0 ;
    DNB_At_Sensor_Radiance:_FillValue = -999.9f ;
    DNB_At_Sensor_Radiance:long_name = "DNB at Sensor Radiance" ;
    DNB_At_Sensor_Radiance:units = "nW/(cm2 sr)" ;
    DNB_At_Sensor_Radiance:scale_factor = 1.f ;
    DNB_At_Sensor_Radiance:add_offset = 0.f ;
short Glint_Angle(phony_dim_0, phony_dim_1) ;
    Glint_Angle:valid_min = -18000 ;
    Glint_Angle:valid_max = 18000 ;
    Glint_Angle:_FillValue = -32768s ;
    Glint_Angle:long_name = "Glint Angle" ;
    Glint_Angle:units = "degrees" ;
    Glint_Angle:scale_factor = 0.01f ;
    Glint_Angle:add_offset = 0.f ;
ubyte Granule(phony_dim_0, phony_dim_1) ;
    Granule:valid_min = 0 ;
    Granule:valid_max = 254 ;
    Granule:_FillValue = 255UB ;
    Granule:long_name = "Number of selected Granule" ;
    Granule:units = "none" ;
    Granule:scale_factor = 1.f ;
    Granule:add_offset = 0.f ;
short Lunar_Azimuth(phony_dim_0, phony_dim_1) ;
    Lunar_Azimuth:valid_min = -18000 ;
    Lunar_Azimuth:valid_max = 18000 ;
    Lunar_Azimuth:_FillValue = -32768s ;
    Lunar_Azimuth:long_name = "Lunar Azimuth Angle" ;
    Lunar_Azimuth:units = "degrees" ;
    Lunar_Azimuth:scale_factor = 0.01f ;
    Lunar_Azimuth:add_offset = 0.f ;
short Lunar_Zenith(phony_dim_0, phony_dim_1) ;
    Lunar_Zenith:valid_min = 0 ;
    Lunar_Zenith:valid_max = 18000 ;
    Lunar_Zenith:_FillValue = -32768s ;
    Lunar_Zenith:long_name = "Lunar Zenith Angle" ;
    Lunar_Zenith:units = "degrees" ;
    Lunar_Zenith:scale_factor = 0.01f ;
    Lunar_Zenith:add_offset = 0.f ;
short Moon_Illumination_Fraction(phony_dim_0, phony_dim_1) ;
    Moon_Illumination_Fraction:valid_min = 0 ;

```

```

Moon_Illumination_Fraction:valid_max = 10000 ;
Moon_Illumination_Fraction:_FillValue = -32768s ;
Moon_Illumination_Fraction:long_name = "Moon Illumination Fraction" ;
Moon_Illumination_Fraction:units = "percentage" ;
Moon_Illumination_Fraction:scale_factor = 0.01f ;
Moon_Illumination_Fraction:add_offset = 0.f ;
short Moon_Phase_Angle(phony_dim_0, phony_dim_1) ;
    Moon_Phase_Angle:valid_min = 0 ;
    Moon_Phase_Angle:valid_max = 18000 ;
    Moon_Phase_Angle:_FillValue = -32768s ;
    Moon_Phase_Angle:long_name = "Moon Phase Angle" ;
    Moon_Phase_Angle:units = "degrees" ;
    Moon_Phase_Angle:scale_factor = 0.01f ;
    Moon_Phase_Angle:add_offset = 0.f ;
ushort QF_Cloud_Mask(phony_dim_0, phony_dim_1) ;
    QF_Cloud_Mask:valid_min = 0 ;
    QF_Cloud_Mask:valid_max = 65534 ;
    QF_Cloud_Mask:_FillValue = 65535US ;
    QF_Cloud_Mask:long_name = "Cloud Mask Status" ;
    QF_Cloud_Mask:units = "flag, no units" ;
    QF_Cloud_Mask:flag_meanings = "bit 0: Night, 1=Day\n bits 1-3: Land/Water 000=Land & Desert, 001=Land & no Desert, 010=Inland Water, 011=Sea Water, 101=Coastal\n bits 4-5: Cloud Mask Quality 00=Poor, 01=Low, 10=Medium, 11=High\n bits 6-7: Cloud Confidence 00=Confident Clear, 01=Probably Clear, 10=Probably Cloudy, 11=Confident Cloudy\n bit 8: Shadow Detected 1=Yes, 0=No\n bit 9: Cirrus Detection (IR) 1=Cloud, 0=No Cloud\n bit 10: Snow/Ice 1=Snow/Ice, 0=No Snow/Ice\n bit 11: VI used\n bit 12: aurora detected\n bit 13: lunar eclipse detected , bits 11-13: 1=Yes; 0=No " ;
    ushort QF_DNB(phony_dim_0, phony_dim_1) ;
        QF_DNB:valid_min = 0 ;
        QF_DNB:valid_max = 65534 ;
        QF_DNB:_FillValue = 65535US ;
        QF_DNB:long_name = "DNB QF" ;
        QF_DNB:units = " flag, no units " ;
    ushort QF_VIIRS_M10(phony_dim_0, phony_dim_1) ;
        QF_VIIRS_M10:valid_min = 0 ;
        QF_VIIRS_M10:valid_max = 65534 ;
        QF_VIIRS_M10:_FillValue = 65535US ;
        QF_VIIRS_M10:long_name = "Quality Flag of Band M10" ;
        QF_VIIRS_M10:units = " flag, no units " ;
    ushort QF_VIIRS_M11(phony_dim_0, phony_dim_1) ;
        QF_VIIRS_M11:valid_min = 0 ;
        QF_VIIRS_M11:valid_max = 65534 ;
        QF_VIIRS_M11:_FillValue = 65535US ;
        QF_VIIRS_M11:long_name = "Quality Flag of Band M11" ;
        QF_VIIRS_M11:units = "flag, no units " ;
    ushort QF_VIIRS_M12(phony_dim_0, phony_dim_1) ;
        QF_VIIRS_M12:valid_min = 0 ;
        QF_VIIRS_M12:valid_max = 65534 ;
        QF_VIIRS_M12:_FillValue = 65535US ;
        QF_VIIRS_M12:long_name = "Quality Flag of Band M12" ;
        QF_VIIRS_M12:units = "flag, no units " ;
    ushort QF_VIIRS_M13(phony_dim_0, phony_dim_1) ;
        QF_VIIRS_M13:valid_min = 0 ;
        QF_VIIRS_M13:valid_max = 65534 ;
        QF_VIIRS_M13:_FillValue = 65535US ;
        QF_VIIRS_M13:long_name = "Quality Flag of Band M13" ;
        QF_VIIRS_M13:units = "flag, no units " ;
    ushort QF_VIIRS_M15(phony_dim_0, phony_dim_1) ;
        QF_VIIRS_M15:valid_min = 0 ;
        QF_VIIRS_M15:valid_max = 65534 ;
        QF_VIIRS_M15:_FillValue = 65535US ;
        QF_VIIRS_M15:long_name = "Quality Flag of Band M15" ;
        QF_VIIRS_M15:units = " flag, no units " ;
    ushort QF_VIIRS_M16(phony_dim_0, phony_dim_1) ;
        QF_VIIRS_M16:valid_min = 0 ;
        QF_VIIRS_M16:valid_max = 65534 ;
        QF_VIIRS_M16:_FillValue = 65535US ;
        QF_VIIRS_M16:long_name = "Quality Flag of Band M16" ;
        QF_VIIRS_M16:units = "flag, no units " ;
    ushort Radiance_M10(phony_dim_0, phony_dim_1) ;
        Radiance_M10:valid_min = 0 ;
        Radiance_M10:valid_max = 65534 ;
        Radiance_M10:_FillValue = 65535US ;
        Radiance_M10:long_name = "Band M10 Radiance" ;
        Radiance_M10:units = "W/(m2 micron sr)" ;
        Radiance_M10:scale_factor = 0.0013f ;
        Radiance_M10:add_offset = -0.04f ;
    ushort Radiance_M11(phony_dim_0, phony_dim_1) ;
        Radiance_M11:valid_min = 0 ;
        Radiance_M11:valid_max = 65534 ;

```

```

Radiance_M11:_FillValue = 65535US ;
Radiance_M11:long_name = "Band M11 Radiance" ;
Radiance_M11:units = "W/(m2 micron sr)" ;
Radiance_M11:scale_factor = 0.00058f ;
Radiance_M11:add_offset = -0.02f ;
short Sensor_Azimuth(phony_dim_0, phony_dim_1) ;
  Sensor_Azimuth:valid_min = -18000 ;
  Sensor_Azimuth:valid_max = 18000 ;
  Sensor_Azimuth:_FillValue = -32768s ;
  Sensor_Azimuth:long_name = "Sensor Azimuth Angle" ;
  Sensor_Azimuth:units = "degrees" ;
  Sensor_Azimuth:scale_factor = 0.01f ;
  Sensor_Azimuth:add_offset = 0.f ;
short Sensor_Zenith(phony_dim_0, phony_dim_1) ;
  Sensor_Zenith:valid_min = 0 ;
  Sensor_Zenith:valid_max = 9000 ;
  Sensor_Zenith:_FillValue = -32768s ;
  Sensor_Zenith:long_name = "Sensor Zenith Angle" ;
  Sensor_Zenith:units = "degrees" ;
  Sensor_Zenith:scale_factor = 0.01f ;
  Sensor_Zenith:add_offset = 0.f ;
short Solar_Azimuth(phony_dim_0, phony_dim_1) ;
  Solar_Azimuth:valid_min = -18000 ;
  Solar_Azimuth:valid_max = 18000 ;
  Solar_Azimuth:_FillValue = -32768s ;
  Solar_Azimuth:long_name = "Solar Azimuth Angle" ;
  Solar_Azimuth:units = "degrees" ;
  Solar_Azimuth:scale_factor = 0.01f ;
  Solar_Azimuth:add_offset = 0.f ;
short Solar_Zenith(phony_dim_0, phony_dim_1) ;
  Solar_Zenith:valid_min = 0 ;
  Solar_Zenith:valid_max = 18000 ;
  Solar_Zenith:_FillValue = -32768s ;
  Solar_Zenith:long_name = "Solar Zenith Angle" ;
  Solar_Zenith:units = "degrees" ;
  Solar_Zenith:scale_factor = 0.01f ;
  Solar_Zenith:add_offset = 0.f ;
float UTC_Time(phony_dim_0, phony_dim_1) ;
  UTC_Time:valid_min = 0 ;
  UTC_Time:valid_max = 24 ;
  UTC_Time:_FillValue = -999.9f ;
  UTC_Time:long_name = "View Time (UTC)" ;
  UTC_Time:units = "decimal hours" ;
  UTC_Time:scale_factor = 1.f ;
  UTC_Time:add_offset = 0.f ;
double lat(phony_dim_0) ;
  lat:long_name = "latitude" ;
  lat:units = "degrees_north" ;
  lat:_CoordinateAxisType = "Lat" ;
  lat:valid_min = -90.f ;
  lat:valid_max = 90.f ;
  lat:_FillValue = -999.9f ;
double lon(phony_dim_0) ;
  lon:long_name = "longitude" ;
  lon:units = "degrees_east" ;
  lon:_CoordinateAxisType = "Lon" ;
  lon:valid_min = -180.f ;
  lon:valid_max = 180.f ;
  lon:_FillValue = -999.9f ;
} // group Data\ Fields
} // group VIIRS_Grid_DNB_2d
} // group GRIDS
} // group HDFEOS

group: HDFEOS\ INFORMATION {
variables:
  string StructMetadata.0 ;

// group attributes:
  :HDFEOSVersion = "HDFEOS_5.1.16" ;
} // group HDFEOS\ INFORMATION
}

```

Appendix B: Metadata (Attributes) in VNP46A2 Product

```

netcdf VNP46A2.A2024100.h10v04.002.2024147200718.h5 {
    // global attributes:
        :identifier_product_doi = "10.5067/VIIRS/VNP46A2.002" ;
        :RangeEndingDate = "2024-04-09" ;
        :VerticalTileNumber = "04" ;
        :DataResolution = "15 arc-second" ;
        :creator_url = "https://ladsweb.modaps.eosdis.nasa.gov" ;
        :SensorShortname = "VIIRS" ;
        :EndTime = "2024-04-09 23:59:59.000" ;
        :TileID = "61010004" ;
        :NorthBoundingCoord = 50.f ;
        :SatelliteInstrument = "NPP_OPS" ;
        :creator_name = "VIIRS Land SIPS Processing Group" ;
        :GranuleDayNightFlag = "Night" ;
        :publisher_name = "LAADS" ;
        :LongName = "VIIRS/NPP Gap-Filled Lunar BRDF-Adjusted Nighttime Lights Daily L3 Global 15 arc-second Linear Lat Lon Grid" ;
        :naming_authority = "gov.nasa.gsfc.VIIRSLand" ;
        :InputPointer =
    "VNPLG09GA.A2024100.h10v04.002.2024143025114.h5,VNPLG43DNBA1.A2024100.h10v04.002.2024147193254.h5,MCD12Q1.A2013001.Global.005.T1.Geo.h10v04.bin,MCD12Q1.A2013001.Global.005.T3.Geo.h10v04.bin,VNP46A1.A2024100.h10v04.002.2024101084459.h5,VNP04LGA.A2024100.h10v04.002.2024147200632.hdf,MODLG44W.A2012001.h10v04.006.2020176000000.bin,VNP46A2_DB.A2024099.h10v04.001.2024147192523.hdf"
;

        :PGEVersion = "2.0.4" ;
        :creator_email = "modis-ops@lists.nasa.gov" ;
        :VersionID = "002" ;
        :SouthBoundingCoord = 40.f ;
        :RangeEndingTime = "23:59:59.000" ;
        :identifier_product_doi_authority = "https://doi.org" ;
        :comment = "For additional information regarding traceability for reference-based sensor calibration, VIIRS Level-1B measurement uncertainty, and radiometric accuracy, refer to the following DOIs: identifier_product_doi = 10.5067/VIIRS/VNP02IMG.002; 10.5067/VIIRS/VNP02MOD.002; 10.5067/VIIRS/VNP02DNB.002; For additional information regarding geometric correction methods and reference data sources, and geometric accuracy of the L1 data, refer to the following DOI: identifier_product_doi = 10.5067/VIIRS/VNP03IMG.002; 10.5067/VIIRS/VNP03MOD.002; 10.5067/VIIRS/VNP03DNB.002" ;
        :ProcessingCenter = "LandSIPS" ;
        :Conventions = "CF-1.6" ;
        :ProcessingEnvironment = "Linux minion20013 5.4.0-1093-fips #103-Ubuntu SMP Thu Feb 8 14:02:37 UTC 2024 x86_64 x86_64 x86_64
GNU/Linux" ;
        :HorizontalTileNumber = "10" ;
        :PGE_Name = "PGE555" ;
        :EastBoundingCoord = -70.f ;
        :PGE_EndTime = "2024-04-09 23:59:59.000" ;
        :ShortName = "VNP46A2" ;
        :StartTime = "2024-04-09 00:00:00.000" ;
        :DayNightFlag = "Night" ;
        :RangeBeginningTime = "00:00:00.000" ;
        :publisher_url = "https://ladsweb.modaps.eosdis.nasa.gov" ;
        :GRingPointLongitude = -80., -80., -70., -70. ;
        :PGENumber = "555" ;
        :RangeBeginningDate = "2024-04-09" ;
        :PlatformShortName = "SUOMI-NPP" ;
        :PGE_StartTime = "2024-04-09 00:00:00.000" ;
        :GRingPointLatitude = 40., 50., 50., 40. ;
        :GRingPointSequenceNo = 1, 2, 3, 4 ;
        :AlgorithmVersion = "NPP_PR46A2 1.0.3" ;
        :publisher_email = "modis-ops@lists.nasa.gov" ;
        :LocalGranuleID = "VNP46A2.A2024100.h10v04.002.2024147200718.h5" ;
        :AlgorithmType = "SCI" ;
        :WestBoundingCoord = -80.f ;
        :ProductionTime = "2024-05-26 20:07:18.000" ;

group: HDFEOS {
    group: ADDITIONAL {
        group: FILE_ATTRIBUTES {
            } // group FILE_ATTRIBUTES
        } // group ADDITIONAL
    group: GRIDS {
        group: VIIRS_Grid_DNB_2d {
            group: Data\Fields {

```

```

dimensions:
    phony_dim_0 = 2400 ;
    phony_dim_1 = 2400 ;
variables:
    float DNB_BRDF-Corrected_NTL(phony_dim_0, phony_dim_1) ;
        DNB_BRDF-Corrected_NTL:_FillValue = -999.9f ;
        DNB_BRDF-Corrected_NTL:long_name = "BRDF Corrected DNB Radiance" ;
        DNB_BRDF-Corrected_NTL:units = "nWatts/(cm^2 sr)\n" ;
        DNB_BRDF-Corrected_NTL:valid_range = ">=0.0 \n" ;
        DNB_BRDF-Corrected_NTL:scale_factor = 1.0 ;
        DNB_BRDF-Corrected_NTL:offset = 0. ;
    ushort DNB_Lunar_Irradiance(phony_dim_0, phony_dim_1) ;
        DNB_Lunar_Irradiance:_FillValue = 65535US ;
        DNB_Lunar_Irradiance:long_name = "Lunar Irradiance" ;
        DNB_Lunar_Irradiance:units = "nWatts/cm^2 \n" ;
        DNB_Lunar_Irradiance:valid_range = "0-65534 \n" ;
        DNB_Lunar_Irradiance:offset = 0. ;
        DNB_Lunar_Irradiance:scale_factor = 0.1 ;
    float Gap_Filled_DNB_BRDF-Corrected_NTL(phony_dim_0, phony_dim_1) ;
        Gap_Filled_DNB_BRDF-Corrected_NTL:_FillValue = -999.9f ;
        Gap_Filled_DNB_BRDF-Corrected_NTL:long_name = "Gap Filled BRDF Corrected DNB Radiance" ;
        Gap_Filled_DNB_BRDF-Corrected_NTL:units = "nWatts/(cm^2 sr)\n" ;
        Gap_Filled_DNB_BRDF-Corrected_NTL:valid_range = ">=0.0 \n" ;
        Gap_Filled_DNB_BRDF-Corrected_NTL:offset = 0. ;
        Gap_Filled_DNB_BRDF-Corrected_NTL:scale_factor = 1.0 ;
    ubyte Latest_High_Quality_Retrieval(phony_dim_0, phony_dim_1) ;
        Latest_High_Quality_Retrieval:_FillValue = 255UB ;
        Latest_High_Quality_Retrieval:units = "Number of Days \n" ;
        Latest_High_Quality_Retrieval:long_name = "The Latest High Quality BRDF Corrected DNB Radiance Retrieval" ;
        Latest_High_Quality_Retrieval:valid_range = "0 - 254 \n" ;
        Latest_High_Quality_Retrieval:scale_factor = 1. ;
        Latest_High_Quality_Retrieval:offset = 0. ;
    ubyte Mandatory_Quality_Flag(phony_dim_0, phony_dim_1) ;
        Mandatory_Quality_Flag:_FillValue = 255UB ;
        Mandatory_Quality_Flag:units = "flag, no units \n" ;
        Mandatory_Quality_Flag:long_name = "Mandatory Quality Flag of BRDF Corrected DNB Radiance" ;
        Mandatory_Quality_Flag:valid_range = "0 - 5 \n" ;
        Mandatory_Quality_Flag:Description = "00\High-Quality\Main Algorithm \n01\Poor-Quality\Main Algorithm (Outlier, Potential cloud contamination or other issues)\n02\Poor-Quality\Main Algorithm (high solar zenith angle 102-108 degrees)\n03\Poor-Quality\Main Algorithm (Lunar eclipse)\n04\Poor-Quality\Main Algorithm (Aurora)\n05\Poor-Quality\Main Algorithm (glint)\n255\No Retrieval\Fill Value \n" ;
    ushort QF_Cloud_Mask(phony_dim_0, phony_dim_1) ;
        QF_Cloud_Mask:_FillValue = 65535US ;
        QF_Cloud_Mask:long_name = "Cloud Mask Status" ;
        QF_Cloud_Mask:units = " flag, no units \n" ;
        QF_Cloud_Mask:valid_range = "0 - 65534 \n" ;
        QF_Cloud_Mask:Description = "bit   Flag description key: \n0\Day/Night \n  0=Night 1=Day \n1-3\Land/Water Background \n\n000=Land & Desert \n001=Land no Desert \n010=Inland Water \n011=Sea Water \n012=Coastal \n4-5\Cloud Mask Quality \n\n0=Poor \n01=Low \n10=Medium \n11=High \n6-7\Cloud Detection Results & Confidence Indicator \n\n0=Confident Clear \n\n01=Probably Clear \n10=Probably Cloudy \n11=Confident Cloudy \n8\Shadow Detected \n\n1=Yes 0=No \n9\Cirrus Detection (IR) (BTM15-BTM16) \n10=Cloud 0-No Cloud \n101=Snow/Ice \n  1=Snow/Ice, 0=No Snow/Ice \n11=VI used \n\n1=Yes 0=No \n12=Aurora detected \n\n1=Yes 0=No \n13=Lunar eclipse detected \n\n1=Yes 0=No \n" ;
    ubyte Snow_Flag(phony_dim_0, phony_dim_1) ;
        Snow_Flag:_FillValue = 255UB ;
        Snow_Flag:long_name = "Snow/Ice Status" ;
        Snow_Flag:units = " flag, no units \n" ;
        Snow_Flag:valid_range = "0 - 1 \n" ;
        Snow_Flag:Description = "0 = No snow/ice \n 1 = snow/ice \n" ;
double lat(phony_dim_0) ;
    lat:long_name = "latitude" ;
    lat:units = "degrees_north" ;
    lat:_CoordinateAxisType = "Lat" ;
    lat:valid_min = -90.f ;
    lat:valid_max = 90.f ;
    lat:_FillValue = -999.9f ;
double lon(phony_dim_0) ;
    lon:long_name = "longitude" ;
    lon:units = "degrees_east" ;
    lon:_CoordinateAxisType = "Lon" ;
    lon:valid_min = -180.f ;
    lon:valid_max = 180.f ;
    lon:_FillValue = -999.9f ;
} // group Data\ Fields
} // group VIIRS_Grid_DNB_2d
} // group GRIDS
} // group HDFEOS
group: HDFEOS\ INFORMATION {
variables:

```

```

string StructMetadata.0 ;

// group attributes:
:HDFEOSVersion = "HDFEOS_5.1.16" ;
} // group HDFEOS\ INFORMATION
}

netcdf VNP46A3.A2012183.h10v04.002.2024192174224.h5 {

// global attributes:
:identifier_product_doi = "10.5067/VIIRS/VNP46A3.002" ;
:RangeEndingDate = "2012-07-31" ;
:VerticalTileNumber = "04" ;
:NumberofInputGranules = "31" ;
:DataResolution = "15 arc second" ;
:creator_url = "https://ladsweb.modaps.eosdis.nasa.gov" ;
:SensorShortname = "VIIRS" ;
:EndTime = "2012-08-01 00:00:00" ;
:TileID = "61010004" ;
:NorthBoundingCoord = 50.f ;
:SatelliteInstrument = "NPP_OPS" ;
:creator_name = "VIIRS Land SIPS Processing Group" ;
:GranuleDayNightFlag = "Night" ;
:publisher_name = "LAADS" ;
:LongName = "VIIRS/NPP Lunar BRDF-Adjusted Nighttime Lights Monthly L3 Global 15 arc second Linear Lat Lon Grid" ;
:ProcessVersion = "002" ;
:naming_authority = "gov.nasa.gsfc.VIIRSland" ;
:InputPointer =
"VNP46A1.A2012183.h10v04.002.2024129083350.h5,VNP46A1.A2012184.h10v04.002.2024129085927.h5,VNP46A1.A2012185.h10v04.002.2024129093651.h5,VNP46A1.A2012186.h10v04.002.2024129101257.h5,VNP46A1.A2012187.h10v04.002.2024129105025.h5,VNP46A1.A2012188.h10v04.002.2024129112543.h5,VNP46A1.A2012189.h10v04.002.2024129120305.h5,VNP46A1.A2012190.h10v04.002.2024129123842.h5,VNP46A1.A2012191.h10v04.002.2024129131741.h5,VNP46A1.A2012192.h10v04.002.2024129140304.h5,VNP46A1.A2012193.h10v04.002.2024129145409.h5,VNP46A1.A2012194.h10v04.002.2024129154810.h5,VNP46A1.A2012195.h10v04.002.2024129165300.h5,VNP46A1.A2012196.h10v04.002.2024129175909.h5,VNP46A1.A2012197.h10v04.002.2024129185612.h5,VNP46A1.A2012198.h10v04.002.2024129194549.h5,VNP46A1.A2012199.h10v04.002.2024129203302.h5, VNP46A1.A2012200.h10v04.002.2024129212352.h5,VNP46A1.A2012201.h10v04.002.2024129221522.h5,VNP46A1.A2012202.h10v04.002.202412923 0447.h5,VNP46A1.A2012203.h10v04.002.2024129235428.h5,VNP46A1.A2012204.h10v04.002.2024130004507.h5,VNP46A1.A2012205.h10v04.002.2024130013327.h5,VNP46A1.A2012206.h10v04.002.2024130022233.h5,VNP46A1.A2012207.h10v04.002.2024130031109.h5,VNP46A1.A2012208.h10v04.002.2024130040122.h5,VNP46A1.A2012209.h10v04.002.2024130044755.h5,VNP46A1.A2012210.h10v04.002.2024130053034.h5,VNP46A1.A20122 11.h10v04.002.2024130061104.h5,VNP46A1.A2012212.h10v04.002.2024130080153.h5,VNP46A1.A2012213.h10v04.002.2024130085711.h5,VNP46A2 .A2012183.h10v04.002.2024177151244.h5,VNP46A2.A2012184.h10v04.002.2024177153436.h5,VNP46A2.A2012185.h10v04.002.2024177160448.h5, VNP46A2.A2012186.h10v04.002.202417717163830.h5,VNP46A2.A2012187.h10v04.002.2024177170247.h5,VNP46A2.A2012188.h10v04.002.2024177174 009.h5,VNP46A2.A2012189.h10v04.002.2024177181216.h5,VNP46A2.A2012190.h10v04.002.2024177184631.h5,VNP46A2.A2012191.h10v04.002.202 4177191116.h5,VNP46A2.A2012192.h10v04.002.2024177195051.h5,VNP46A2.A2012193.h10v04.002.2024177202338.h5,VNP46A2.A2012194.h10v04 .002.2024177205215.h5,VNP46A2.A2012195.h10v04.002.2024177212237.h5,VNP46A2.A2012196.h10v04.002.2024177215300.h5,VNP46A2.A201219 7.h10v04.002.2024177221858.h5,VNP46A2.A2012198.h10v04.002.2024177225111.h5,VNP46A2.A2012199.h10v04.002.2024177232341.h5,VNP46A2 .A2012200.h10v04.002.2024177234949.h5,VNP46A2.A2012201.h10v04.002.2024178003018.h5,VNP46A2.A2012202.h10v04.002.2024178005628.h5, VNP46A2.A2012203.h10v04.002.2024178013049.h5,VNP46A2.A2012204.h10v04.002.2024178020145.h5,VNP46A2.A2012205.h10v04.002.202417802 911.h5,VNP46A2.A2012206.h10v04.002.2024178025651.h5,VNP46A2.A2012207.h10v04.002.2024178032319.h5,VNP46A2.A2012208.h10v04.002.202 4178035247.h5,VNP46A2.A2012209.h10v04.002.2024178042501.h5,VNP46A2.A2012210.h10v04.002.2024178044915.h5,VNP46A2.A2012211.h10v04 .002.2024178052000.h5,VNP46A2.A2012212.h10v04.002.2024178054648.h5,VNP46A2.A2012213.h10v04.002.2024178062055.h5" ;
:PGEVersion = "2.0.3" ;
:creator_email = "modis-ops@lists.nasa.gov" ;
:VersionID = "002" ;
:SouthBoundingCoord = 40.f ;
:RangeEndingTime = "23:59:00.000000" ;
:identifier_product_doi_authority = "https://doi.org" ;
:ProcessingCenter = "LandSIPS" ;
:Conventions = "CF-1.6" ;
:ProcessingEnvironment = "Linux minion20200 5.4.0-1093-fips #103-Ubuntu SMP Thu Feb 8 14:02:37 UTC 2024 x86_64 x86_64 x86_64"

GNU/Linux ;
:HorizontalTileNumber = "10" ;
:PGE_Name = "PGE556" ;
:EastBoundingCoord = -70.f ;
:PGE_EndTime = "2012-08-01 00:00:00.000" ;
:ShortName = "VNP46A3" ;
:StarTime = "2012-07-01 00:00:00" ;
:DayNightFlag = "Night" ;
:RangeBeginningTime = "00:00:00.000000" ;
:publisher_url = "https://ladsweb.modaps.eosdis.nasa.gov" ;
:GRingPointLongitude = -80., -80., -70., -70. ;
:PGENumber = "556" ;
:RangeBeginningDate = "2012-07-01" ;
}

```

```

:PlatformShortName = "SUOMI-NPP" ;
:PGE_StartTime = "2012-07-01 00:00:00.000" ;
:GRingPointLatitude = 40., 50., 50., 40. ;
:GRingPointSequenceNo = 1, 2, 3, 4 ;
:AlgorithmVersion = "NPP_PR46A3 2.0.0" ;
:publisher_email = "modis-ops@lists.nasa.gov" ;
:LocalGranuleID = "VNP46A3.A2012183.h10v04.002.2024192174224.h5" ;
:AlgorithmType = "SCI" ;
:WestBoundingCoord = -80.f ;
:ProductionTime = "2024-07-10 17:42:24.000" ;

group: HDFEOS {
    group: ADDITIONAL {
        group: FILE_ATTRIBUTES {
            } // group FILE_ATTRIBUTES
        } // group ADDITIONAL
    group: GRIDS {
        group: VIIRS_Grid_DNB_2d {
            group: Data\ Fields {
                dimensions:
                    phony_dim_0 = 2400 ;
                    phony_dim_1 = 2400 ;
                variables:
                    float AllAngle_Composite_Snow_Covered(phony_dim_0, phony_dim_1) ;
                    AllAngle_Composite_Snow_Covered:_FillValue = -999.9f ;
                    AllAngle_Composite_Snow_Covered:long_name = "Temporal Radiance Composite Using All Observations During Snow-covered Period" ;
                    AllAngle_Composite_Snow_Covered:units = "nWatts/(cm^2 sr)" ;
                    AllAngle_Composite_Snow_Covered:valid_range = ">= 0.0\n" ;
                    AllAngle_Composite_Snow_Covered:scale_factor = 1. ;
                    AllAngle_Composite_Snow_Covered:offset = 0. ;
                    AllAngle_Composite_Snow_Covered:coordinates = "latitude longitude" ;
                    ushort AllAngle_Composite_Snow_Covered_Num(phony_dim_0, phony_dim_1) ;
                    AllAngle_Composite_Snow_Covered_Num:_FillValue = 65535US ;
                    AllAngle_Composite_Snow_Covered_Num:long_name = "Number of Observations of Temporal Radiance Composite Using All Observations During Snow-covered Period" ;
                    AllAngle_Composite_Snow_Covered_Num:units = "number of observations" ;
                    AllAngle_Composite_Snow_Covered_Num:valid_range = 0US, 65534US ;
                    AllAngle_Composite_Snow_Covered_Num:scale_factor = 1. ;
                    AllAngle_Composite_Snow_Covered_Num:offset = 0. ;
                    AllAngle_Composite_Snow_Covered_Num:coordinates = "latitude longitude" ;
                    ubyte AllAngle_Composite_Snow_Covered_Quality(phony_dim_0, phony_dim_1) ;
                    AllAngle_Composite_Snow_Covered_Quality:_FillValue = 255UB ;
                    AllAngle_Composite_Snow_Covered_Quality:long_name = "Quality Flag of Temporal Radiance Composite Using All Observations During Snow-covered Period" ;
                    AllAngle_Composite_Snow_Covered_Quality:units = "flag, no units" ;
                    AllAngle_Composite_Snow_Covered_Quality:valid_range = 0UB, 254UB ;
                    AllAngle_Composite_Snow_Covered_Quality:scale_factor = 1. ;
                    AllAngle_Composite_Snow_Covered_Quality:offset = 0. ;
                    AllAngle_Composite_Snow_Covered_Quality:Description = "Quality:\n\t 0 = Good quality\n\t 1 = Poor quality\n\t 2 = Gap filled\n\t 255 = Fill value\n\t" ;
                    AllAngle_Composite_Snow_Covered_Quality:coordinates = "latitude longitude" ;
                    float AllAngle_Composite_Snow_Covered_Std(phony_dim_0, phony_dim_1) ;
                    AllAngle_Composite_Snow_Covered_Std:_FillValue = -999.9f ;
                    AllAngle_Composite_Snow_Covered_Std:long_name = "Standard Deviation of Temporal Radiance Composite Using All Observations During Snow-covered Period" ;
                    AllAngle_Composite_Snow_Covered_Std:units = "nWatts/(cm^2 sr)" ;
                    AllAngle_Composite_Snow_Covered_Std:valid_range = ">= 0.0 \n" ;
                    AllAngle_Composite_Snow_Covered_Std:scale_factor = 1. ;
                    AllAngle_Composite_Snow_Covered_Std:offset = 0. ;
                    AllAngle_Composite_Snow_Covered_Std:coordinates = "latitude longitude" ;
                    float AllAngle_Composite_Snow_Free(phony_dim_0, phony_dim_1) ;
                    AllAngle_Composite_Snow_Free:_FillValue = -999.9f ;
                    AllAngle_Composite_Snow_Free:long_name = "Temporal Radiance Composite Using All Observations During Snow-free Period" ;
                    AllAngle_Composite_Snow_Free:units = "nWatts/(cm^2 sr)" ;
                    AllAngle_Composite_Snow_Free:valid_range = ">= 0.0 \n" ;
                    AllAngle_Composite_Snow_Free:scale_factor = 1. ;
                    AllAngle_Composite_Snow_Free:offset = 0. ;
                    AllAngle_Composite_Snow_Free:coordinates = "latitude longitude" ;
                    ushort AllAngle_Composite_Snow_Free_Num(phony_dim_0, phony_dim_1) ;
                    AllAngle_Composite_Snow_Free_Num:_FillValue = 65535US ;
                    AllAngle_Composite_Snow_Free_Num:long_name = "Number of Observations of Temporal Radiance Composite Using All Observations During Snow-free Period" ;
            } // group Data\ Fields
        } // group GRIDS
    } // group HDFEOS
}
```

```

AllAngle_Composite_Snow_Free_Num:units = "number of observations" ;
AllAngle_Composite_Snow_Free_Num:valid_range = 0US, 65534US ;
AllAngle_Composite_Snow_Free_Num:scale_factor = 1. ;
AllAngle_Composite_Snow_Free_Num:offset = 0. ;
AllAngle_Composite_Snow_Free_Num:coordinates = "latitude longitude" ;
ubyte AllAngle_Composite_Snow_Free_Quality(phony_dim_0, phony_dim_1) ;
    AllAngle_Composite_Snow_Free_Quality:_FillValue = 255UB ;
    AllAngle_Composite_Snow_Free_Quality:long_name = "Quality Flag of Temporal Radiance Composite Using All Observations During
Snow-free Period" ;
        AllAngle_Composite_Snow_Free_Quality:units = "flag, no units" ;
        AllAngle_Composite_Snow_Free_Quality:valid_range = 0UB, 254UB ;
        AllAngle_Composite_Snow_Free_Quality:scale_factor = 1. ;
        AllAngle_Composite_Snow_Free_Quality:offset = 0. ;
        AllAngle_Composite_Snow_Free_Quality:Description = "Quality:\n\t 0 = Good quality\n\t 1 = Poor quality\n\t 2 = Gap filled\n\t 255 =
Fill value\n\t" ;
            AllAngle_Composite_Snow_Free_Quality:coordinates = "latitude longitude" ;
            float AllAngle_Composite_Snow_Free_Std(phony_dim_0, phony_dim_1) ;
                AllAngle_Composite_Snow_Free_Std:_FillValue = -999.9f ;
                AllAngle_Composite_Snow_Free_Std:long_name = "Standard Deviation of Temporal Radiance Composite Using All Observations During
Snow-free Period" ;
                    AllAngle_Composite_Snow_Free_Std:units = "nWatts/(cm^2 sr)" ;
                    AllAngle_Composite_Snow_Free_Std:valid_range = ">= 0.0 \n" ;
                    AllAngle_Composite_Snow_Free_Std:scale_factor = 1. ;
                    AllAngle_Composite_Snow_Free_Std:offset = 0. ;
                    AllAngle_Composite_Snow_Free_Std:coordinates = "latitude longitude" ;
                    ubyte DNB_Platform(phony_dim_0, phony_dim_1) ;
                        DNB_Platform:_FillValue = 255UB ;
                        DNB_Platform:long_name = "Platform" ;
                        DNB_Platform:units = "platform, no units" ;
                        DNB_Platform:valid_range = 0UB, 254UB ;
                        DNB_Platform:scale_factor = 1. ;
                        DNB_Platform:offset = 0. ;
                        DNB_Platform:Description = "Platform:\n\t 0 = Suomi-NPP\n\t 1 = NOAA20\n\t 2 = NOAA21 \n\t 3 = NOAA20 and NOAA21 combined
\n\t" ;
                            DNB_Platform:coordinates = "latitude longitude" ;
                            ubyte Land_Water_Mask(phony_dim_0, phony_dim_1) ;
                                Land_Water_Mask:_FillValue = 255UB ;
                                Land_Water_Mask:long_name = "Land Water Mask" ;
                                Land_Water_Mask:units = "land water mask, no units" ;
                                Land_Water_Mask:valid_range = 0UB, 254UB ;
                                Land_Water_Mask:scale_factor = 1. ;
                                Land_Water_Mask:offset = 0. ;
                                Land_Water_Mask:Description = "Land/Water:\n\t 0 = Land & Desert \n\t 1 = Land no Desert \n\t 2 = Inland Water \n\t 3 = Sea Water
\n\t 5 = Coastal \n\t" ;
                                    Land_Water_Mask:coordinates = "latitude longitude" ;
                                    float NearNadir_Composite_Snow_Covered(phony_dim_0, phony_dim_1) ;
                                        NearNadir_Composite_Snow_Covered:_FillValue = -999.9f ;
                                        NearNadir_Composite_Snow_Covered:long_name = "Temporal Radiance Composite Using Near Nadir Angle Observations (View Zenith
Angle 0-20 degree) During Snow-covered Period" ;
                                            NearNadir_Composite_Snow_Covered:units = "nWatts/(cm^2 sr)" ;
                                            NearNadir_Composite_Snow_Covered:valid_range = ">= 0.0 \n" ;
                                            NearNadir_Composite_Snow_Covered:scale_factor = 1. ;
                                            NearNadir_Composite_Snow_Covered:offset = 0. ;
                                            NearNadir_Composite_Snow_Covered:coordinates = "latitude longitude" ;
                                            ushort NearNadir_Composite_Snow_Covered_Num(phony_dim_0, phony_dim_1) ;
                                                NearNadir_Composite_Snow_Covered_Num:_FillValue = 65535US ;
                                                NearNadir_Composite_Snow_Covered_Num:long_name = "Number of Observations of Temporal Radiance Composite Using Near Nadir
Angle Observations (View Zenith Angle 0-20 degree) During Snow-covered Period" ;
                                                    NearNadir_Composite_Snow_Covered_Num:units = "number of observations" ;
                                                    NearNadir_Composite_Snow_Covered_Num:valid_range = 0US, 65534US ;
                                                    NearNadir_Composite_Snow_Covered_Num:scale_factor = 1. ;
                                                    NearNadir_Composite_Snow_Covered_Num:offset = 0. ;
                                                    NearNadir_Composite_Snow_Covered_Num:coordinates = "latitude longitude" ;
                                                    ubyte NearNadir_Composite_Snow_Covered_Quality(phony_dim_0, phony_dim_1) ;
                                                        NearNadir_Composite_Snow_Covered_Quality:_FillValue = 255UB ;
                                                        NearNadir_Composite_Snow_Covered_Quality:long_name = "Quality Flag of Temporal Radiance Composite Using Near Nadir Angle
Observations (View Zenith Angle 0-20 degree) During Snow-covered Period" ;
                                                            NearNadir_Composite_Snow_Covered_Quality:units = "flag, no units" ;
                                                            NearNadir_Composite_Snow_Covered_Quality:valid_range = 0UB, 254UB ;
                                                            NearNadir_Composite_Snow_Covered_Quality:scale_factor = 1. ;
                                                            NearNadir_Composite_Snow_Covered_Quality:offset = 0. ;
                                                            NearNadir_Composite_Snow_Covered_Quality:Description = "Quality:\n\t 0 = Good quality\n\t 1 = Poor quality\n\t 2 = Gap filled\n\t
255 = Fill value\n\t" ;
                                                                NearNadir_Composite_Snow_Covered_Quality:coordinates = "latitude longitude" ;
                                                                float NearNadir_Composite_Snow_Covered_Std(phony_dim_0, phony_dim_1) ;
                                                                    NearNadir_Composite_Snow_Covered_Std:_FillValue = -999.9f ;
                                                                    NearNadir_Composite_Snow_Covered_Std:long_name = "Standard Deviation of Temporal Radiance Composite Using Near Nadir Angle
Observations (View Zenith Angle 0-20 degree) During Snow-covered Period" ;

```

```

NearNadir_Composite_Snow_Covered_Std:units = "nWatts/(cm^2 sr)" ;
NearNadir_Composite_Snow_Covered_Std:valid_range = ">= 0.0 \n" ;
NearNadir_Composite_Snow_Covered_Std:scale_factor = 1. ;
NearNadir_Composite_Snow_Covered_Std:offset = 0. ;
NearNadir_Composite_Snow_Covered_Std:coordinates = "latitude longitude" ;
float NearNadir_Composite_Snow_Free(phony_dim_0, phony_dim_1) ;
NearNadir_Composite_Snow_Free:_FillValue = -999.9f ;
NearNadir_Composite_Snow_Free:long_name = "Temporal Radiance Composite Using Near Nadir Angle Observations (View Zenith
Angle 0-20 degree) During Snow-free Period" ;
NearNadir_Composite_Snow_Free:units = "nWatts/(cm^2 sr)" ;
NearNadir_Composite_Snow_Free:valid_range = ">= 0.0 \n" ;
NearNadir_Composite_Snow_Free:scale_factor = 1. ;
NearNadir_Composite_Snow_Free:offset = 0. ;
NearNadir_Composite_Snow_Free:coordinates = "latitude longitude" ;
ushort NearNadir_Composite_Snow_Free_Num(phony_dim_0, phony_dim_1) ;
NearNadir_Composite_Snow_Free_Num:_FillValue = 65535US ;
NearNadir_Composite_Snow_Free_Num:long_name = "Number of Observations of Temporal Radiance Composite Using Near Nadir
Angle Observations (View Zenith Angle 0-20 degree) During Snow-free Period" ;
NearNadir_Composite_Snow_Free_Num:units = "number of observations" ;
NearNadir_Composite_Snow_Free_Num:valid_range = 0US, 65534US ;
NearNadir_Composite_Snow_Free_Num:scale_factor = 1. ;
NearNadir_Composite_Snow_Free_Num:offset = 0. ;
NearNadir_Composite_Snow_Free_Num:coordinates = "latitude longitude" ;
ubyte NearNadir_Composite_Snow_Free_Quality(phony_dim_0, phony_dim_1) ;
NearNadir_Composite_Snow_Free_Quality:_FillValue = 255UB ;
NearNadir_Composite_Snow_Free_Quality:long_name = "Quality Flag of Temporal Radiance Composite Using Near Nadir Angle
Observations (View Zenith Angle 0-20 degree) During Snow-free Period" ;
NearNadir_Composite_Snow_Free_Quality:units = "flag, no units" ;
NearNadir_Composite_Snow_Free_Quality:valid_range = 0UB, 254UB ;
NearNadir_Composite_Snow_Free_Quality:scale_factor = 1. ;
NearNadir_Composite_Snow_Free_Quality:offset = 0. ;
NearNadir_Composite_Snow_Free_Quality:Description = "Quality:\n\t 0 = Good quality\n\t 1 = Poor quality\n\t 2 = Gap filled\n\t 255 =
Fill value\n\t" ;
NearNadir_Composite_Snow_Free_Quality:coordinates = "latitude longitude" ;
float NearNadir_Composite_Snow_Free_Std(phony_dim_0, phony_dim_1) ;
NearNadir_Composite_Snow_Free_Std:_FillValue = -999.9f ;
NearNadir_Composite_Snow_Free_Std:long_name = "Standard Deviation of Temporal Radiance Composite Using Near Nadir Angle
Observations (View Zenith Angle 0-20 degree) During Snow-free Period" ;
NearNadir_Composite_Snow_Free_Std:units = "nWatts/(cm^2 sr)" ;
NearNadir_Composite_Snow_Free_Std:valid_range = ">= 0.0 \n" ;
NearNadir_Composite_Snow_Free_Std:scale_factor = 1. ;
NearNadir_Composite_Snow_Free_Std:offset = 0. ;
NearNadir_Composite_Snow_Free_Std:coordinates = "latitude longitude" ;
float OffNadir_Composite_Snow_Covered(phony_dim_0, phony_dim_1) ;
OffNadir_Composite_Snow_Covered:_FillValue = -999.9f ;
OffNadir_Composite_Snow_Covered:long_name = "Temporal Radiance Composite Using Off Nadir Angle Observations (View Zenith
Angle 40-60 degree) During Snow-covered Period" ;
OffNadir_Composite_Snow_Covered:units = "nWatts/(cm^2 sr)" ;
OffNadir_Composite_Snow_Covered:valid_range = ">= 0.0 \n" ;
OffNadir_Composite_Snow_Covered:scale_factor = 1. ;
OffNadir_Composite_Snow_Covered:offset = 0. ;
OffNadir_Composite_Snow_Covered:coordinates = "latitude longitude" ;
ushort OffNadir_Composite_Snow_Covered_Num(phony_dim_0, phony_dim_1) ;
OffNadir_Composite_Snow_Covered_Num:_FillValue = 65535US ;
OffNadir_Composite_Snow_Covered_Num:long_name = "Number of Observations of Temporal Radiance Composite Using Off Nadir
Angle Observations (View Zenith Angle 40-60 degree) During Snow-covered Period" ;
OffNadir_Composite_Snow_Covered_Num:units = "number of observations" ;
OffNadir_Composite_Snow_Covered_Num:valid_range = 0US, 65534US ;
OffNadir_Composite_Snow_Covered_Num:scale_factor = 1. ;
OffNadir_Composite_Snow_Covered_Num:offset = 0. ;
OffNadir_Composite_Snow_Covered_Num:coordinates = "latitude longitude" ;
ubyte OffNadir_Composite_Snow_Covered_Quality(phony_dim_0, phony_dim_1) ;
OffNadir_Composite_Snow_Covered_Quality:_FillValue = 255UB ;
OffNadir_Composite_Snow_Covered_Quality:long_name = "Quality Flag of Temporal Radiance Composite Using Off Nadir Angle
Observations (View Zenith Angle 40-60 degree) During Snow-covered Period" ;
OffNadir_Composite_Snow_Covered_Quality:units = "flag, no units" ;
OffNadir_Composite_Snow_Covered_Quality:valid_range = 0UB, 254UB ;
OffNadir_Composite_Snow_Covered_Quality:scale_factor = 1. ;
OffNadir_Composite_Snow_Covered_Quality:offset = 0. ;
OffNadir_Composite_Snow_Covered_Quality:Description = "Quality:\n\t 0 = Good quality\n\t 1 = Poor quality\n\t 2 = Gap filled\n\t 255 =
Fill value\n\t" ;
OffNadir_Composite_Snow_Covered_Quality:coordinates = "latitude longitude" ;
float OffNadir_Composite_Snow_Covered_Std(phony_dim_0, phony_dim_1) ;
OffNadir_Composite_Snow_Covered_Std:_FillValue = -999.9f ;
OffNadir_Composite_Snow_Covered_Std:long_name = "Standard Deviation of Temporal Radiance Composite Using Off Nadir Angle
Observations (View Zenith Angle 40-60 degree) During Snow-covered Period" ;
OffNadir_Composite_Snow_Covered_Std:units = "nWatts/(cm^2 sr)" ;
OffNadir_Composite_Snow_Covered_Std:valid_range = ">= 0.0 \n" ;

```

```

OffNadir_Composite_Snow_Covered_Std:scale_factor = 1. ;
OffNadir_Composite_Snow_Covered_Std:offset = 0. ;
OffNadir_Composite_Snow_Covered_Std:coordinates = "latitude longitude" ;
float OffNadir_Composite_Snow_Free(phony_dim_0, phony_dim_1) ;
OffNadir_Composite_Snow_Free:_FillValue = -999.9f ;
OffNadir_Composite_Snow_Free:long_name = "Temporal Radiance Composite Using Off Nadir Angle Observations (View Zenith Angle 40-60 degree) During Snow-free Period" ;
OffNadir_Composite_Snow_Free:units = "nWatts/(cm^2 sr)" ;
OffNadir_Composite_Snow_Free:valid_range = ">= 0.0 \n" ;
OffNadir_Composite_Snow_Free:scale_factor = 1. ;
OffNadir_Composite_Snow_Free:offset = 0. ;
OffNadir_Composite_Snow_Free:coordinates = "latitude longitude" ;
ushort OffNadir_Composite_Snow_Free_Num(phony_dim_0, phony_dim_1) ;
OffNadir_Composite_Snow_Free_Num:_FillValue = 65535US ;
OffNadir_Composite_Snow_Free_Num:long_name = "Number of Observations of Temporal Radiance Composite Using Off Nadir Angle Observations (View Zenith Angle 40-60 degree) During Snow-free Period" ;
OffNadir_Composite_Snow_Free_Num:units = "number of observations" ;
OffNadir_Composite_Snow_Free_Num:valid_range = 0US, 65534US ;
OffNadir_Composite_Snow_Free_Num:scale_factor = 1. ;
OffNadir_Composite_Snow_Free_Num:offset = 0. ;
OffNadir_Composite_Snow_Free_Num:coordinates = "latitude longitude" ;
ubyte OffNadir_Composite_Snow_Free_Quality(phony_dim_0, phony_dim_1) ;
OffNadir_Composite_Snow_Free_Quality:_FillValue = 255UB ;
OffNadir_Composite_Snow_Free_Quality:long_name = "Quality Flag of Temporal Radiance Composite Using Off Nadir Angle Observations (View Zenith Angle 40-60 degree) During Snow-free Period" ;
OffNadir_Composite_Snow_Free_Quality:units = "flag, no units" ;
OffNadir_Composite_Snow_Free_Quality:valid_range = 0UB, 254UB ;
OffNadir_Composite_Snow_Free_Quality:scale_factor = 1. ;
OffNadir_Composite_Snow_Free_Quality:offset = 0. ;
OffNadir_Composite_Snow_Free_Quality:Description = "Quality:\n\t 0 = Good quality\n\t 1 = Poor quality\n\t 2 = Gap filled\n\t 255 = Fill value\n\t" ;
OffNadir_Composite_Snow_Free_Quality:coordinates = "latitude longitude" ;
float OffNadir_Composite_Snow_Free_Std(phony_dim_0, phony_dim_1) ;
OffNadir_Composite_Snow_Free_Std:_FillValue = -999.9f ;
OffNadir_Composite_Snow_Free_Std:long_name = "Standard Deviation of Temporal Radiance Composite Using Off Nadir Angle Observations (View Zenith Angle 40-60 degree) During Snow-free Period" ;
OffNadir_Composite_Snow_Free_Std:units = "nWatts/(cm^2 sr)" ;
OffNadir_Composite_Snow_Free_Std:valid_range = ">= 0.0 \n" ;
OffNadir_Composite_Snow_Free_Std:scale_factor = 1. ;
OffNadir_Composite_Snow_Free_Std:offset = 0. ;
OffNadir_Composite_Snow_Free_Std:coordinates = "latitude longitude" ;
double lat(phony_dim_0) ;
lat:long_name = "latitude" ;
lat:units = "degrees_north" ;
lat:_CoordinateAxisType = "Lat" ;
lat:valid_min = -90.f ;
lat:valid_max = 90.f ;
lat:_FillValue = -999.9f ;
double lon(phony_dim_0) ;
lon:long_name = "longitude" ;
lon:units = "degrees_east" ;
lon:_CoordinateAxisType = "Lon" ;
lat:valid_min = -180.f ;
lat:valid_max = 180.f ;
lat:_FillValue = -999.9f ;
} // group Data\ Fields
} // group VIIRS_Grid_DNB_2d
} // group GRIDS
} // group HDFEOS
}

group: HDFEOS\ INFORMATION {
variables:
string StructMetadata.0 ;

// group attributes:
:HDFEOSVersion = "HDFEOS_5.1.16" ;
} // group HDFEOS\ INFORMATION
}

```

Appendix D: Metadata (Attributes) in VNP46A4 Product

netcdf VNP46A4.A2021001.h10v05.002.2024130162723.h5 {

```

// global attributes:
:identifier_product_doi = "10.5067/VIIRS/VNP46A4.002" ;
:RangeEndingDate = "2021-12-31" ;
:VerticalTileNumber = "05" ;
:NumberofInputGranules = "363" ;
:DataResolution = "15 arc second" ;
:creator_url = "https://ladsweb.modaps.eosdis.nasa.gov" ;
:SensorShortname = "VIIRS" ;
:EndTime = "2022-01-01 00:00:00" ;
:TileID = "61010005" ;
:NorthBoundingCoord = 40.f ;
:SatelliteInstrument = "NPP_OPS" ;
:creator_name = "VIIRS Land SIPS Processing Group" ;
:GranuleDayNightFlag = "Night" ;
:publisher_name = "LAADS" ;
:LongName = "VIIRS/NPP Lunar BRDF-Adjusted Nighttime Lights Yearly L3 Global 15 arc second Linear Lat Lon Grid" ;
:ProcessVersion = "002" ;
:naming_authority = "gov.nasa.gsfc.VIIRSland" ;
:InputPointer =
"VNP46A1.A2021001.h10v05.002.2023184124429.h5,VNP46A1.A2021002.h10v05.002.2023184133156.h5,VNP46A1.A2021003.h10v05.002.20231841
45311.h5,VNP46A1.A2021004.h10v05.002.2023184154440.h5,VNP46A1.A2021005.h10v05.002.2023184170537.h5,VNP46A1.A2021006.h10v05.002.2
023184175801.h5,VNP46A1.A2021007.h10v05.002.2023184194654.h5,VNP46A1.A2021008.h10v05.002.2023184205537.h5,VNP46A1.A2021009.h10v
05.002.2023184221618.h5,VNP46A1.A2021010.h10v05.002.2023184233026.h5,VNP46A1.A2021011.h10v05.002.2023185005250.h5,VNP46A1.A2021
012.h10v05.002.2023185020736.h5,VNP46A1.A2021013.h10v05.002.2023185032203.h5,VNP46A1.A2021014.h10v05.002.2023185044326.h5,VNP46A
1.A2021015.h10v05.002.2023185061633.h5,VNP46A1.A2021016.h10v05.002.2023185080104.h5,VNP46A1.A2021017.h10v05.002.2023185092749.h5,
VNP46A1.A2021018.h10v05.002.2023185111745.h5,VNP46A1.A2021019.h10v05.002.2023185125309.h5,VNP46A1.A2021020.h10v05.002.202318514
1203.h5,VNP46A1.A2021021.h10v05.002.2023185153107.h5,VNP46A1.A2021022.h10v05.002.2023185162459.h5,VNP46A1.A2021023.h10v05.002.20
23185170933.h5,VNP46A1.A2021024.h10v05.002.2023185175922.h5,VNP46A1.A2021025.h10v05.002.2023185184307.h5,VNP46A1.A2021026.h10v0
5.002.2023185192537.h5,VNP46A1.A2021027.h10v05.002.2023185201429.h5,VNP46A1.A2021028.h10v05.002.2023185210343.h5,VNP46A1.A20210
29.h10v05.002.2023185214728.h5,VNP46A1.A2021030.h10v05.002.2023185223243.h5,VNP46A1.A2021031.h10v05.002.2023185232120.h5,VNP46A1
.A2021032.h10v05.002.2023186000510.h5,VNP46A1.A2021033.h10v05.002.2023186010105.h5,VNP46A1.A2021034.h10v05.002.2023186014215.h5,V
NP46A1.A2021035.h10v05.002.2023186023133.h5,VNP46A1.A2021036.h10v05.002.2023186032655.h5,VNP46A1.A2021037.h10v05.002.2023186043
650.h5,VNP46A1.A2021038.h10v05.002.2023186055901.h5,VNP46A1.A2021039.h10v05.002.2023186072528.h5,VNP46A1.A2021040.h10v05.002.202
3186085646.h5,VNP46A1.A2021041.h10v05.002.2023186102423.h5,VNP46A1.A2021042.h10v05.002.2023186115903.h5,VNP46A1.A2021043.h10v05
.002.2023186131803.h5,VNP46A1.A2021044.h10v05.002.2023186150936.h5,VNP46A1.A2021045.h10v05.002.2023186193837.h5,VNP46A1.A202104
6.h10v05.002.2023186210130.h5,VNP46A1.A2021047.h10v05.002.2023186224627.h5,VNP46A1.A2021048.h10v05.002.2023187001827.h5,VNP46A1
.A2021049.h10v05.002.2023187015711.h5,VNP46A1.A2021050.h10v05.002.2023187035244.h5,VNP46A1.A2021051.h10v05.002.2023187061555.h5,V
NP46A1.A2021052.h10v05.002.2023187080716.h5,VNP46A1.A2021053.h10v05.002.2023187091036.h5,VNP46A1.A2021054.h10v05.002.2023187101
935.h5,VNP46A1.A2021055.h10v05.002.2023187111727.h5,VNP46A1.A2021056.h10v05.002.2023187121418.h5,VNP46A1.A2021057.h10v05.002.202
3187132124.h5,VNP46A1.A2021058.h10v05.002.2023187141435.h5,VNP46A1.A2021059.h10v05.002.2023187150926.h5,VNP46A1.A2021060.h10v05
.002.2023187163421.h5,VNP46A1.A2021061.h10v05.002.2023187183559.h5,VNP46A1.A2021062.h10v05.002.2023187194314.h5,VNP46A1.A202106
3.h10v05.002.2023187204613.h5,VNP46A1.A2021064.h10v05.002.2023187220806.h5,VNP46A1.A2021065.h10v05.002.2023187231117.h5,VNP46A1
.A2021066.h10v05.002.2023188005626.h5,VNP46A1.A2021067.h10v05.002.2023188023749.h5,VNP46A1.A2021068.h10v05.002.2023188041723.h5,V
NP46A1.A2021069.h10v05.002.2023188061705.h5,VNP46A1.A2021070.h10v05.002.2023188083940.h5,VNP46A1.A2021071.h10v05.002.2023188105
234.h5,VNP46A1.A2021072.h10v05.002.2023188124406.h5,VNP46A1.A2021073.h10v05.002.2023188143408.h5,VNP46A1.A2021074.h10v05.002.202
3188160719.h5,VNP46A1.A2021075.h10v05.002.2023188173747.h5,VNP46A1.A2021076.h10v05.002.2023188192103.h5,VNP46A1.A2021077.h10v05
.002.2023188205854.h5,VNP46A1.A2021078.h10v05.002.2023188223757.h5,VNP46A1.A2021079.h10v05.002.2023189000635.h5,VNP46A1.A202108
0.h10v05.002.2023189014036.h5,VNP46A1.A2021081.h10v05.002.2023189025628.h5,VNP46A1.A2021082.h10v05.002.2023189035911.h5,VNP46A1
.A2021083.h10v05.002.2023189045309.h5,VNP46A1.A2021084.h10v05.002.2023189065413.h5,VNP46A1.A2021085.h10v05.002.2023189074605.h5,V
NP46A1.A2021086.h10v05.002.2023189100147.h5,VNP46A1.A2021087.h10v05.002.2023189110716.h5,VNP46A1.A2021088.h10v05.002.2023189121
019.h5,VNP46A1.A2021089.h10v05.002.2023189131735.h5,VNP46A1.A2021090.h10v05.002.2023189141101.h5,VNP46A1.A2021091.h10v05.002.202
3189151607.h5,VNP46A1.A2021092.h10v05.002.2023189160744.h5,VNP46A1.A2021093.h10v05.002.2023189170811.h5,VNP46A1.A2021094.h10v05
.002.2023189180800.h5,VNP46A1.A2021095.h10v05.002.2023189192156.h5,VNP46A1.A2021096.h10v05.002.2023189204140.h5,VNP46A1.A202109
7.h10v05.002.2023189221155.h5,VNP46A1.A2021098.h10v05.002.2023189233958.h5,VNP46A1.A2021099.h10v05.002.2023190011904.h5,VNP46A1
.A2021100.h10v05.002.2023190024219.h5,VNP46A1.A2021101.h10v05.002.2023190042055.h5,VNP46A1.A2021102.h10v05.002.2023190055547.h5,V
NP46A1.A2021103.h10v05.002.2023190073255.h5,VNP46A1.A2021104.h10v05.002.2023190085702.h5,VNP46A1.A2021105.h10v05.002.2023190103
316.h5,VNP46A1.A2021106.h10v05.002.2023190121429.h5,VNP46A1.A2021107.h10v05.002.2023190134718.h5,VNP46A1.A2021108.h10v05.002.202
3190152227.h5,VNP46A1.A2021109.h10v05.002.2023190164207.h5,VNP46A1.A2021110.h10v05.002.2023190175119.h5,VNP46A1.A2021111.h10v05
.002.2023190190539.h5,VNP46A1.A2021112.h10v05.002.2023190200130.h5,VNP46A1.A2021113.h10v05.002.2023190205912.h5,VNP46A1.A202111
4.h10v05.002.2023190221444.h5,VNP46A1.A2021115.h10v05.002.2023190231535.h5,VNP46A1.A2021116.h10v05.002.2023191001100.h5,VNP46A1
.A2021117.h10v05.002.2023191012841.h5,VNP46A1.A2021118.h10v05.002.2023191024003.h5,VNP46A1.A2021119.h10v05.002.2023191033543.h5,V
NP46A1.A2021120.h10v05.002.2023191042409.h5,VNP46A1.A2021121.h10v05.002.2023191075923.h5,VNP46A1.A2021122.h10v05.002.2023191092
222.h5,VNP46A1.A2021123.h10v05.002.2023191104616.h5,VNP46A1.A2021124.h10v05.002.2023191120536.h5,VNP46A1.A2021125.h10v05.002.202
3191132724.h5,VNP46A1.A2021126.h10v05.002.2023191144859.h5,VNP46A1.A2021127.h10v05.002.2023191160326.h5,VNP46A1.A2021128.h10v05
.002.2023191174533.h5,VNP46A1.A2021129.h10v05.002.2023191191421.h5,VNP46A1.A2021130.h10v05.002.2023191203431.h5,VNP46A1.A202113
1.h10v05.002.2023191214711.h5,VNP46A1.A2021132.h10v05.002.2023191230619.h5,VNP46A1.A2021133.h10v05.002.2023192002358.h5,VNP46A1
.A2021134.h10v05.002.2023192013818.h5,VNP46A1.A2021135.h10v05.002.2023192030027.h5,VNP46A1.A2021136.h10v05.002.2023192041501.h5,V
NP46A1.A2021137.h10v05.002.20231920449.h5,VNP46A1.A2021138.h10v05.002.2023192071229.h5,VNP46A1.A2021139.h10v05.002.2023192082
938.h5,VNP46A1.A2021140.h10v05.002.2023192094948.h5,VNP46A1.A2021141.h10v05.002.2023192111557.h5,VNP46A1.A2021142.h10v05.002.202
3192121540.h5,VNP46A1.A2021143.h10v05.002.2023192131046.h5,VNP46A1.A2021144.h10v05.002.2023192140458.h5,VNP46A1.A2021145.h10v05
.002.2023192145323.h5,VNP46A1.A2021146.h10v05.002.2023192154707.h5,VNP46A1.A2021147.h10v05.002.2023192163616.h5,VNP46A1.A202114
8.h10v05.002.2023192172437.h5,VNP46A1.A2021149.h10v05.002.2023192181058.h5,VNP46A1.A2021150.h10v05.002.2023192185924.h5,VNP46A1
.A2021151.h10v05.002.2023192195305.h5,VNP46A1.A2021152.h10v05.002.2023192204614.h5,VNP46A1.A2021153.h10v05.002.2023192213456.h5,V
NP46A1.A2021154.h10v05.002.2023192223550.h5,VNP46A1.A2021155.h10v05.002.2023192234910.h5,VNP46A1.A2021156.h10v05.002.2023193010
836.h5,VNP46A1.A2021157.h10v05.002.2023193022329.h5,VNP46A1.A2021158.h10v05.002.2023193034904.h5,VNP46A1.A2021159.h10v05.002.202
3193053920.h5,VNP46A1.A2021160.h10v05.002.2023193063430.h5,VNP46A1.A2021161.h10v05.002.2023193081009.h5,VNP46A1.A2021162.h10v05
.002.2023193100622.h5,VNP46A1.A2021163.h10v05.002.2023193115358.h5,VNP46A1.A2021164.h10v05.002.2023193133625.h5,VNP46A1.A202116
5.h10v05.002.2023193145000.h5,VNP46A1.A2021166.h10v05.002.2023193160832.h5,VNP46A1.A2021167.h10v05.002.2023193172109.h5,VNP46A1.

```


A2021025.h10v05.002.2024078153831.h5,VNP46A2.A2021026.h10v05.002.2024078174352.h5,VNP46A2.A2021027.h10v05.002.2024078181704.h5,VNP46A2.A2021028.h10v05.002.2024078184935.h5,VNP46A2.A2021029.h10v05.002.2024078192112.h5,VNP46A2.A2021030.h10v05.002.2024078194910.h5,VNP46A2.A2021031.h10v05.002.2024078202121.h5,VNP46A2.A2021032.h10v05.002.2024078205529.h5,VNP46A2.A2021033.h10v05.002.2024078212630.h5,VNP46A2.A2021034.h10v05.002.2024078220236.h5,VNP46A2.A2021035.h10v05.002.2024078223847.h5,VNP46A2.A2021036.h10v05.002.2024078231937.h5,VNP46A2.A2021037.h10v05.002.2024078235728.h5,VNP46A2.A2021038.h10v05.002.2024079001832.h5,VNP46A2.A2021039.h10v05.002.2024079004044.h5,VNP46A2.A2021040.h10v05.002.2024079010309.h5,VNP46A2.A2021041.h10v05.002.2024079012347.h5,VNP46A2.A2021042.h10v05.002.2024079014502.h5,VNP46A2.A2021043.h10v05.002.2024079020525.h5,VNP46A2.A2021044.h10v05.002.2024079022530.h5,VNP46A2.A2021045.h10v05.002.2024079024710.h5,VNP46A2.A2021046.h10v05.002.2024079030707.h5,VNP46A2.A2021047.h10v05.002.2024079032746.h5,VNP46A2.A2021048.h10v05.002.2024079034738.h5,VNP46A2.A2021049.h10v05.002.2024079041245.h5,VNP46A2.A2021050.h10v05.002.2024079043143.h5,VNP46A2.A2021051.h10v05.002.2024079045249.h5,VNP46A2.A2021052.h10v05.002.2024079051447.h5,VNP46A2.A2021053.h10v05.002.2024079054308.h5,VNP46A2.A2021054.h10v05.002.2024079061813.h5,VNP46A2.A2021055.h10v05.002.2024079065224.h5,VNP46A2.A2021056.h10v05.002.2024079072514.h5,VNP46A2.A2021057.h10v05.002.2024079075404.h5,VNP46A2.A2021058.h10v05.002.2024079082049.h5,VNP46A2.A2021059.h10v05.002.2024079084627.h5,VNP46A2.A2021060.h10v05.002.2024079091354.h5,VNP46A2.A2021061.h10v05.002.2024079094209.h5,VNP46A2.A2021062.h10v05.002.2024079101105.h5,VNP46A2.A2021063.h10v05.002.2024079104507.h5,VNP46A2.A2021064.h10v05.002.2024079112908.h5,VNP46A2.A2021065.h10v05.002.2024079120821.h5,VNP46A2.A2021066.h10v05.002.2024079124142.h5,VNP46A2.A2021067.h10v05.002.2024079130837.h5,VNP46A2.A2021068.h10v05.002.2024079133257.h5,VNP46A2.A2021069.h10v05.002.2024079135276.h5,VNP46A2.A2021070.h10v05.002.2024079141823.h5,VNP46A2.A2021071.h10v05.002.2024079144055.h5,VNP46A2.A2021072.h10v05.002.2024079150705.h5,VNP46A2.A2021073.h10v05.002.2024079153243.h5,VNP46A2.A2021074.h10v05.002.2024079155518.h5,VNP46A2.A2021075.h10v05.002.2024079161724.h5,VNP46A2.A2021076.h10v05.002.2024079164108.h5,VNP46A2.A2021077.h10v05.002.2024079170455.h5,VNP46A2.A2021078.h10v05.002.2024079173003.h5,VNP46A2.A2021079.h10v05.002.2024079175634.h5,VNP46A2.A2021080.h10v05.002.2024079182230.h5,VNP46A2.A2021081.h10v05.002.2024079183505.h5,VNP46A2.A2021083.h10v05.002.2024079202627.h5,VNP46A2.A2021084.h10v05.002.2024079211301.h5,VNP46A2.A2021085.h10v05.002.2024079215345.h5,VNP46A2.A2021086.h10v05.002.2024079223517.h5,VNP46A2.A2021087.h10v05.002.2024079231223.h5,VNP46A2.A2021088.h10v05.002.2024079234950.h5,VNP46A2.A2021089.h10v05.002.2024080002309.h5,VNP46A2.A2021090.h10v05.002.2024080010002.h5,VNP46A2.A2021091.h10v05.002.2024080014110.h5,VNP46A2.A2021092.h10v05.002.2024080022252.h5,VNP46A2.A2021093.h10v05.002.2024080030804.h5,VNP46A2.A2021094.h10v05.002.2024080035714.h5,VNP46A2.A2021095.h10v05.002.2024080043902.h5,VNP46A2.A2021096.h10v05.002.2024080050427.h5,VNP46A2.A2021097.h10v05.002.2024080052713.h5,VNP46A2.A2021098.h10v05.002.20240800805012.h5,VNP46A2.A2021099.h10v05.002.2024080060936.h5,VNP46A2.A2021100.h10v05.002.2024080063138.h5,VNP46A2.A2021101.h10v05.002.2024080065300.h5,VNP46A2.A2021102.h10v05.002.2024080071424.h5,VNP46A2.A2021103.h10v05.002.2024080073553.h5,VNP46A2.A2021104.h10v05.002.2024080075819.h5,VNP46A2.A2021105.h10v05.002.2024080082131.h5,VNP46A2.A2021106.h10v05.002.2024080084657.h5,VNP46A2.A2021107.h10v05.002.2024080091247.h5,VNP46A2.A2021108.h10v05.002.2024080093731.h5,VNP46A2.A2021109.h10v05.002.2024080095700.h5,VNP46A2.A2021110.h10v05.002.2024080102037.h5,VNP46A2.A2021111.h10v05.002.2024080104429.h5,VNP46A2.A2021112.h10v05.002.2024080111450.h5,VNP46A2.A2021113.h10v05.002.2024080115925.h5,VNP46A2.A2021114.h10v05.002.2024080123846.h5,VNP46A2.A2021115.h10v05.002.2024080132004.h5,VNP46A2.A2021116.h10v05.002.2024080135827.h5,VNP46A2.A2021117.h10v05.002.2024080143625.h5,VNP46A2.A2021118.h10v05.002.2024080151411.h5,VNP46A2.A2021119.h10v05.002.2024081094635.h5,VNP46A2.A2021120.h10v05.002.2024081103218.h5,VNP46A2.A2021121.h10v05.002.2024081111141.h5,VNP46A2.A2021122.h10v05.002.2024081114837.h5,VNP46A2.A2021123.h10v05.002.2024081123556.h5,VNP46A2.A2021124.h10v05.002.2024081132432.h5,VNP46A2.A2021125.h10v05.002.2024081134854.h5,VNP46A2.A2021126.h10v05.002.2024081142108.h5,VNP46A2.A2021127.h10v05.002.2024081144250.h5,VNP46A2.A2021128.h10v05.002.2024081150648.h5,VNP46A2.A2021129.h10v05.002.2024081153114.h5,VNP46A2.A2021130.h10v05.002.2024081155146.h5,VNP46A2.A2021131.h10v05.002.2024081161222.h5,VNP46A2.A2021132.h10v05.002.2024081163350.h5,VNP46A2.A2021133.h10v05.002.2024081165810.h5,VNP46A2.A2021134.h10v05.002.2024081172011.h5,VNP46A2.A2021135.h10v05.002.2024081174152.h5,VNP46A2.A2021136.h10v05.002.2024081180323.h5,VNP46A2.A2021137.h10v05.002.2024081182601.h5,VNP46A2.A2021138.h10v05.002.2024081184740.h5,VNP46A2.A2021139.h10v05.002.2024081190838.h5,VNP46A2.A2021140.h10v05.002.2024081193112.h5,VNP46A2.A2021141.h10v05.002.2024081200154.h5,VNP46A2.A2021142.h10v05.002.2024081203609.h5,VNP46A2.A2021143.h10v05.002.2024081210929.h5,VNP46A2.A2021144.h10v05.002.2024081220112.h5,VNP46A2.A2021145.h10v05.002.2024081224034.h5,VNP46A2.A2021146.h10v05.002.2024081231905.h5,VNP46A2.A2021147.h10v05.002.2024081235905.h5,VNP46A2.A2021148.h10v05.002.2024081235905.h5,VNP46A2.A2021149.h10v05.002.2024081235905.h5,VNP46A2.A2021150.h10v05.002.2024082040412.h5,VNP46A2.A2021151.h10v05.002.202408204435.h5,VNP46A2.A2021152.h10v05.002.2024082033638.h5,VNP46A2.A2021153.h10v05.002.2024082041629.h5,VNP46A2.A2021154.h10v05.002.2024082045324.h5,VNP46A2.A2021155.h10v05.002.2024082054930.h5,VNP46A2.A2021156.h10v05.002.2024082061520.h5,VNP46A2.A2021157.h10v05.002.2024082063830.h5,VNP46A2.A2021158.h10v05.002.20240820707114.h5,VNP46A2.A2021159.h10v05.002.2024082072745.h5,VNP46A2.A2021160.h10v05.002.2024082072745.h5,VNP46A2.A2021161.h10v05.002.2024082081027.h5,VNP46A2.A2021162.h10v05.002.2024082083410.h5,VNP46A2.A2021163.h10v05.002.2024082110421.h5,VNP46A2.A2021164.h10v05.002.2024082112946.h5,VNP46A2.A2021165.h10v05.002.2024082115157.h5,VNP46A2.A2021166.h10v05.002.202408212136.h5,VNP46A2.A2021167.h10v05.002.2024082123612.h5,VNP46A2.A2021168.h10v05.002.2024082130154.h5,VNP46A2.A2021169.h10v05.002.2024082132457.h5,VNP46A2.A2021170.h10v05.002.2024082134911.h5,VNP46A2.A2021171.h10v05.002.2024082141042.h5,VNP46A2.A2021172.h10v05.002.2024082143613.h5,VNP46A2.A2021173.h10v05.002.2024082151025.h5,VNP46A2.A2021174.h10v05.002.2024082154325.h5,VNP46A2.A2021175.h10v05.002.2024082162012.h5,VNP46A2.A2021176.h10v05.002.2024082165538.h5,VNP46A2.A2021177.h10v05.002.2024082172804.h5,VNP46A2.A2021178.h10v05.002.2024082181355.h5,VNP46A2.A2021179.h10v05.002.2024082184931.h5,VNP46A2.A2021180.h10v05.002.2024082192124.h5,VNP46A2.A2021181.h10v05.002.2024082195408.h5,VNP46A2.A2021182.h10v05.002.2024082202742.h5,VNP46A2.A2021183.h10v05.002.2024082211752.h5,VNP46A2.A2021184.h10v05.002.2024082214329.h5,VNP46A2.A2021185.h10v05.002.2024082222054.h5,VNP46A2.A2021186.h10v05.002.2024082230827.h5,VNP46A2.A2021187.h10v05.002.2024082234506.h5,VNP46A2.A2021188.h10v05.002.202408300447.h5,VNP46A2.A2021189.h10v05.002.2024083002824.h5,VNP46A2.A2021190.h10v05.002.2024083004835.h5,VNP46A2.A2021191.h10v05.002.2024083011120.h5,VNP46A2.A2021192.h10v05.002.202408302130.h5,VNP46A2.A2021193.h10v05.002.2024083023356.h5,VNP46A2.A2021196.h10v05.002.2024083025647.h5,VNP46A2.A2021197.h10v05.002.2024083032116.h5,VNP46A2.A2021198.h10v05.002.2024083034346.h5,VNP46A2.A2021199.h10v05.002.2024083040627.h5,VNP46A2.A2021200.h10v05.002.2024083040627.h5,VNP46A2.A2021201.h10v05.002.2024083045847.h5,VNP46A2.A2021202.h10v05.002.2024083052302.h5,VNP46A2.A2021203.h10v05.002.2024083051339.h5,VNP46A2.A2021204.h10v05.002.202408306216.h5,VNP46A2.A2021205.h10v05.002.2024083070122.h5,VNP46A2.A2021206.h10v05.002.2024083073452.h5,VNP46A2.A2021207.h10v05.002.2024083080953.h5,VNP46A2.A2021208.h10v05.002.2024083085458.h5,VNP46A2.A2021209.h10v05.002.2024083092842.h5,VNP46A2.A2021210.h10v05.002.2024083100449.h5,VNP46A2.A2021211.h10v05.002.2024083103753.h5,VNP46A2.A2021212.h10v05.002.2024083111019.h5,VNP46A2.A2021213.h10v05.002.2024083114236.h5,VNP46A2.A2021214.h10v05.002.2024083121809.h5,VNP46A2.A2021217.h10v05.002.2024086162838.h5,VNP46A2.A2021218.h10v05.002.2024086170126.h5,VNP46A2.A2021219.h10v05.002.2024086172507.h5,VNP46A2.A2021220.h10v05.002.2024086174851.h5,VNP46A2.A2021221.h10v05.002.2024086181843.h5,VNP46A2.A2021222.h10v05.002.20240861843.h5,VNP46A2.A2021223.h10v05.002.2024086190859.h5,VNP46A2.A2021224.h10v05.002.2024086193201.h5,VNP46A2.A2021225.h10v05.002.2024086195338.h5,VNP46A2.A2021226.h10v05.002.2024086201511.h5,VNP46A2.A2021227.h10v05.002.2024086204143.h5,VNP46A2.A2021228.h10v05.002.2024086224431.h5,VNP46A2.A2021229.h10v05.002.2024086224431.h5,VNP46A2.A2021230.h10v05.002.2024086214435.h5,VNP46A2.A2021231.h10v05.002.2024086220614.h5,VNP46A2.A2021232.h10v05.002.2024086224431.h5,VNP46A2.A2021233.h10v05.002.2024086232317.h5,VNP46A2.A2021234.h10v05.002.2024087000222.h5,VNP46A2.A2021235.h10v05.002.2024087003717.h5,VNP46A2.A2021236.h10v05.002.2024087011025.h5,VNP46A2.A2021237.h10v05.002.2024087014614.h5,VNP46A2.A2021238.h10v05.002.2024087021752.h5,VNP46A2.A2021239.h10v05.002.2024087024222.h5,VNP46A2.A2021240.h10v05.002.2024087031728.h5,VNP46A2.A2021241.h10v05.002.2024087034909.h5,VNP46A2.A2021242.h10v05.002.2024087042022.h5,VNP46A2.A2021243.h10v05.002.2024087050839.h5,VNP46A2.A2021244.h10v05.002.2024087054249.h5,VNP46A2.A2021245.h10v05.002.2024087063404.h5,VNP46A2.A2021246.h10v05.002.2024087071419.h5,VNP46A2.A2021247.h10v05.002.2024087073942.h5,VNP46A2.

A2021248.h10v05.002.2024087080146.h5,VNP46A2.A2021249.h10v05.002.2024087083246.h5,VNP46A2.A2021250.h10v05.002.2024087085635.h5,VNP46A2.A2021251.h10v05.002.2024087092105.h5,VNP46A2.A2021252.h10v05.002.2024087094618.h5,VNP46A2.A2021253.h10v05.002.2024087101314.h5,VNP46A2.A2021254.h10v05.002.2024087104220.h5,VNP46A2.A2021255.h10v05.002.2024087110842.h5,VNP46A2.A2021256.h10v05.002.2024087113306.h5,VNP46A2.A2021257.h10v05.002.2024087115739.h5,VNP46A2.A2021258.h10v05.002.2024087122207.h5,VNP46A2.A2021259.h10v05.002.2024087125017.h5,VNP46A2.A2021260.h10v05.002.2024087131044.h5,VNP46A2.A2021261.h10v05.002.2024087133844.h5,VNP46A2.A2021262.h10v05.002.2024087142242.h5,VNP46A2.A2021263.h10v05.002.2024087150031.h5,VNP46A2.A2021264.h10v05.002.2024087153512.h5,VNP46A2.A2021265.h10v05.002.2024087160624.h5,VNP46A2.A2021266.h10v05.002.2024087164505.h5,VNP46A2.A2021267.h10v05.002.2024087171311.h5,VNP46A2.A2021268.h10v05.002.2024087174303.h5,VNP46A2.A2021269.h10v05.002.2024087181347.h5,VNP46A2.A2021270.h10v05.002.2024087184347.h5,VNP46A2.A2021271.h10v05.002.2024087191444.h5,VNP46A2.A2021272.h10v05.002.2024087194720.h5,VNP46A2.A2021273.h10v05.002.202408720157.h5,VNP46A2.A2021274.h10v05.002.2024087210045.h5,VNP46A2.A2021275.h10v05.002.2024087214036.h5,VNP46A2.A2021276.h10v05.002.2024087221559.h5,VNP46A2.A2021277.h10v05.002.2024087223932.h5,VNP46A2.A2021278.h10v05.002.2024087230511.h5,VNP46A2.A2021279.h10v05.002.2024087232633.h5,VNP46A2.A2021280.h10v05.002.2024087235624.h5,VNP46A2.A2021281.h10v05.002.2024088001841.h5,VNP46A2.A2021282.h10v05.002.2024088004137.h5,VNP46A2.A2021283.h10v05.002.2024088010728.h5,VNP46A2.A2021284.h10v05.002.2024088013344.h5,VNP46A2.A2021285.h10v05.002.2024088015723.h5,VNP46A2.A2021286.h10v05.002.2024088022114.h5,VNP46A2.A2021287.h10v05.002.2024089145600.h5,VNP46A2.A2021288.h10v05.002.2024089152047.h5,VNP46A2.A2021289.h10v05.002.2024089154551.h5,VNP46A2.A2021290.h10v05.002.2024089162827.h5,VNP46A2.A2021291.h10v05.002.2024089170921.h5,VNP46A2.A2021292.h10v05.002.2024089174623.h5,VNP46A2.A2021293.h10v05.002.2024089182411.h5,VNP46A2.A2021294.h10v05.002.2024089185919.h5,VNP46A2.A2021295.h10v05.002.2024089193153.h5,VNP46A2.A2021296.h10v05.002.2024089200030.h5,VNP46A2.A2021297.h10v05.002.2024089203611.h5,VNP46A2.A2021298.h10v05.002.2024089210438.h5,VNP46A2.A2021299.h10v05.002.2024089213839.h5,VNP46A2.A2021300.h10v05.002.2024089221024.h5,VNP46A2.A2021301.h10v05.002.2024089225044.h5,VNP46A2.A2021302.h10v05.002.2024089233058.h5,VNP46A2.A2021303.h10v05.002.2024090001015.h5,VNP46A2.A2021304.h10v05.002.2024090005151.h5,VNP46A2.A2021305.h10v05.002.2024090013654.h5,VNP46A2.A2021306.h10v05.002.2024090020254.h5,VNP46A2.A2021307.h10v05.002.2024090022918.h5,VNP46A2.A2021308.h10v05.002.2024090025454.h5,VNP46A2.A2021309.h10v05.002.2024090031451.h5,VNP46A2.A2021310.h10v05.002.2024090034057.h5,VNP46A2.A2021311.h10v05.002.2024090040651.h5,VNP46A2.A2021312.h10v05.002.2024090043220.h5,VNP46A2.A2021313.h10v05.002.2024090045224.h5,VNP46A2.A2021314.h10v05.002.2024090051242.h5,VNP46A2.A2021315.h10v05.002.2024090053816.h5,VNP46A2.A2021316.h10v05.002.2024090060722.h5,VNP46A2.A2021317.h10v05.002.2024090063134.h5,VNP46A2.A2021318.h10v05.002.2024090065705.h5,VNP46A2.A2021319.h10v05.002.2024090072524.h5,VNP46A2.A2021320.h10v05.002.2024090080222.h5,VNP46A2.A2021321.h10v05.002.2024090084250.h5,VNP46A2.A2021322.h10v05.002.2024090092212.h5,VNP46A2.A2021323.h10v05.002.2024090095437.h5,VNP46A2.A2021324.h10v05.002.2024090103004.h5,VNP46A2.A2021325.h10v05.002.2024090110413.h5,VNP46A2.A2021326.h10v05.002.2024090113202.h5,VNP46A2.A2021327.h10v05.002.2024090115930.h5,VNP46A2.A2021328.h10v05.002.2024090122719.h5,VNP46A2.A2021329.h10v05.002.2024090130124.h5,VNP46A2.A2021323.h10v05.002.2024090145041.h5,VNP46A2.A2021333.h10v05.002.2024090145225.h5,VNP46A2.A2021334.h10v05.002.2024090161513.h5,VNP46A2.A2021335.h10v05.002.2024090172455.h5,VNP46A2.A2021338.h10v05.002.2024090174918.h5,VNP46A2.A2021339.h10v05.002.2024090181055.h5,VNP46A2.A2021340.h10v05.002.2024090183053.h5,VNP46A2.A2021341.h10v05.002.2024090185042.h5,VNP46A2.A2021342.h10v05.002.2024090191047.h5,VNP46A2.A2021343.h10v05.002.2024090193132.h5,VNP46A2.A2021344.h10v05.002.2024090195244.h5,VNP46A2.A2021345.h10v05.002.2024090201335.h5,VNP46A2.A2021346.h10v05.002.2024090203436.h5,VNP46A2.A2021347.h10v05.002.2024090205458.h5,VNP46A2.A2021348.h10v05.002.2024090212203.h5,VNP46A2.A2021349.h10v05.002.2024090215642.h5,VNP46A2.A2021350.h10v05.002.2024090223304.h5,VNP46A2.A2021351.h10v05.002.2024090231522.h5,VNP46A2.A2021352.h10v05.002.2024090235114.h5,VNP46A2.A2021353.h10v05.002.2024091002547.h5,VNP46A2.A2021354.h10v05.002.2024091010028.h5,VNP46A2.A2021355.h10v05.002.2024091012446.h5,VNP46A2.A2021356.h10v05.002.2024091014926.h5,VNP46A2.A2021357.h10v05.002.2024091021433.h5,VNP46A2.A2021358.h10v05.002.2024091023827.h5,VNP46A2.A2021359.h10v05.002.2024091031111.h5,VNP46A2.A2021360.h10v05.002.2024091034224.h5,VNP46A2.A2021361.h10v05.002.2024091041358.h5,VNP46A2.A2021362.h10v05.002.2024091045424.h5,VNP46A2.A2021363.h10v05.002.2024091053034.h5,VNP46A2.A2021364.h10v05.002.2024091061815.h5,VNP46A2.A2021365.h10v05.002.2024091064924.h5";
 :PGEVersion = "2.0.3-0";
 :creator_email = "modis-ops@lists.nasa.gov";
 :VersionID = "002";
 :SouthBoundingCoord = 30.f;
 :RangeEndingTime = "23:59:00.000000";
 :Identifier_product_doi_authority = "https://doi.org";
 :ProcessingCenter = "LandSIPS";
 :Conventions = "CF-1.6";
 :ProcessingEnvironment = "Linux minion20180 5.4.0-1082-fips #91-Ubuntu SMP Wed Jul 19 21:56:44 UTC 2023 x86_64 x86_64 x86_64"

GNU/Linux ;

:HorizontalTileNumber = "10";
 :PGE_Name = "PGE557";
 :EastBoundingCoord = -70.f;
 :PGE_EndTime = "2022-01-01 00:00:00.000";
 :ShortName = "VNP46A4";
 :StartTime = "2021-01-01 00:00:00";
 :DayNightFlag = "Night";
 :RangeBeginningTime = "00:00:00.000000";
 :publisher_url = "https://ladsweb.modaps.eosdis.nasa.gov";
 :GRingPointLongitude = -80., -80., -70., -70.;
 :PGENumber = "557";
 :RangeBeginningDate = "2021-01-01";
 :PlatformShortName = "SUOMI-NPP";
 :PGE_StartTime = "2021-01-01 00:00:00.000";
 :GRingPointLatitude = 30., 40., 40., 30. ;
 :GRingPointSequenceNo = 1, 2, 3, 4 ;
 :AlgorithmVersion = "NPP_PR46A3 2.0.0";
 :publisher_email = "modis-ops@lists.nasa.gov";
 :LocalGranuleID = "VNP46A4.A2021001.h10v05.002.2024130162723.h5";
 :AlgorithmType = "SCI";
 :WestBoundingCoord = -80.f;
 :ProductionTime = "2024-05-09 16:27:23.000";

group: HDFEOS {

group: ADDITIONAL {

```

group: FILE_ATTRIBUTES {
    } // group FILE_ATTRIBUTES
} // group ADDITIONAL

group: GRIDS {

group: VIIRS_Grid_DNB_2d {

group: Data|Fields {
dimensions:
    phony_dim_0 = 2400 ;
    phony_dim_1 = 2400 ;
variables:
    float AllAngle_Composite_Snow_Covered(phony_dim_0, phony_dim_1) ;
        AllAngle_Composite_Snow_Covered:_FillValue = -999.9f ;
        AllAngle_Composite_Snow_Covered:long_name = "Temporal Radiance Composite Using All Observations During Snow-covered Period"
    ;
        AllAngle_Composite_Snow_Covered:units = "nWatts/(cm^2 sr)" ;
        AllAngle_Composite_Snow_Covered:valid_range = ">= 0.0\n" ;
        AllAngle_Composite_Snow_Covered:scale_factor = 1. ;
        AllAngle_Composite_Snow_Covered:offset = 0. ;
        AllAngle_Composite_Snow_Covered:coordinates = "latitude longitude" ;
    ushort AllAngle_Composite_Snow_Covered_Num(phony_dim_0, phony_dim_1) ;
        AllAngle_Composite_Snow_Covered_Num:_FillValue = 65535US ;
        AllAngle_Composite_Snow_Covered_Num:long_name = "Number of Observations of Temporal Radiance Composite Using All Observations During Snow-covered Period" ;
        AllAngle_Composite_Snow_Covered_Num:units = "number of observations" ;
        AllAngle_Composite_Snow_Covered_Num:valid_range = 0US, 65534US ;
        AllAngle_Composite_Snow_Covered_Num:scale_factor = 1. ;
        AllAngle_Composite_Snow_Covered_Num:offset = 0. ;
        AllAngle_Composite_Snow_Covered_Num:coordinates = "latitude longitude" ;
    ubyte AllAngle_Composite_Snow_Covered_Quality(phony_dim_0, phony_dim_1) ;
        AllAngle_Composite_Snow_Covered_Quality:_FillValue = 255UB ;
        AllAngle_Composite_Snow_Covered_Quality:long_name = "Quality Flag of Temporal Radiance Composite Using All Observations During Snow-covered Period" ;
        AllAngle_Composite_Snow_Covered_Quality:units = "flag, no units" ;
        AllAngle_Composite_Snow_Covered_Quality:valid_range = 0UB, 254UB ;
        AllAngle_Composite_Snow_Covered_Quality:scale_factor = 1. ;
        AllAngle_Composite_Snow_Covered_Quality:offset = 0. ;
        AllAngle_Composite_Snow_Covered_Quality:Description = "Quality:\n\t 0 = Good quality\n\t 1 = Poor quality\n\t 2 = Gap filled\n\t 255 = Fill value\n\t" ;
        AllAngle_Composite_Snow_Covered_Quality:coordinates = "latitude longitude" ;
    float AllAngle_Composite_Snow_Covered_Std(phony_dim_0, phony_dim_1) ;
        AllAngle_Composite_Snow_Covered_Std:_FillValue = -999.9f ;
        AllAngle_Composite_Snow_Covered_Std:long_name = "Standard Deviation of Temporal Radiance Composite Using All Observations During Snow-covered Period" ;
        AllAngle_Composite_Snow_Covered_Std:units = "nWatts/(cm^2 sr)" ;
        AllAngle_Composite_Snow_Covered_Std:valid_range = ">= 0.0 \n" ;
        AllAngle_Composite_Snow_Covered_Std:scale_factor = 1. ;
        AllAngle_Composite_Snow_Covered_Std:offset = 0. ;
        AllAngle_Composite_Snow_Covered_Std:coordinates = "latitude longitude" ;
    float AllAngle_Composite_Snow_Free(phony_dim_0, phony_dim_1) ;
        AllAngle_Composite_Snow_Free:_FillValue = -999.9f ;
        AllAngle_Composite_Snow_Free:long_name = "Temporal Radiance Composite Using All Observations During Snow-free Period" ;
        AllAngle_Composite_Snow_Free:units = "nWatts/(cm^2 sr)" ;
        AllAngle_Composite_Snow_Free:valid_range = "<= 0.0 \n" ;
        AllAngle_Composite_Snow_Free:scale_factor = 1. ;
        AllAngle_Composite_Snow_Free:offset = 0. ;
        AllAngle_Composite_Snow_Free:coordinates = "latitude longitude" ;
    ushort AllAngle_Composite_Snow_Free_Num(phony_dim_0, phony_dim_1) ;
        AllAngle_Composite_Snow_Free_Num:_FillValue = 65535US ;
        AllAngle_Composite_Snow_Free_Num:long_name = "Number of Observations of Temporal Radiance Composite Using All Observations During Snow-free Period" ;
        AllAngle_Composite_Snow_Free_Num:units = "number of observations" ;
        AllAngle_Composite_Snow_Free_Num:valid_range = 0US, 65534US ;
        AllAngle_Composite_Snow_Free_Num:scale_factor = 1. ;
        AllAngle_Composite_Snow_Free_Num:offset = 0. ;
        AllAngle_Composite_Snow_Free_Num:coordinates = "latitude longitude" ;
    ubyte AllAngle_Composite_Snow_Free_Quality(phony_dim_0, phony_dim_1) ;
        AllAngle_Composite_Snow_Free_Quality:_FillValue = 255UB ;
        AllAngle_Composite_Snow_Free_Quality:long_name = "Quality Flag of Temporal Radiance Composite Using All Observations During Snow-free Period" ;
        AllAngle_Composite_Snow_Free_Quality:units = "flag, no units" ;
        AllAngle_Composite_Snow_Free_Quality:valid_range = 0UB, 254UB ;
        AllAngle_Composite_Snow_Free_Quality:scale_factor = 1. ;
        AllAngle_Composite_Snow_Free_Quality:offset = 0. ;
}
}

```

```

AllAngle_Composite_Snow_Free_Quality:Description = "Quality:\n\t 0 = Good quality\n\t 1 = Poor quality\n\t 2 = Gap filled\n\t 255 =
Fill value\n\t" ;
    AllAngle_Composite_Snow_Free_Quality:coordinates = "latitude longitude" ;
    float AllAngle_Composite_Snow_Free_Std(phony_dim_0, phony_dim_1) ;
        AllAngle_Composite_Snow_Free_Std:_FillValue = -999.9f ;
        AllAngle_Composite_Snow_Free_Std:long_name = "Standard Deviation of Temporal Radiance Composite Using All Observations During
Snow-free Period" ;
            AllAngle_Composite_Snow_Free_Std:units = "nWatts/(cm^2 sr)" ;
            AllAngle_Composite_Snow_Free_Std:valid_range = ">= 0.0 \n" ;
            AllAngle_Composite_Snow_Free_Std:scale_factor = 1. ;
            AllAngle_Composite_Snow_Free_Std:offset = 0. ;
            AllAngle_Composite_Snow_Free_Std:coordinates = "latitude longitude" ;
        ubyte DNB_Platform(phony_dim_0, phony_dim_1) ;
            DNB_Platform:_FillValue = 255UB ;
            DNB_Platform:long_name = "Platform" ;
            DNB_Platform:units = "platform, no units" ;
            DNB_Platform:valid_range = 0UB, 254UB ;
            DNB_Platform:scale_factor = 1. ;
            DNB_Platform:offset = 0. ;
            DNB_Platform:Description = "Platform:\n\t 0 = Suomi-NPP\n\t 1 = NOAA20\n\t 2 = NOAA21 \n\t 3 = NOAA20 and NOAA21 combined
\n\t" ;
                DNB_Platform:coordinates = "latitude longitude" ;
            ubyte Land_Water_Mask(phony_dim_0, phony_dim_1) ;
                Land_Water_Mask:_FillValue = 255UB ;
                Land_Water_Mask:long_name = "Land Water Mask" ;
                Land_Water_Mask:units = "land water mask, no units" ;
                Land_Water_Mask:valid_range = 0UB, 254UB ;
                Land_Water_Mask:scale_factor = 1. ;
                Land_Water_Mask:offset = 0. ;
                Land_Water_Mask:Description = "Land/Water:\n\t 0 = Land & Desert \n\t 1 = Land no Desert \n\t 2 = Inland Water \n\t 3 = Sea Water
\n\t 5 = Coastal \n\t" ;
                    Land_Water_Mask:coordinates = "latitude longitude" ;
                float NearNadir_Composite_Snow_Covered(phony_dim_0, phony_dim_1) ;
                    NearNadir_Composite_Snow_Covered:_FillValue = -999.9f ;
                    NearNadir_Composite_Snow_Covered:long_name = "Temporal Radiance Composite Using Near Nadir Angle Observations (View Zenith
Angle 0-20 degree) During Snow-covered Period" ;
                        NearNadir_Composite_Snow_Covered:units = "nWatts/(cm^2 sr)" ;
                        NearNadir_Composite_Snow_Covered:valid_range = ">= 0.0 \n" ;
                        NearNadir_Composite_Snow_Covered:scale_factor = 1. ;
                        NearNadir_Composite_Snow_Covered:offset = 0. ;
                        NearNadir_Composite_Snow_Covered:coordinates = "latitude longitude" ;
                    ushort NearNadir_Composite_Snow_Covered_Num(phony_dim_0, phony_dim_1) ;
                        NearNadir_Composite_Snow_Covered_Num:_FillValue = 65535US ;
                        NearNadir_Composite_Snow_Covered_Num:long_name = "Number of Observations of Temporal Radiance Composite Using Near Nadir
Angle Observations (View Zenith Angle 0-20 degree) During Snow-covered Period" ;
                            NearNadir_Composite_Snow_Covered_Num:units = "number of observations" ;
                            NearNadir_Composite_Snow_Covered_Num:valid_range = 0US, 65534US ;
                            NearNadir_Composite_Snow_Covered_Num:scale_factor = 1. ;
                            NearNadir_Composite_Snow_Covered_Num:offset = 0. ;
                            NearNadir_Composite_Snow_Covered_Num:coordinates = "latitude longitude" ;
                        ubyte NearNadir_Composite_Snow_Covered_Quality(phony_dim_0, phony_dim_1) ;
                            NearNadir_Composite_Snow_Covered_Quality:_FillValue = 255UB ;
                            NearNadir_Composite_Snow_Covered_Quality:long_name = "Quality Flag of Temporal Radiance Composite Using Near Nadir Angle
Observations (View Zenith Angle 0-20 degree) During Snow-covered Period" ;
                                NearNadir_Composite_Snow_Covered_Quality:units = "flag, no units" ;
                                NearNadir_Composite_Snow_Covered_Quality:valid_range = 0UB, 254UB ;
                                NearNadir_Composite_Snow_Covered_Quality:scale_factor = 1. ;
                                NearNadir_Composite_Snow_Covered_Quality:offset = 0. ;
                                NearNadir_Composite_Snow_Covered_Quality:Description = "Quality:\n\t 0 = Good quality\n\t 1 = Poor quality\n\t 2 = Gap filled\n\t
255 = Fill value\n\t" ;
                                    NearNadir_Composite_Snow_Covered_Quality:coordinates = "latitude longitude" ;
                                float NearNadir_Composite_Snow_Covered_Std(phony_dim_0, phony_dim_1) ;
                                    NearNadir_Composite_Snow_Covered_Std:_FillValue = -999.9f ;
                                    NearNadir_Composite_Snow_Covered_Std:long_name = "Standard Deviation of Temporal Radiance Composite Using Near Nadir Angle
Observations (View Zenith Angle 0-20 degree) During Snow-covered Period" ;
                                        NearNadir_Composite_Snow_Covered_Std:units = "nWatts/(cm^2 sr)" ;
                                        NearNadir_Composite_Snow_Covered_Std:valid_range = ">= 0.0 \n" ;
                                        NearNadir_Composite_Snow_Covered_Std:scale_factor = 1. ;
                                        NearNadir_Composite_Snow_Covered_Std:offset = 0. ;
                                        NearNadir_Composite_Snow_Covered_Std:coordinates = "latitude longitude" ;
                                    float NearNadir_Composite_Snow_Free(phony_dim_0, phony_dim_1) ;
                                        NearNadir_Composite_Snow_Free:_FillValue = -999.9f ;
                                        NearNadir_Composite_Snow_Free:long_name = "Temporal Radiance Composite Using Near Nadir Angle Observations (View Zenith
Angle 0-20 degree) During Snow-free Period" ;
                                            NearNadir_Composite_Snow_Free:units = "nWatts/(cm^2 sr)" ;
                                            NearNadir_Composite_Snow_Free:valid_range = ">= 0.0 \n" ;
                                            NearNadir_Composite_Snow_Free:scale_factor = 1. ;
                                            NearNadir_Composite_Snow_Free:offset = 0. ;

```

```

NearNadir_Composite_Snow_Free:coordinates = "latitude longitude" ;
ushort NearNadir_Composite_Snow_Free_Num(phony_dim_0, phony_dim_1) ;
NearNadir_Composite_Snow_Free_Num:_FillValue = 65535US ;
NearNadir_Composite_Snow_Free_Num:long_name = "Number of Observations of Temporal Radiance Composite Using Near Nadir Angle Observations (View Zenith Angle 0-20 degree) During Snow-free Period" ;
NearNadir_Composite_Snow_Free_Num:units = "number of observations" ;
NearNadir_Composite_Snow_Free_Num:valid_range = 0US, 65534US ;
NearNadir_Composite_Snow_Free_Num:scale_factor = 1. ;
NearNadir_Composite_Snow_Free_Num:offset = 0. ;
NearNadir_Composite_Snow_Free_Num:coordinates = "latitude longitude" ;
ubyte NearNadir_Composite_Snow_Free_Quality(phony_dim_0, phony_dim_1) ;
NearNadir_Composite_Snow_Free_Quality:_FillValue = 255UB ;
NearNadir_Composite_Snow_Free_Quality:long_name = "Quality Flag of Temporal Radiance Composite Using Near Nadir Angle Observations (View Zenith Angle 0-20 degree) During Snow-free Period" ;
NearNadir_Composite_Snow_Free_Quality:units = "flag, no units" ;
NearNadir_Composite_Snow_Free_Quality:valid_range = 0UB, 254UB ;
NearNadir_Composite_Snow_Free_Quality:scale_factor = 1. ;
NearNadir_Composite_Snow_Free_Quality:offset = 0. ;
NearNadir_Composite_Snow_Free_Quality:Description = "Quality:\n\t 0 = Good quality\n\t 1 = Poor quality\n\t 2 = Gap filled\n\t 255 = Fill value\n\t" ;
NearNadir_Composite_Snow_Free_Quality:coordinates = "latitude longitude" ;
float NearNadir_Composite_Snow_Free_Std(phony_dim_0, phony_dim_1) ;
NearNadir_Composite_Snow_Free_Std:_FillValue = -999.9f ;
NearNadir_Composite_Snow_Free_Std:long_name = "Standard Deviation of Temporal Radiance Composite Using Near Nadir Angle Observations (View Zenith Angle 0-20 degree) During Snow-free Period" ;
NearNadir_Composite_Snow_Free_Std:units = "nWatts/(cm^2 sr)" ;
NearNadir_Composite_Snow_Free_Std:valid_range = ">= 0.0 \n" ;
NearNadir_Composite_Snow_Free_Std:scale_factor = 1. ;
NearNadir_Composite_Snow_Free_Std:offset = 0. ;
NearNadir_Composite_Snow_Free_Std:coordinates = "latitude longitude" ;
float OffNadir_Composite_Snow_Covered(phony_dim_0, phony_dim_1) ;
OffNadir_Composite_Snow_Covered:_FillValue = -999.9f ;
OffNadir_Composite_Snow_Covered:long_name = "Temporal Radiance Composite Using Off Nadir Angle Observations (View Zenith Angle 40-60 degree) During Snow-covered Period" ;
OffNadir_Composite_Snow_Covered:units = "nWatts/(cm^2 sr)" ;
OffNadir_Composite_Snow_Covered:valid_range = ">= 0.0 \n" ;
OffNadir_Composite_Snow_Covered:scale_factor = 1. ;
OffNadir_Composite_Snow_Covered:offset = 0. ;
OffNadir_Composite_Snow_Covered:coordinates = "latitude longitude" ;
ushort OffNadir_Composite_Snow_Covered_Num(phony_dim_0, phony_dim_1) ;
OffNadir_Composite_Snow_Covered_Num:_FillValue = 65535US ;
OffNadir_Composite_Snow_Covered_Num:long_name = "Number of Observations of Temporal Radiance Composite Using Off Nadir Angle Observations (View Zenith Angle 40-60 degree) During Snow-covered Period" ;
OffNadir_Composite_Snow_Covered_Num:units = "number of observations" ;
OffNadir_Composite_Snow_Covered_Num:valid_range = 0US, 65534US ;
OffNadir_Composite_Snow_Covered_Num:scale_factor = 1. ;
OffNadir_Composite_Snow_Covered_Num:offset = 0. ;
OffNadir_Composite_Snow_Covered_Num:coordinates = "latitude longitude" ;
ubyte OffNadir_Composite_Snow_Covered_Quality(phony_dim_0, phony_dim_1) ;
OffNadir_Composite_Snow_Covered_Quality:_FillValue = 255UB ;
OffNadir_Composite_Snow_Covered_Quality:long_name = "Quality Flag of Temporal Radiance Composite Using Off Nadir Angle Observations (View Zenith Angle 40-60 degree) During Snow-covered Period" ;
OffNadir_Composite_Snow_Covered_Quality:units = "flag, no units" ;
OffNadir_Composite_Snow_Covered_Quality:valid_range = 0UB, 254UB ;
OffNadir_Composite_Snow_Covered_Quality:scale_factor = 1. ;
OffNadir_Composite_Snow_Covered_Quality:offset = 0. ;
OffNadir_Composite_Snow_Covered_Quality:Description = "Quality:\n\t 0 = Good quality\n\t 1 = Poor quality\n\t 2 = Gap filled\n\t 255 = Fill value\n\t" ;
OffNadir_Composite_Snow_Covered_Quality:coordinates = "latitude longitude" ;
float OffNadir_Composite_Snow_Covered_Std(phony_dim_0, phony_dim_1) ;
OffNadir_Composite_Snow_Covered_Std:_FillValue = -999.9f ;
OffNadir_Composite_Snow_Covered_Std:long_name = "Standard Deviation of Temporal Radiance Composite Using Off Nadir Angle Observations (View Zenith Angle 40-60 degree) During Snow-covered Period" ;
OffNadir_Composite_Snow_Covered_Std:units = "nWatts/(cm^2 sr)" ;
OffNadir_Composite_Snow_Covered_Std:valid_range = ">= 0.0 \n" ;
OffNadir_Composite_Snow_Covered_Std:scale_factor = 1. ;
OffNadir_Composite_Snow_Covered_Std:offset = 0. ;
OffNadir_Composite_Snow_Covered_Std:coordinates = "latitude longitude" ;
float OffNadir_Composite_Snow_Free(phony_dim_0, phony_dim_1) ;
OffNadir_Composite_Snow_Free:_FillValue = -999.9f ;
OffNadir_Composite_Snow_Free:long_name = "Temporal Radiance Composite Using Off Nadir Angle Observations (View Zenith Angle 40-60 degree) During Snow-free Period" ;
OffNadir_Composite_Snow_Free:units = "nWatts/(cm^2 sr)" ;
OffNadir_Composite_Snow_Free:valid_range = ">= 0.0 \n" ;
OffNadir_Composite_Snow_Free:scale_factor = 1. ;
OffNadir_Composite_Snow_Free:offset = 0. ;
OffNadir_Composite_Snow_Free:coordinates = "latitude longitude" ;
ushort OffNadir_Composite_Snow_Free_Num(phony_dim_0, phony_dim_1) ;

```

```

OffNadir_Composite_Snow_Free_Num:_FillValue = 65535US ;
OffNadir_Composite_Snow_Free_Num:long_name = "Number of Observations of Temporal Radiance Composite Using Off Nadir Angle
Observations (View Zenith Angle 40-60 degree) During Snow-free Period" ;
    OffNadir_Composite_Snow_Free_Num:units = "number of observations" ;
    OffNadir_Composite_Snow_Free_Num:valid_range = 0US, 65534US ;
    OffNadir_Composite_Snow_Free_Num:scale_factor = 1. ;
    OffNadir_Composite_Snow_Free_Num:offset = 0. ;
    OffNadir_Composite_Snow_Free_Num:coordinates = "latitude longitude" ;
    ubyte OffNadir_Composite_Snow_Free_Quality(phony_dim_0, phony_dim_1) ;
        OffNadir_Composite_Snow_Free_Quality:_FillValue = 255UB ;
        OffNadir_Composite_Snow_Free_Quality:long_name = "Quality Flag of Temporal Radiance Composite Using Off Nadir Angle
Observations (View Zenith Angle 40-60 degree) During Snow-free Period" ;
            OffNadir_Composite_Snow_Free_Quality:units = "flag, no units" ;
            OffNadir_Composite_Snow_Free_Quality:valid_range = 0UB, 254UB ;
            OffNadir_Composite_Snow_Free_Quality:scale_factor = 1. ;
            OffNadir_Composite_Snow_Free_Quality:offset = 0. ;
            OffNadir_Composite_Snow_Free_Quality:Description = "Quality:\n\t 0 = Good quality\n\t 1 = Poor quality\n\t 2 = Gap filled\n\t 255 =
Fill value\n\t" ;
                OffNadir_Composite_Snow_Free_Quality:coordinates = "latitude longitude" ;
                float OffNadir_Composite_Snow_Free_Std(phony_dim_0, phony_dim_1) ;
                    OffNadir_Composite_Snow_Free_Std:_FillValue = -999.9f ;
                    OffNadir_Composite_Snow_Free_Std:long_name = "Standard Deviation of Temporal Radiance Composite Using Off Nadir Angle
Observations (View Zenith Angle 40-60 degree) During Snow-free Period" ;
                        OffNadir_Composite_Snow_Free_Std:units = "nWatts/(cm^2 sr)" ;
                        OffNadir_Composite_Snow_Free_Std:valid_range = ">= 0.0 \n" ;
                        OffNadir_Composite_Snow_Free_Std:scale_factor = 1. ;
                        OffNadir_Composite_Snow_Free_Std:offset = 0. ;
                        OffNadir_Composite_Snow_Free_Std:coordinates = "latitude longitude" ;
                        double lat(phony_dim_0) ;
                            lat:long_name = "latitude" ;
                            lat:units = "degrees_north" ;
                            lat:CoordinateAxisType = "Lat" ;
                            lat:valid_min = -90.f ;
                            lat:valid_max = 90.f ;
                            lat:_FillValue = -999.9f ;
                        double lon(phony_dim_0) ;
                            lon:long_name = "longitude" ;
                            lon:units = "degrees_east" ;
                            lon:CoordinateAxisType = "Lon" ;
                            lon:valid_min = -180.f ;
                            lon:valid_max = 180.f ;
                            lon:_FillValue = -999.9f ;
                    } // group Data\ Fields
                } // group VIIRS_Grid_DNB_2d
            } // group GRIDS
        } // group HDFEOS
    }

group: HDFEOS\ INFORMATION {
variables:
    string StructMetadata.0 ;

// group attributes:
    :HDFEOSVersion = "HDFEOS_5.1.16" ;
} // group HDFEOS\ INFORMATION
}

```